BIOMECHANICAL STUDIES OF DEVELOPING ZEBRAFISH HEART *IN-VIVO*

by

NABID SALEHIN

DISSERTATION

Submitted in partial fulfillment of the requirements
for the degree of Doctor of Philosophy at
The University of Texas at Arlington
May, 2021

Arlington, Texas

Supervising Committee:

Cheng-Jen Chuong, Supervising Professor

Juhyun Lee

Hanli Liu

Jun Liao

ABSTRACT

Biomechanical Studies of Developing Zebrafish Heart *In-Vivo*

Nabid Salehin, Ph.D.

The University of Texas at Arlington, 2021

Supervising Professor: Cheng-Jen Chuong

The heart is an electrically controlled mechanical pump that provides the cardiac output required by the body to function properly and flexibly adapts to changing demand and working conditions. In vertebrate embryos, the heart is the first organ that starts functioning and the function is initiated well before structural organogenesis is complete, with its early mechanical function affecting its own development. During development, the heart transforms from a valveless linear peristaltic tube into a multi-chambered pulsatile pump with blood flow regulating valves while continuing to serve the metabolic needs of the embryo. The zebrafish has emerged as a popular model system for *in vivo* studies of developmental biology due to its unique features including high fecundity, external fertilization, rapid organ development and optical transparency. In this study, we analyzed the changing mechanical function of the embryonic zebrafish heart in-vivo, both overall and regional, through the developmental period of 3 to 5-days post fertilization (dpf).

For Aim 1, we assessed the changing pressure-volume relationships of the developing ventricle of zebrafish in-vivo. We measured intra-ventricular pressure using servo null method and reconstructed ventricular volume using selective plane illumination microscopy (SPIM), a light sheet fluorescence microscopy technique. Pressure volume (P-V) loops were constructed by

synchronizing measured intra-ventricular pressure and ventricular volume that facilitated hemodynamic analysis. Results indicated significant increases in peak systolic pressure, stroke volume, cardiac output, stroke work, power generation, and a decrease in the total peripheral resistance of the developing heart from 3 to 4 and 5 dpf.

In Aim 2, we examined the regional function of the ventricles from zebrafish embryos at 3, 4, 5 dpf. We developed a method that characterized the regional deformation of the ventricular myocardium by tracking the moving 3D coordinates of the fluorescing cardiomyocytes through cardiac cycles. Our results did not show statistically significant differences in regional area ratios. The ventricular wall myocardium was found to have higher compliance at 3 dpf than 4 and 5 dpf groups. On the other hand, the ventricular myocardium was found to have higher systolic performance index at 4, 5 dpf than at 3 dpf. The developing myocardium becomes stiffer from 3 to 5 dpf and generates higher ventricular pressure at faster rates during ejection. Resolving the deformation into principal stretches λ_1 and λ_2, acting along longitudinal and latitudinal directions respectively, differences were noted. From 4 and 5 dpf groups, end diastolic λ_2 was larger than λ_1 in all three regions and differences between λ_2 and λ_1 also existed at end systolic state. At 5 dpf, significant regional difference was detected in both λ_2 and λ_1. Our results suggest that along with the developmental changes in morphology, vasculature and maturation of valves, the embryos at 4, 5 dpf underwent anisotropic deformation favoring latitudinal direction.

Aim 3 is an extension from Aim 2 wherein we further divided the ventricular surface into 8 sub-regions to systematically map out the differences in deformation characteristics along circumferences at different axial positions and the differences in three dpf groups. Results revealed not only the regional differences but also the tethering effects due to the presence of AV valve and its opening closure through a cardiac cycle when regulating blood flow.

Collectively, results from three aims revealed insights in our understanding of the increasing operational efficiency of the early-stage zebrafish heart when undergoing rapid growth. The development of the heart occurs in time with concurrent changes in myocardium growth, in valve development, in chamber morphology, and in the improving efficiency of the physiological pumping function supplying blood to feed the increasing complexity of the vascular network of the organism.

ACKNOWLEDGEMENTS

I would like to sincerely thank my supervising professor Dr. Cheng-Jen Chuong for the support and guidance he provided through the course of this research. His feedback and cooperation greatly facilitated the completion of this study. I would also like to thank Dr. Juhyun Lee for his valuable advice and for letting me use the facilities in his lab. The experiments for this research were performed in his lab. In addition, I would like to express my gratitude to the committee members, Dr. Hanli Liu and Dr. Jun Liao for their support. I also acknowledge the help and suggestions provided by Dr. Benjamin Dubansky of UNT regarding the use of servo null micro pressure measurement system.

A very special thanks to Tanveer Teranikar, PhD student at UTA, for his help with setting up the light sheet imaging system, imaging the zebrafish embryos, image processing and segmentation. I also sincerely thank Cameron Villareal, MS at UTA, for his help with measuring intra-ventricular pressure of zebrafish embryos.

TABLE OF CONTENTS

LIST OF FIGURES

CHAPTER 2

CHAPTER 3

CHAPTER 4

LIST OF TABLES

CHAPTER 1

CHAPTER 2

CHAPTER 1

Introduction

The heart is an electrically controlled mechanical pump that provides the cardiac output required by the body to function properly and flexibly adapts to changing demands and changing working conditions (*1, 2*). Analysis of overall cardiac pumping function and regional functions of local myocardium have provided useful insights for many cardiovascular diseases in the fetus, the child and the adult (*2*). A properly functioning heart is extremely important for the survival of the embryo and thus the heart starts pumping blood early in embryogenesis (*3*).

In fact, the heart is the first organ that starts functioning in vertebrate embryos and the function is initiated well before structural organogenesis is complete, with its early mechanical function affecting its own development (*4*). During development, the heart transforms from a valveless linear peristaltic tube into a multi-chambered pulsatile pump with regulating valves and all the changes occur under blood flow conditions. This transformation involves a dynamic interaction between genetic and epigenetic (environmental) factors that regulate the processes of growth (volume change), remodeling (property change) and morphogenesis (shape change) (*5*). Biomechanics is a key epigenetic factor, affecting the early stages of heart development, from looping and trabeculation to chamber and valve formation. The genetic blueprint of an organism contains the basic plan for cardiac development (*6*), but hemodynamic events can edit this blueprint. During early stages of development, the heart is very sensitive to biomechanical cues that modulate intrinsic genetic programs (*7-9*). Studies have demonstrated that, the heart does not develop properly in the absence of blood flow and deviations from normal hemodynamic conditions lead to congenital heart defects (*10-12*). Some studies have pointed out the

importance of intrinsic and extrinsic mechanical forces for the looping process (*13, 14*). Biomechanics thus play a critical role in shaping development of the heart.

The cardiac muscle is initially a thin layer of epithelial cells forming the outer layer of the heart tube. With differentiation of these cells into muscle and the accumulation of acto-myosin contractile proteins in the cytoplasm, sarcomere and myofibrils are formed that gradually align to create the complex three-dimensional architecture of the mature heart (*5*). Collagen fibers of the extracellular matrix also cross link to form their own structure (*15*). Because of this remodeling, the stiffness and anisotropy of the myocardium changes during development. The morphology of the heart changes dramatically during development but it functions without interruption to serve the metabolic needs of the rapidly growing embryo, implying the changes are closely coordinated (*5*).

Heart development starts through the formation of a hollow linear tube structure, as two separate masses of pre-cardiac mesoderm meet after migrating to the ventral midline (*3*). The early heart tube consists of three tissue layers: a two-cell thick outer layer of myocardium, a thick middle layer of cardiac jelly and a thin inner layer of endocardium. The cells of the myocardium contain the only contractile elements, the cardiac jelly serves as the extracellular matrix and the one cell thick endocardium lines the lumen of the tube. Before the myocytes start to contract, spontaneous action potentials propagate through the myocardium, that eventually initiates the flow of blood (*16*).

The initial blood flow through the heart is due to a peristaltic wave of contraction. Soon afterwards, the flow becomes pulsatile with regional wall thickening of cardiac jelly called endocardial cushions in the inflow and outflow regions serving as primitive valves (*5*). The

cushions close the lumen locally to preclude back flow with the passing of contractile waves. The physiological attributes (e.g., ventricular pressure-time curve) of the tubular heart are noticeably resembles the mature heart although valves are still being formed. Following the beginning of contraction, the linear heart tube undergoes bending (dextral looping) and twisting through the morphogenetic process of looping and forms an s-shaped curved tube. Studies suggested that forces intrinsic to the heart itself drive the bending component of looping (*13*), while the torsional component of looping might be strongly influenced by extrinsic forces from neighboring tissues (*14*). A series of protrusions: the sinus venosus, the primitive atrium, the ventricle and the conotruncus, also appear along the tube. These protrusions are brought into their proper relative anatomic positions by looping which set the pattern for the final form of the heart.

The process of trabeculation is initiated near the end of looping, when cardiac jelly is displaced from the ventricle's outer curvature and endocardial pouches grow toward the myocardial layer (*17, 18*). The trabecular myocardium is a sponge like network of cardiomyocytes that is critical for contraction and conduction, ventricular septation, papillary muscle formation and wall thickening through the process of compaction (*18*). While trabeculation is regulated by several developmental genes and metabolites (e.g., N – cadherin, neuregulin, ErbB and BMP) (*19, 20*), hemodynamics also modulates trabeculation. It has been reported that reduced shear stress attenuated trabeculation through down regulation of Notch signaling (*9*). Formation of trabeculae greatly increases surface area, myocardial mass and wall stiffness (*21*). The increase in surface area increases passive diffusion of oxygen in the absence of coronary vessels at this early stage (*22*). With progress of trabeculation, direct blood flow through the trabecular spaces supplies nutrients to the myocardium. After a period of trabecular

growth, inter-ventricular septation and chamber formation occur via coalescence and compaction of trabeculae and ballooning of the ventricles (*23*). It has been observed that normal septation does not occur in the presence of aberrant flows (*24*), indicating the importance of hemodynamic forces.

Valvulogenesis, which started with the formation of endocardial cushions in the atrio-ventricular (AV) canal and outflow tract (OFT), continues as the endocardial cushions are colonized by endocardial cells of the AV and OFT when these cells undergo epithelial to mesenchymal transformation. The AV endocardial cushions fuse, condense and then remodel to mitral and tricuspid valves while the OFT cushions remodel into semilunar valve leaflets. More than 100 genes have been identified that play a role in this process (*25*) in addition to the role of hemodynamics. Hemodynamic forces are important mechanical stimuli for valve development as reported by many studies (*4, 7-10*). One study showed that the expression of the relevant gene: klf2a was dependent on the presence of reversing flows (*8*). Another study revealed that shear stress governs the differential expression of miR – 21 in AV canal (*7*). With the formation of valves, the heart resembles its mature form, and the rest of the development is mainly dominated by growth.

Several animal models have been used to study cardiovascular development. Mouse models are very commonly used to study genes important for cardiac development and linked to cardiac defects (*26*) and provide valuable information about the role of genetic perturbation (*3*). In order to avoid the difficulty of accessing embryos within their mother's womb, non-mammalian models of cardiac development have been widely used including chicken (*27*) and zebrafish (*28*). Because of the conservation of developmental processes among vertebrate species, non-mammals are very good models to study cardiovascular development and they

allow easy access to the embryo for imaging and manipulation. The similarity in the process of cardiac development in humans and animal models is notable although the timing of events differs as shown in Table below.

Table: Early stages of heart development in the embryonic human, mouse, chick and zebrafish

	Human (days)	**Mouse**	**Chick**	**Zebrafish (dpf)**	**Milestones**
Linear heart tube	22	E8	HH10-HH11	1	Formation of heart tube; 1st heartbeat
Looping heart	28	E9	HH10-HH24	1.5	Dextral looping; early formation of chambers
Trabeculation	26-32	E10	HH17-HH25	2-5	Replacement of cardiac jelly with trabeculae; stage ends with compaction
Cushion formation	28-37	E9-E11	HH12-HH34	1.5-1.75	Serve as primitive valve
Septation initiation	50-60	E11-E13	HH21-HH26	None	4 chambered heart; 2 chambered in zebrafish
Valve formation	42-70	E12-E17	HH24-HH36	4-5	Cushions fuse and condense to form valve leaflets

E embryonic days in mice, *HH* Hamburger – Hamilton stage in chick, *dpf* days post-fertilization,

References: (*3, 28*)

The zebrafish has emerged as a popular model system for *in vivo* studies of the genetic,

morphological and functional aspects of cardiovascular development. Transgenic varieties of zebrafish have been generated in which fluorescent proteins label individual cells or particular tissues and facilitate visualization of cell and tissue behavior during development. Although zebrafish heart differs from human heart by having only systemic circulation, there are considerable similarities in heart structure and physiology (*28*). Zebrafish possesses some unique characteristics that make it particularly attractive for cardiovascular research. It has high reproduction rate and males externally fertilize the eggs. Because of its external development and relative optical transparency during early developmental period, the zebrafish embryo can be imaged by light microscopy techniques from its earliest stages (*1*). Genetic engineering methods like morpholino oligomer injections are available to induce clinically relevant cardiac defects in zebrafish (*8, 29*). Unlike other model systems, zebrafish embryos are not dependent on circulatory system at early stages of development, since passive diffusion is sufficient for oxygen delivery (*30*). Embryos with abnormal cardiovascular function that can adversely affect blood flow can continue to develop and thus enable phenotypic studies of longer duration compared with mammals (*1*). Because of the close interrelation of structure and function of the heart, it would be best to study it directly inside the body of the developing embryo. With the advancement in light sheet imaging technology, it became possible to image the heart of zebrafish embryo *in vivo* – in three dimensions, at high spatial and temporal resolution (*1*). This enabled the real-time visualization of the highly dynamic process of heart development in zebrafish.

To assess cardiac function, contractility of the heart muscle needs to be evaluated locally. Contribution of cardiac muscles to global ejection performance of the heart and their ability to adapt to changing demands should be examined (*2*). The myocyte, the building block of the heart

muscle, develop force and shorten, when it is electrically activated. The maximum shortening of an individual myocyte is 10 - 15% (*31*). The myocytes combine to form muscle fibers, which through a complex three-dimensional arrangement provide the overall shape of the ventricle with specific curvature and thickness. With activation, the myocytes generate force along their longitudinal direction and the resultant force of differently oriented cells induces a rise in cavity pressure. As the ventricular pressure exceeds the aortic pressure, the aortic valve opens, and the myocytes start to shorten. This deformation of the myocardium leads to a reduction in cavity size and results in ejection of a certain volume of blood into the circulation. Hence, to evaluate cardiac function, both the developed force (pressure) and the resulting deformation (volume ejection) need to be considered.

Due to the relative ease of obtaining measurements of spatial dimensions, cardiac function is currently evaluated by assessing volume-based parameters. End diastolic volume (EDV), end systolic volume (ESV), stroke volume (SV = EDV - ESV), cardiac output (CO, product of SV and heart rate) and ejection fraction (EF = (EDV - ESV) / EDV) are commonly used hemodynamic parameters that indicate global ejection from the ventricle as a result of overall deformation of the ventricle. Measurement of intra-ventricular pressure requires invasive approaches. Peak systolic ventricular pressure (PSVP) and end diastolic ventricular pressure (EDVP) are typically used indicators. Another important hemodynamic parameter is the stroke work (SW), the work done by the ventricle in each cardiac cycle to enable blood circulation in the cardiovascular system. It can be measured from the area enclosed by the pressure volume loop. Ventricular pressure–volume (PV) loop, determined from pressure and volume measurement of the left ventricle over one cardiac cycle, facilitates the quantification of key hemodynamic parameters and is a popular tool for characterizing ventricular function. Relations

between ventricular pressure and volume, as reflected in the P-V loop, provide one of the most precise means of assessing cardiac function. Pressure-volume loop provides physiological insights revealing the effects in ventricular function in response to the changes in preload, afterload and inotropy. Disease models of a model organism can display dramatic changes in cardiac morphology and integrated cardiovascular physiology, and this has greatly enhanced the need for rigorous quantification of cardiac function in intact animals. Developmental changes in stroke volume, intra-ventricular pressure and stroke work have been reported primarily in chick (*32-35*), as it offers the advantage of resembling human heart structure with four-chamber/four-valve configuration and enabling clinically relevant surgical manipulations (*28*). P-V loops have been developed for embryonic chick (*34, 35*) with ventricular volume estimated from 2D images of the ventricle assuming a prolate ellipsoid shape and the developed P-V loops were similar to those for the mature heart. One of the studies tested the effect of reduced placental blood flow on embryonic heart development by venous clipping or ligation of vitelline vein (*34*). Reduced ventricular contractility compared to the normal embryo, derived from P-V loop, suggested that hemodynamic perturbations cause long term and likely permanent effects. Few studies have examined functional changes during heart development in embryonic zebrafish (*36-38*). This led us to the first aim of assessing the changing pressure-volume relationships of the developing zebrafish ventricle from 3 to 5 days post fertilization (dpf).

Because of the inhomogeneity of the ventricle in terms of local shape, morphology, tissue composition and perfusion, regional assessment of force and deformation is required to quantify regional ventricular function. The deformation of a myocardial region during ejection is very complex and multi-dimensional. Deformation is generally quantified in terms of strain that measures how different points in myocardium change position relative to one another over a

certain period of time. The amount of shortening or stretch in the tissue quantifies the normal strain whereas the sliding of tissues parallel to a border quantifies the shear (*39*). The normal components of strain are longitudinal (in the base-to-apex direction), circumferential (along the short-axis circumference), and radial (from epi- to endocardium). There are also three shear components that cause change of angles. For a number of cardiac diseases, the dysfunction of the heart can be detected early with myocardial strain analysis compared to traditional (overall) function measurements (*40*). Multi-dimensional deformations can be described by principal strain analysis which identifies the effective directions along which strains develop as well as the magnitude of the strains (*41*).

The complex three-dimensional arrangement of muscle fibers in the wall of the mature heart results in ejection fractions of approximately 60% although individual muscle fibers can only shorten by 10–15%. A change in the orientation of the muscle fibers across the myocardial wall ensures such efficient ejection of blood (*2*). The fibers are oriented longitudinally at the epicardial surface, then gradually change angles, and become circumferentially oriented at the mid myocardium. The endocardial fibers are oriented longitudinally again. While contracting, fibers deform along their fiber direction, so that contraction of longitudinally oriented fibers causes deformation in the apex to base direction. Contraction of circumferential fibers result in a decrease of the short-axis diameter. Because of incompressibility, longitudinal and circumferential shortening result in thickening in the radial direction. The slight oblique orientation of epicardial and endocardial fiber causes rotation of the basal plane relative to the apical plane. The overall 3D deformation of a region is the resultant of all the deformation components.

Different components of deformation can be affected in different ways by disease processes. For example, assessment of only volume changes may not reveal the decreased longitudinal function, if it is compensated by an increased circumferential contraction (*42*). Also, during the iso-volumetric contraction (*43*) or relaxation period, there may be regional interaction causing deformation of regions that does not induce volume changes. Thus, quantifying regional ventricular function requires an examination of all potential geometric changes during the cardiac cycle. For embryonic zebrafish, assessment of regional ventricular deformation and associated developmental changes are yet to be carried out. This led us to the second aim of developing a method to characterize the regional deformation of the ventricular myocardium of developing zebrafish heart. In aim three, we want to apply the method developed in aim two and create a map of regional deformation in order to gain insights from regional contributions of ventricular myocardium to global pumping function of the heart through cardiac development.

CHAPTER 2

ASSESSING PRESSURE-VOLUME RELATIONSHIP IN DEVELOPING HEART OF ZEBRAFISH *IN-VIVO*[1]

Nabid Salehin, Cameron Villareal, Tanveer Teranikar, Benjamin Dubansky, Juhyun Lee &

Cheng-Jen Chuong

Citation:

Salehin, N., Villareal, C., Teranikar, T. et al. Assessing Pressure-Volume Relationship in Developing Heart of Zebrafish *In-Vivo*. *Ann Biomed Eng* (2021). https://doi.org/10.1007/s10439-021-02731-0

[1]Used with permission of the publisher, 2021

Introduction

Despite ongoing technological advances, it remains challenging to adequately visualize and study the development of the embryonic human heart. Animal models such as the mouse (*26*) and bird (*44*) are widely used to study cardiovascular development and pathogenesis from the level of molecular underpinnings to the associated morphological, behavioral and physiological phenotypes. The zebrafish has emerged as a leading *in vivo* model for developmental biology due to its relatively low cost, fast development in culture, and the fact that its early developmental stages can be imaged using light microscopy due to the relative transparency (*1*). Researchers have heavily leveraged the large molecular toolkit available for the fully sequenced and well-annotated zebrafish genome to detect or induce gene-level modifications while monitoring the morphological landmarks of clinically relevant cardiac defects (*8, 29*). As such, the zebrafish has emerged as a venerable model for studying human cardiovascular developmental defects and diseases (*45-47*). However, the zebrafish's small size has meant tools to directly measure cardiovascular variables lagging the relatively rapid development of molecular (and behavioral) tools.

In contrast to the four chambered mammalian heart, the zebrafish heart is composed of only two chambers (one ventricle and one atrium) (*47*). Blood comes from the venous system through the sinoatrial valve into the atrium of the zebrafish heart, which pumps blood through the atrio-ventricular (AV) valve into the ventricle. The ventricle then pumps blood out of the heart through the ventriculo-bulbar (VB) valve into the outflow tract where the bulbus arteriosus (BA) receives the blood under ventricle-generated pressure. This pressure stretches the elastin-rich BA (*48*), creating a "capacitor" that stores and releases elastic energy to maintain continuous blood flow away from the heart and into the gills where oxygen and ion transport occur (*36*). The

oxygenated blood then flows through the body and back to the heart in a single systemic circuit (*47*).

Despite having only two chambers, the zebrafish heart is a venerable model for early cardiovascular development. Early heart development is highly conserved across vertebrates, such that all hearts proceed through the same general developmental landmarks. In zebrafish, the formation of the heart tube starts ~16 hours post fertilization (hpf) in embryos incubated at 28° C. The tube-shaped heart, which starts to contract in a rhythmic peristaltic manner near 24 hpf, begins to loop into an "S–shape" near 33 hpf in a similar pattern as other vertebrates. Pumping mechanisms transform from slow peristaltic waves into sequential chamber contractions at approximately 36 hpf, just prior to valve formation (*28*). As the chambers differentiate, bumps of tissue between the chambers called endocardial cushions start transforming into primitive valve leaflets at ~40 hpf. Functional valve development is completed by 96-120 hpf (*8, 49*). Organogenesis for zebrafish incubated at 28° C is largely completed by 5 days post fertilization (*10*) (Fig. 1.)

To best leverage the zebrafish developmental program as a model for human cardiovascular pathophysiology, it is crucial to understand the complex physiological phenotypes that may arise from physical and pharmacological stressors as well as from induced and acquired genetic variation (*50*). However, it has been difficult to measure relevant cardiovascular parameters such as blood flow, blood pressure and the electrical events that occur during the cardiac cycle in developing zebrafish. Indeed, few devices are available that enable the direct measurement of cardiac physiology in these small model organisms (≈ 4 mm long when newly hatched).

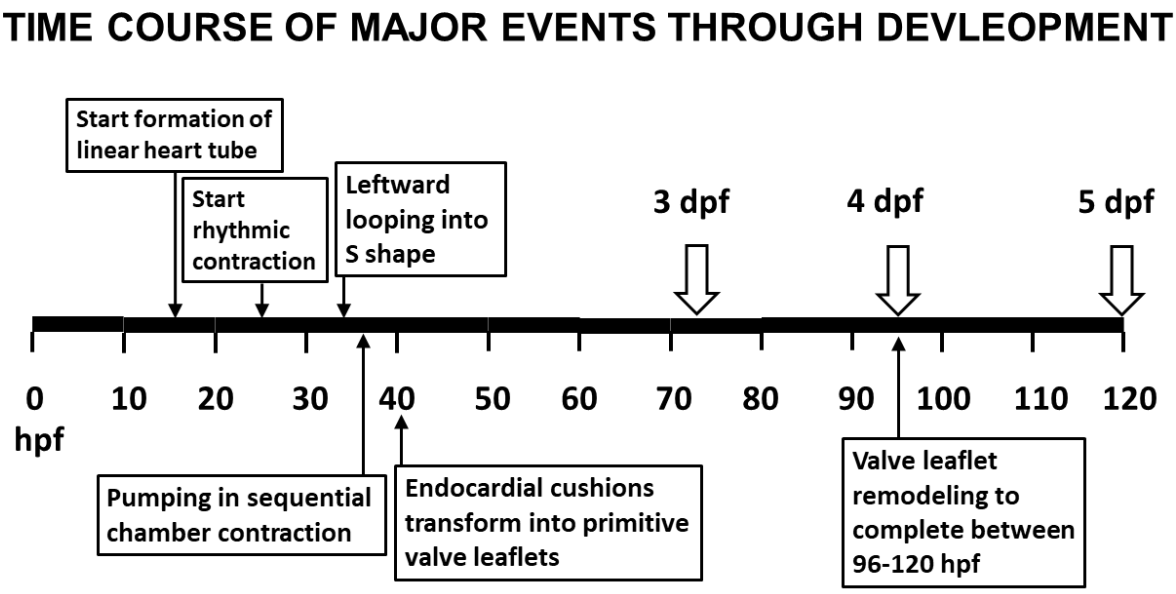

Figure 1: Heart development in zebrafish with major milestones indicated

The pressure-volume loop (PV loop) is a tool to visualize changes in pressure and blood volume in the heart ventricles (*51*). By incorporating changes in both pressure and volume during the cardiac cycle, the resultant plot of pressure versus volume provides deep physiological insights into ventricular function (*52*). Indeed, nuances in PV loops can indicate fine-scale effects from cardioactive stressors such as changes in preload, afterload and inotropy. The embryonic zebrafish's small size, however, has made it challenging to directly measure intra-ventricular pressure and volume. Here, we separately measured ventricular pressure and volume in developing zebrafish *in vivo* at 3, 4 and 5 dpf. We used servo null micro-pressure measurement technology (*36, 47*) to measure intra-ventricular pressure. Next, we used 4-D (3-D + time) selective plane illumination microscopy (SPIM) (*9, 29*) to measure ventricular volume and the function of the AV and VB valves during early development. With this recorded data, we generated PV loops for zebrafish at 3, 4 and 5 dpf and used these measurements to calculate

hemodynamic parameters, including stroke volume, heart rate, cardiac output, ejection fraction, stroke work, power, and total peripheral resistance. Collectively, these data describe the improved mechanical performance of the developing zebrafish heart at 3, 4, and 5 dpf. These data provide new insight for assessing hemodynamic parameters in the zebrafish embryo, and strongly highlights the need for reliable technologies to directly measure cardiovascular physiology.

Materials and Methods

a. Zebrafish and preparation for imaging

Transgenic zebrafish embryos Tg*(cmlc2:* mCherry*; fli1a:* GFP*)* at 3, 4, 5 dpf expressing mCherry fluorescent signal in myocardium and green fluorescent signal in endocardium were used for imaging and calculating ventricular volume and AV and VB valve analyses in this study. Embryos were bred and maintained at the UT Arlington animal care facility. Embryos were incubated at 28^0C in zebrafish embryo media (E3 media) with 0.003% phenylthiourea (PTU) added at 20 hpf to maintain embryo transparency (*53*). For imaging, embryos were anesthetized in 0.05% tricaine and immersed in 0.5% low melting point agarose which was refractive indice-matched to water. Embryos were transferred to a fluorinated ethylene propylene (FEP) tube for embryo mounting and manipulation for light sheet microscopy. Husbandry and experiments were performed in compliance with our Institutional Animal Care and Use Committee (IACUC) protocols.

b. Image acquisition

Three separate embryos at each of 3, 4, 5 dpf time point were imaged by SPIM. A laser (CNI Laser, PSU – III - LED) operated at 473 and 532 nm was used to provide the excitation for GFP and mCherry respectively, and a 10X objective lens (NA = 0.2) was used for detection. The illumination and the detection path are orthogonal to each other with the sample placed at the intersection of the two axes. Only the fluorophores in the focal plane of the detection objective lens are excited and the emission light is collected through the detection optics and recorded using a digital camera (Hamamatsu, ORCA Flash 4.0 sCMOS, see schematic in Fig. S1). A single 2D image can thus be obtained at the focal plane without scanning. Dynamic 3D volumes

of the embryonic zebrafish heart were acquired by collecting 2D image sequences while moving the sample along the detection axis at a fixed 2 μm step size. We captured 2D image sequence stacks of the heart from the cranial to the caudal end. Each slice sequence in the stack consisted of 500 frames (512 x 512 pixels), imaged at 10 ms exposure time per frame with 80 - 120 overlapping z-slices recorded. 4D images were reconstructed from the slice sequences with a voxel size of 0.65 x 0.65 x 2 μm^3. Custom LABVIEW (National Instruments) code was used to control the process of image acquisition and recording.

c. 4-D images of the embryonic zebrafish heart

Acquired image slices were processed with software we previously developed (*9, 29*). Briefly, dynamic 3D volumes were reconstructed by a non-gated synchronization algorithm that rearranged the slice sequences to find the minimum error of the cardiac phase of each layer, with respect to time (*54, 55*). The synchronization algorithm was based on a criterion to minimize least squares intensity differences implemented in custom MATLAB code (MathWorks).

d. Estimation of ventricular volume reconstructed from 3-D images

We recovered the dynamic events of the ventricle over cardiac cycles using reconstructed 4D images of the embryonic zebrafish hearts. At each time point through a cardiac cycle, individual slices that made up the ventricular volume were manually segmented to delineate the endocardial surface of the ventricle as well as the positioning of the AV and VB valve leaflets. Figure 2A is a representative slice image from a 5 dpf fish when its AV valve was fully open and VB valve was closed during diastolic filling; whereas Figure 2B is that when the AV valve was closed, and VB valve was fully open during ejection. In both, we added yellow dot lines to delineate the endocardial surface. The corresponding blood volume enclosed by the endocardial surface was calculated as the product of the confined area multiplied by the slice thickness of the

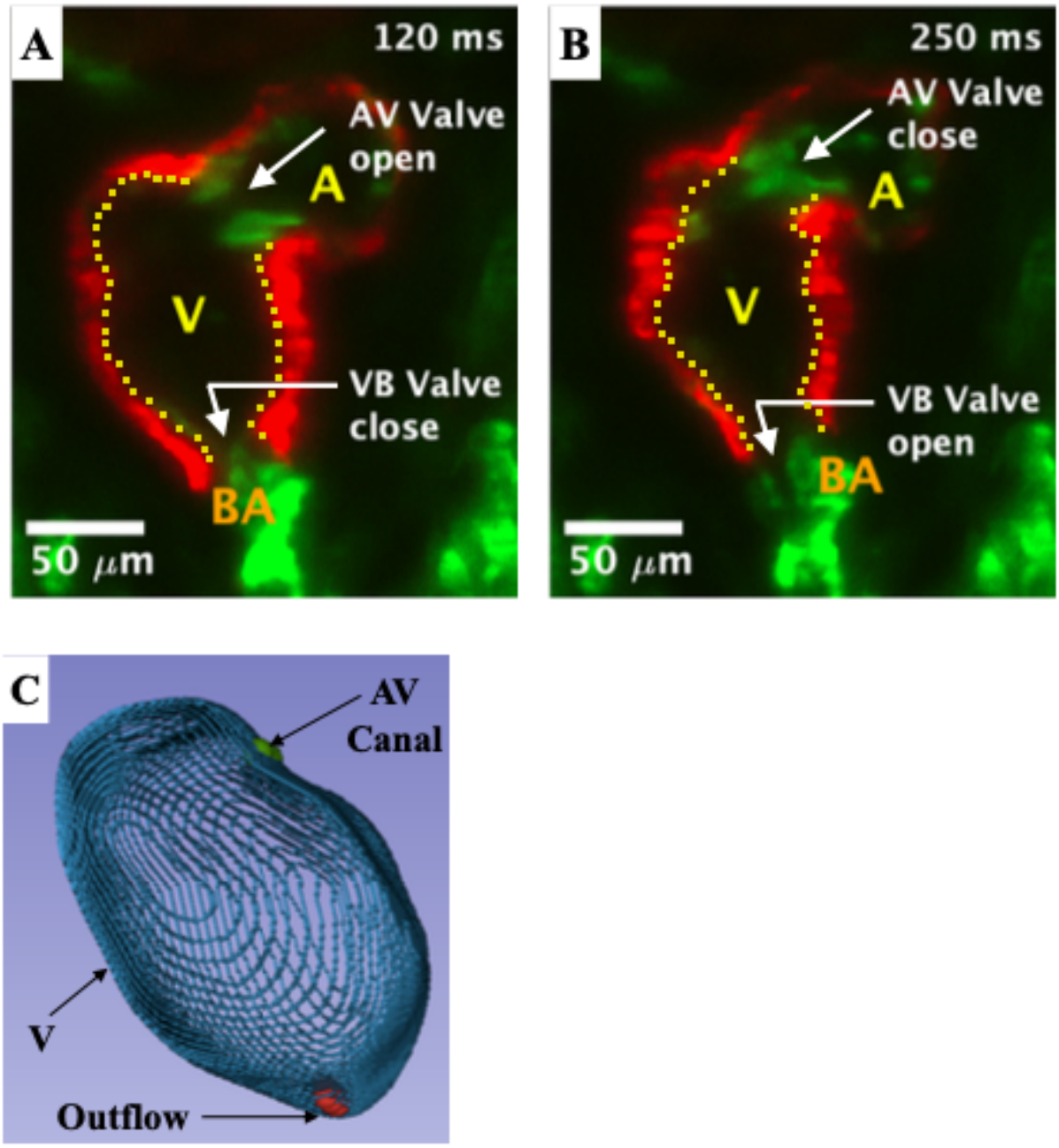

Figure 2: SPIM images of the developing Tg*(cmlc2:* mcherry*; fli1a:* gfp*)* zebrafish heart at 5 dpf, **A)** when AV valve fully open and VB valve closed during diastolic filling and **B)** when AV valve closed and VB valve fully open during ejection. Myocardium: Red; Endocardium: Green; Endocardial surfaces: Yellow dot lines; V: Ventricle; A: Atrium; BA: Bulbus arteriosus. **C)** Stack of endocardial surface contours based on which we calculated the ventricular volume at each of the time steps in a cardiac cycle. AV canal and outflow are shown in green and red color.

image. The instantaneous ventricular blood volume was obtained by summing the volume of the segmented stacks at the time step (Fig. 2C). The stroke volume of the beating heart was then calculated as the difference in the ventricular volume between end-diastole and end-systole states. Image analysis of the volume renderings was performed using Slicer 3D (www.slicer.org).

e. Calculation of blood flow rate into the ventricle and out of the ventricle to bulbus arteriosus (BA)

Knowing the moment-to-moment blood flow rate enables assessment of the effects of the instantaneous driving pressure from the contracting atrium, and the impedance of the ventricle in accommodating the blood influx during filling phase. Likewise, it enables examination of the effect of the instantaneous driving potential of the contracting ventricular myocardium and the impedance of the BA to accommodate the blood influx during ejection phase. In larger animals, blood flow rate can be measured by invasive (indicator dilution, radiolabel tracer washout) or non-invasive (Doppler ultrasound, contrast-enhanced ultrasonography) techniques. Because of the technical difficulty associated with the small size of the embryonic heart, we chose to use an indirect method to calculate the flow rate by taking the time derivative of the reconstructed ventricular volume: $\dot{Q} = \frac{d\,(vol)}{dt}$. For improved accuracy of the numerical differentiation at each time step, four neighboring time points were considered making up a five-point stencil.

f. Measurements of intra-ventricular pressure and that of BA

Since ventricular pressure measurements are destructive, separate organisms were used for individual ventricular pressure measurements (see Limitations section). Five separate

embryos per time point were anesthetized in 0.05% tricaine and placed in an agarose-filled petri dish with customized depressions in the agarose that helped to stabilize the embryo. Intra-ventricular pressure of zebrafish embryos was measured using a 900A servo null micro-pressure system (World Precision Instruments). Briefly, a glass electrode with a 2-5 μm tip diameter was pulled from borosilicate glass and filled with 1 M NaCl and the tip was inserted into the ventricle. Changes in ventricular pressure cause a change in electrical resistance at the tip of the micropipette which is offset by system generated compensatory positive or negative pressure. Known pressure pulses of 5-20 mmHg were used for calibration. Prior to each measurement, the system was recalibrated to zero, such that reported pressures are relative to the external fluid pressure just outside the heart. Data were sampled at 100 Hz and passed through an IIR Butterworth filter to eliminate high frequency noise with cut-off frequency determined from spectrum analysis. Recorded analog signals were filtered using a MATLAB (MathWorks) code. Pressure of the BA from embryos at 3, 4, 5 dpf group were measured by the same steps.

g. Open – close activities of AV and VB valve

We monitored the time courses AV and VB valve operation during cardiac cycles. The distance between the tips of the two AV valve leaflets was measured in each video image frame to track the valve opening and closure during the cardiac cycle. Embryos at 3 dpf did not yet have working valves and were thus excluded from these analyses. VB valve activity was measured starting at 4 dpf by calculating the change in area of the proximal region of the BA during the cardiac cycle. We considered the VB valve cycle to begin at the instant when the BA area began to increase (due to increasing volume at blood influx), and the VB valve closure process began the moment the BA area started to decrease. Image analysis was performed in MATLAB (MathWorks).

h. Synchronization of pressure and volume

Since pressure and volume cannot yet be measured simultaneously on a single fish, synchronization of data was needed (see Limitations section). We identified the end of isovolumic relaxation and the end of diastole as the respective time points at which the AV valve opened and closed. Similarly, the time points when the VB valve opened, and the VB valve closed respectively marked the start and the end of ejection. From the time course of intra-ventricular pressure, the end of isovolumic relaxation was identified as the time point at which the first derivative of ventricular pressure (*dP/dt)* reached zero following its minimum. Similarly, the time at which dP/dt started rising sharply toward its maximum value marked the end diastole. For synchronization of pressure and volume, these events in the cardiac cycle were matched in time from the volume-time curve and the pressure-time curve.

i. Hemodynamic parameters and the P-V loops

From the reconstructed ventricular volume time courses, we identified end diastolic volume (*EDV*), end systolic volume (*ESV*), stroke volume ($SV = EDV - ESV$), and heart rate (*HR*) to calculate cardiac output ($CO = SV\ x\ HR$), and ejection fraction ($EF = \frac{(EDV - ESV)}{EDV}$). From intra-ventricular pressure recordings, we identified peak systolic ventricular pressure (*PSVP*) and end diastolic ventricular pressure (*EDVP*). Synchronized pressure and volume were combined to generate the pressure-volume (*PV*) loops to allow the assessment of cardiac function. We further calculated stroke work from $SW = -\oint p \cdot d(vol)$, the work done by the ventricle in each of the cardiac cycles to enable blood circulation in the cardiovascular system, and the power generation was calculated as ($Power = SW\ x\ HR$). Additionally, we calculated total peripheral resistance (*TPR*) from $TPR = \frac{\overline{P_{BA}}}{CO} = \frac{1}{CO} \frac{\int_{t_1}^{t_2} P_{BA}(t)\, dt}{(t_2 - t_1)}$ with $P_{BA}(t)$ from BA

pressure recordings and t_1, t_2 denote the start and end time point of a cardiac cycle. Collectively, we examined the changes in these hemodynamic parameters and indices in zebrafish at 3, 4, 5 dpf that revealed functional changes in cardiac performance of the developing heart.

j. Statistical treatment

Results from intraventricular pressure (*PSVP, EDVP*, and *HR*) were expressed as mean ± SD of the measurement with n = 5 for each of 3, 4, 5 dpf time point. Results from reconstructed ventricular volume and derived parameters (*SV, EF, CO*) were expressed as mean $\pm$ SD with n = 3 for each time point. Results incorporating measurements from the BA (*TPR* and $\overline{P_{BA}}$) were expressed as means ± SD with n = 3 for each of three time points. Differences in each of *PSVP, EDVP, HR, SV, EF, CO, SW,* $\overline{P_{BA}}$ and *TPR* among time points were tested for with a one-way ANOVA followed by Tukey's multiple comparison test with $p < 0.05$ chosen for statistical significance.

Results

Representative time courses of intraventricular pressure measurements, reconstructed ventricular volume, blood flow rate, and regulating valve activities over two cardiac cycles are presented in Figs. 3, 4, 5 for embryonic zebrafish at 3, 4, and 5 dpf, respectively. In Figs. 4, 5, red vertical dash lines demarcate the four phases of the cardiac cycle: filling, isovolumic contraction, ejection, and isovolumic relaxation. No data is reported for valves at 3 dpf, since the remodeling of valve leaflets is yet to be complete at this point in development. In Fig. 3, ECG signals from 3 dpf zebrafish, adapted from Dhillon et al (*56*), was used to time scale our measurement data to the known corresponding physiological events in the heart. Key hemodynamic parameters extracted from these measurements are summarized with statistics in Table 1 and depicted in Fig. 6 A-D.

Intra-ventricular pressure: From embryos at 3 dpf, the *PSVP* were found to be at 7.52$\pm$0.77 mmHg. At 4, 5 dpf, their *PSVP* were found to increase to 10.64$\pm$1.64, to 11.26$\pm$1.31 mmHg respectively, accounting for 41% and 50% increases above that at 3 dpf. The changes in *EDVP* appeared to undergo a relatively small decrease from 1.36$\pm$0.52 to 1.28$\pm$0.31 to 1.32$\pm$0.19 mmHg, accounting for 6% and 3% decreases from that at 3 dpf. There were significant increases in *PSVP* between 3 and 4 dpf groups ($p = 0.0063$) and between 3 and 5 dpf groups ($p = 0.0017$), however, the change in *EDVP* was not significant.

From pressure recordings, we found the *HR* to be at 112.87±8.58, 130.02±5.04, and 139.16±6.70 beats/min for 3, 4, and 5 dpf embryos, respectively. Statistical testing indicated a statistically significant difference from 3 to 4 dpf ($p = 0.005$), and from 3 to 5 dpf ($p = 0.001$). While there was no significant difference when comparing the *HR* of 4 to 5 dpf ($p = 0.134$). All data of intraventricular pressure measurement are included in Supplementary Materials Fig. S2.

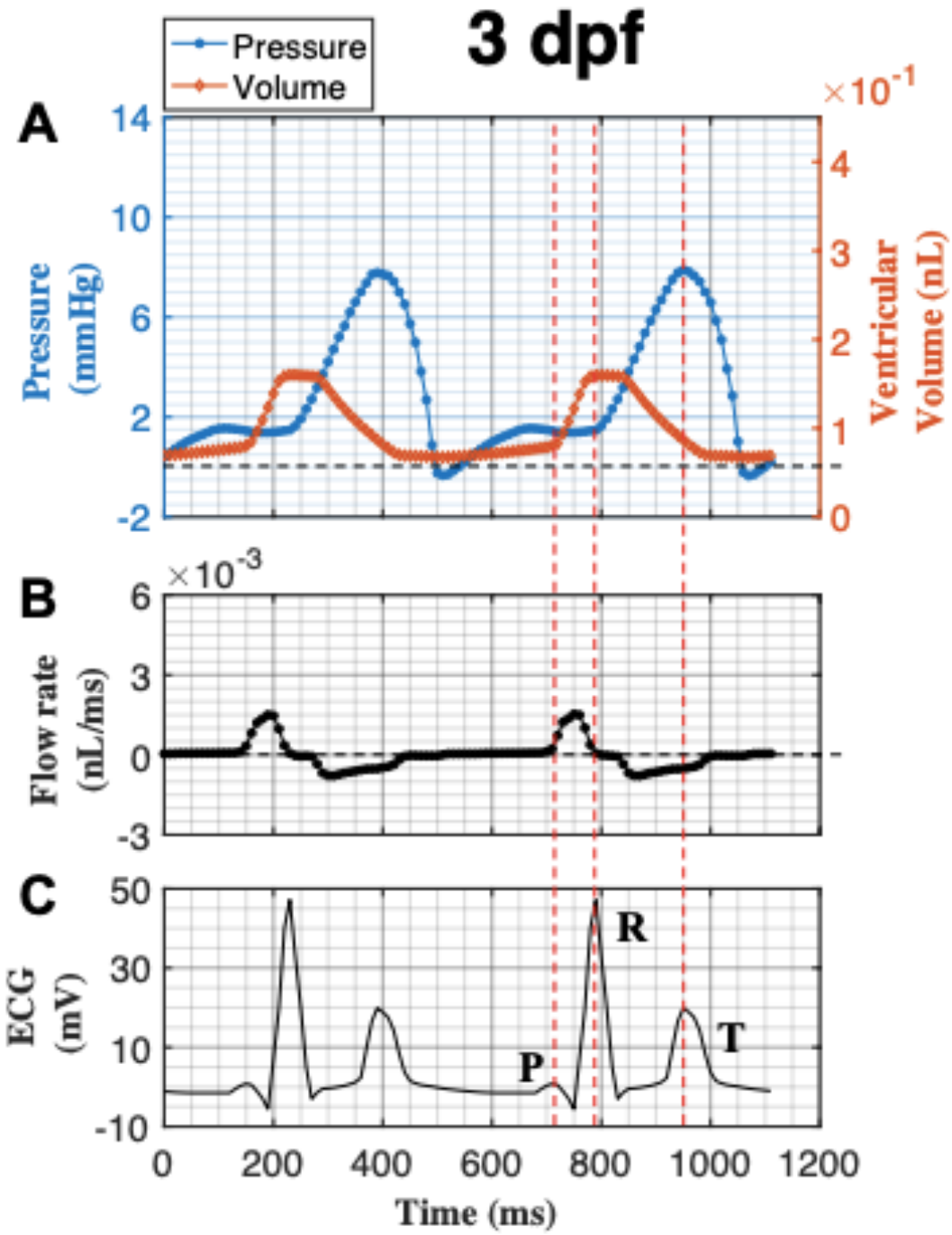

Figure 3: Representative time course of **A)** Intra-ventricular pressure and ventricular volume, **B)** Moment-to-moment blood flow rate calculated as the time derivative of the ventricular volume over two cycles from developing zebrafish heart at 3 dpf, **C)** ECG signals from zebrafish at 3 dpf with P, R, T waves marked, adapted from Dhillon et al (*56*) with time scaled to our measurements. Pressure and volume data are representative of measurements with n = 5 for pressure and n = 3 for volume, see Table-1 and Fig. 6 for statistical details.

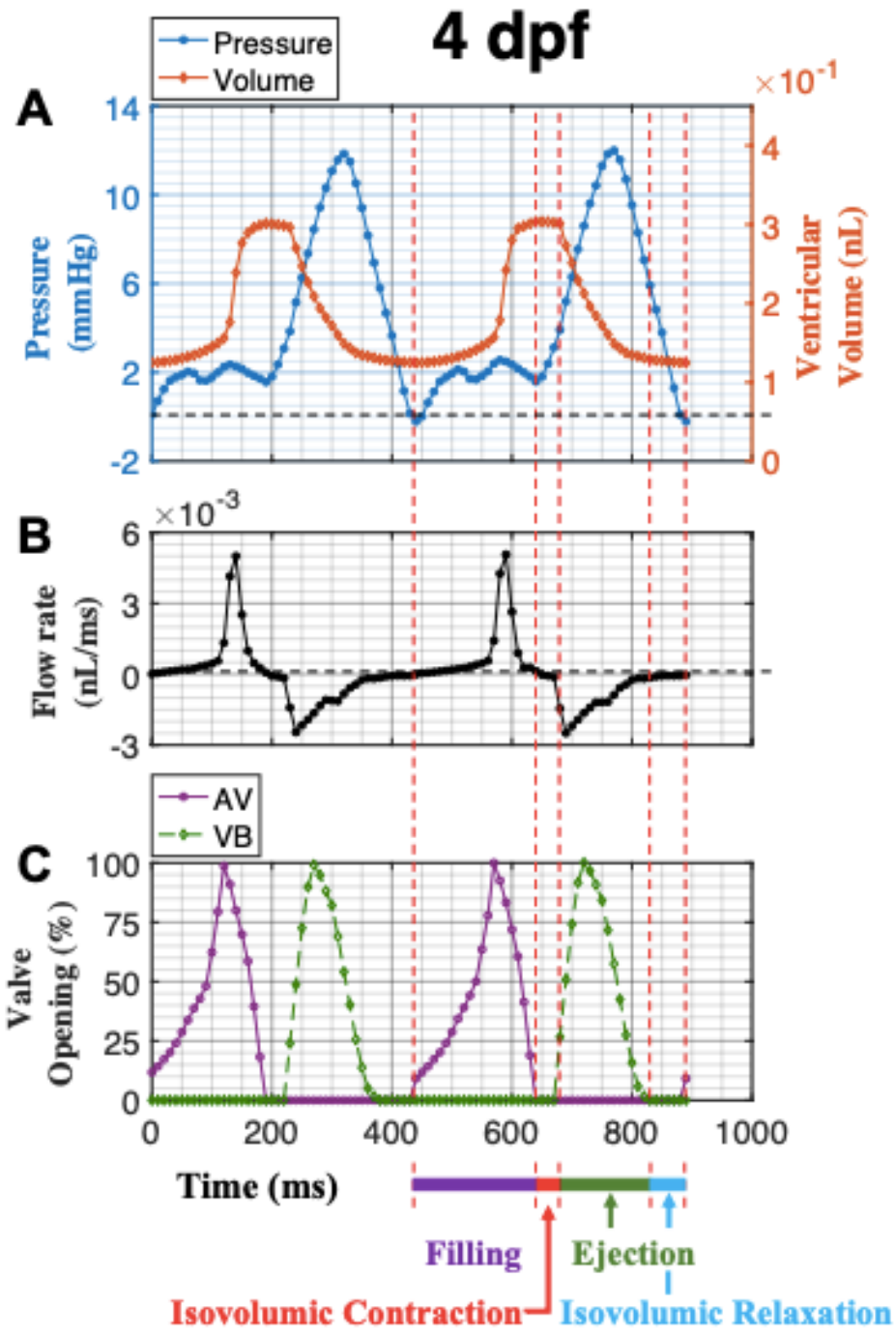

Figure 4: Representative time course of **A)** Intra-ventricular pressure and ventricular volume, **B)** Moment-to-moment blood flow rate calculated as the time derivative of the ventricular volume, and **C)** Valve activities (Normalized) over two cycles from developing zebrafish heart at 4 dpf. Four phases in the cardiac cycle can be identified as marked. Pressure and volume data are representative of measurements with n = 5 for pressure and n = 3 for volume, see Table-1 and Fig. 6 for statistical details.

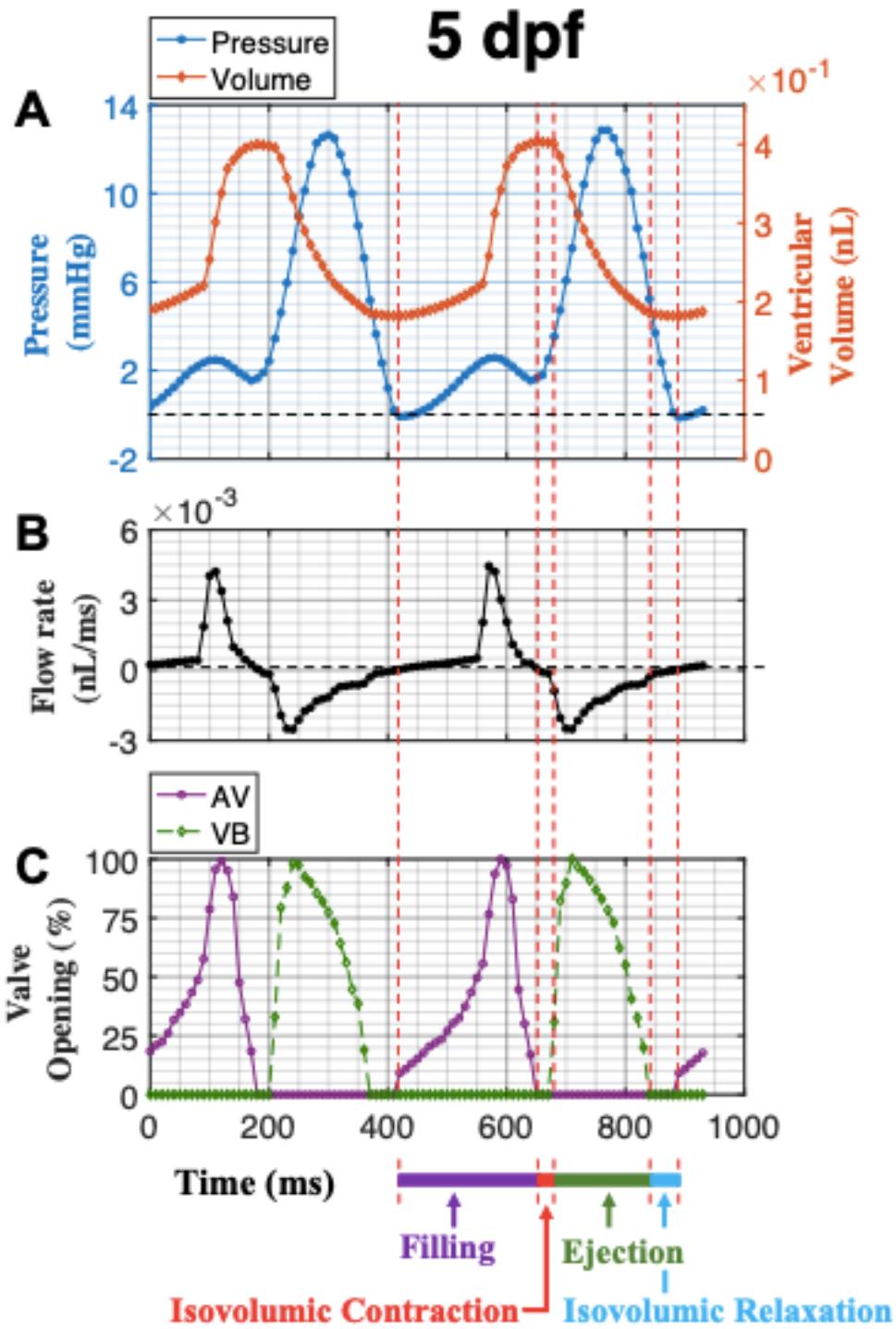

Figure 5: Representative time course of **A)** Intra-ventricular pressure and ventricular volume, **B**) Moment-to-moment blood flow rate calculated as the time derivative of the ventricular volume, and **C)** Valve activities (Normalized) over two cycles from developing zebrafish heart at 5 dpf. Four phases in the cardiac cycle can be identified as marked. Pressure and volume data are representative of measurements with n = 5 for pressure and n = 3 for volume, see Table-1 and Fig. 6 for statistical details.

Ventricular volumes, Stroke Volume, Cardiac Output, and Ejection Fraction: The *EDV* were found to be 0.18±0.02 nL from 3 dpf embryos. The *EDV* values were found to increase to 0.33±0.02 and 0.40±0.03 nL from embryos at 4 and 5 dpf, respectively. Their corresponding values in *ESV* were found to be 0.08±0.01 nL from embryo at 3 dpf, which increased to 0.14±0.01 and 0.18±0.01 nL from embryos at 4 and 5 dpf, accounting for 73% and 134% increases, respectively.

From 3 dpf embryos the *SV* was 0.10±0.01 nL. From 4 and 5 dpf groups their *SV* were found to increase to 0.19±0.01 and 0.21±0.02 nL, which account for 96% and 120% increases from that at 3 dpf. Using HR measurements, the *CO* was calculated at 10.5±0.6 nL/min at 3 dpf, which increased to 25.3±1.7 at 4 dpf and then to 29.1±2.18 nL/min at 5 dpf. *CO* at the latter two time points account for 142% and 178% increases, respectively, compared to 3 dpf values. Calculated *EF* were found to bear no significant changes, being 55.3±2.4%, 58.3±0.9% and 53.6±0.5% from embryos at 3, 4 and 5 dpf, respectively.

Calculated blood flow rates: During filling phase, from 3 dpf embryo we noted very little blood flow from atrium to ventricle until the onset of atrium contraction and reached a peak of 1.5 x 10^{-3} nL/ms. From 4 and 5 dpf embryos, the flow rates were also slow but reached a peak at 5.1 and 4.5 x 10^{-3} nL/ms, respectively, at atrial contraction. Hence there were increases in the peak values of inflow rate by 200-240 % from 3 to 4, 5 dpf. During ejection phase, we found a peak outflow of -0.8 x 10^{-3} nL/ms from 3 dpf embryos. From 4 and 5 dpf embryos, the peaks in outflow rates were found to be at -2.5 and -2.5 x 10^{-3} nL/ms, respectively, at ventricular contraction. That is, the peaks in outflow rates were found to increase by 213% from 3 to 4, 5 dpf. From the plots of blood flow rates, we noted that in both filling and ejection phases, it took

Table 1

Hemodynamic parameters of developing Tg*(cmlc2:* mcherry*; fli1a:* gfp*)* zebrafish at 3, 4 and 5 dpf. (% in parenthesis indicates % changes from that of 3 dpf)

Parameters	**Units**	**3 dpf**	**4 dpf**	**5 dpf**
PSVP (Peak Systolic Ventricular Pressure) *n = 5 for each dpf group*	mmHg	7.52±0.77	10.64±1.64 (↑ 41%)	11.26±1.31 (↑ 50%)
EDVP (End Diastolic Ventricular Pressure) *n = 5 for each dpf group*	mmHg	1.36±0.52	1.28±0.31 (↓ 6%)	1.32±0.19 (↓ 3%)
EDV (End Diastolic Volume) *n = 3 for each dpf group*	nL	0.18±0.02	0.33±0.02 (↑ 86%)	0.40±0.03 (↑ 126%)
ESV (End Systolic Volume) *n=3 for each dpf group*	nL	0.08±0.01	0.14±0.01 (↑ 73%)	0.18±0.01 (↑ 134%)
SV (Stroke Volume) *n=3 for each dpf group*	nL	0.10±0.01	0.19±0.01 (↑ 96%)	0.21±0.02 (↑ 120%)
HR (Heart Rate) *n = 5 for each dpf group*	beats/min	112.87±8.58	130.02±5.04 (↑ 15%)	139.16±6.70 (↑ 23%)
CO (Cardiac Output) *n=3 for each dpf group*	nL/min	10.5±0.6	25.3±1.7 (↑ 142%)	29.1±2.18 (↑ 178%)
EF (Ejection Fraction) *n=3 for each dpf group*	%	55.3±2.4	58.3±0.9 (↑ 5%)	53.6±0.5 (↓ 3%)
SW (Stroke Work) *n=3 for each dpf group*	nJ	0.062±0.008	0.158±0.020 (↑ 154%)	0.200±0.023 (↑ 222%)
Power *n=3 for each dpf group*	nano Watts	0.11±0.01	0.35±0.04 (↑ 218%)	0.46±0.06 (↑ 315%)
$\overline{P_{BA}}$ (Mean BA pressure) *n = 3 for each dpf group*	mmHg	4.900±0.339	9.865±0.646 (↑101%)	9.944±0.045 (↑ 103%)
TPR (Total Peripheral Resistance) *n = 3 for each dpf group*	mmHg.min/nL	0.504±0.035	0.423±0.028 (↓16%)	0.357 ±0.002 (↓29%)

Unit conversion: 1 mmHg · nL = 0.133 nJ

1 nL = 10^6 μm^3

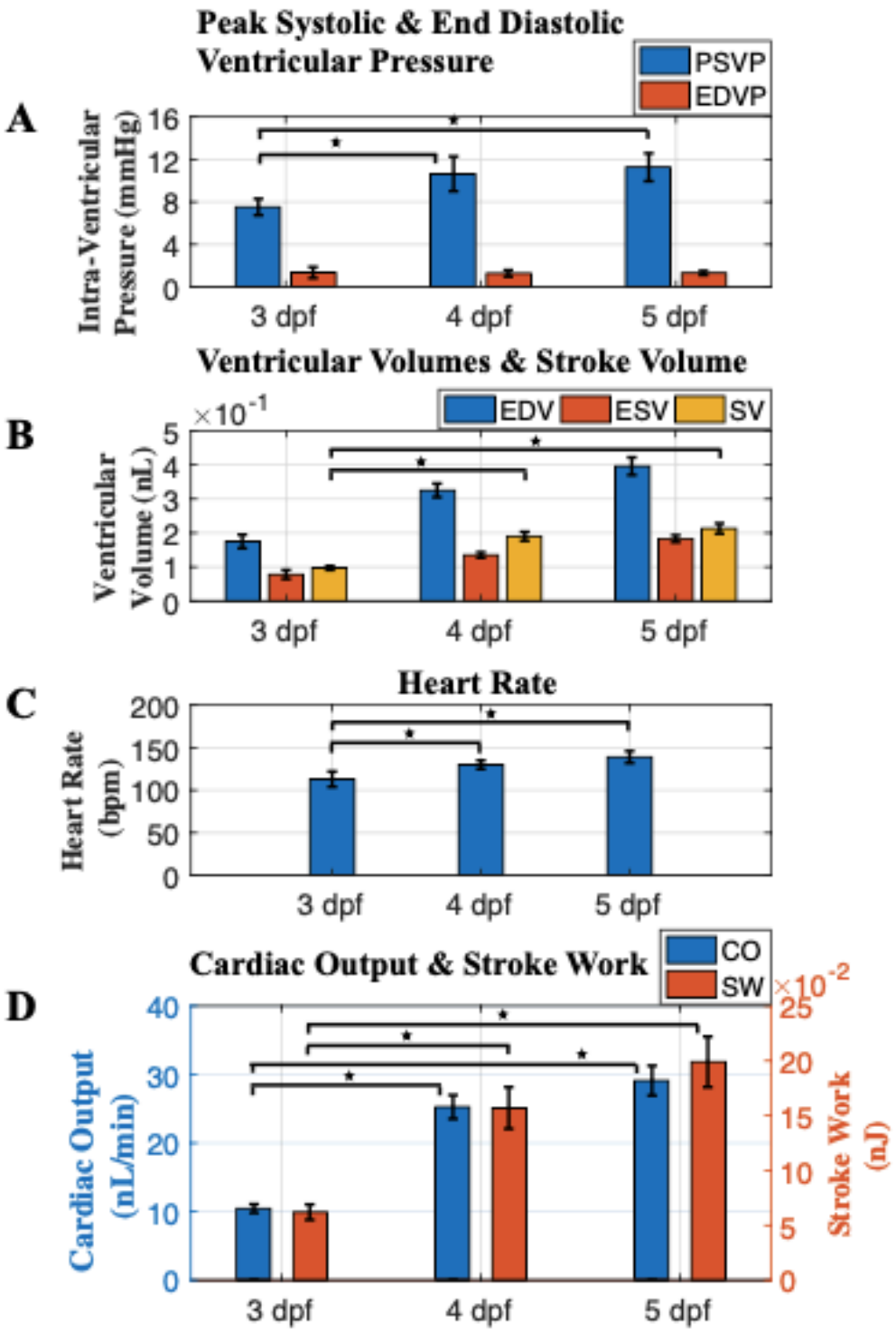

Figure 6: Comparison of **A)** Intra-ventricular pressure (n=5), **B)** Ventricular volumes (n=3), **C)** Heart Rates (n=5), and **D)** Cardiac Output and Stroke Work (n=3), among developing zebrafish heart at each of 3, 4, and 5 dpf. *PSVP*: Peak Systolic Ventricular Pressure; *EDVP*: End Diastolic Ventricular Pressure; *EDV*: End diastolic volume; *ESV*: End systolic volume; *SV*: Stroke volume;

CO: Cardiac Output; *SW*: Stroke Work. In **A)-D)**, statistically significant differences are denoted by *.

longer time duration for the embryonic zebrafish at 3 dpf than that at 4 and 5 dpf, being ~280 ms and 180 ms from 3 dpf, as summarized in Table 2.

Table 2

Time duration of filling and ejection phases from embryonic zebrafish at 3, 4, 5 dpf. Start and end time points refer to the results of Figs. 3B, 4B and 5 B.

dpf	Filling			Ejection		
	Start (ms)	End (ms)	Duration (ms)	Start (ms)	End (ms)	Duration (ms)
3	510	790	**280**	840	1020	**180**
4	440	640	200	680	830	150
5	420	650	230	680	840	160

Pressure-Volume loops: Representative pressure-volume loops constructed from synchronized intra-ventricular pressure measurements and reconstructed ventricular volume are presented in Fig. 7 for embryonic zebrafish at 3, 4 and 5 dpf, respectively. The *SW*, the mechanical work performed by the myocardium to pump the blood, was found to be 0.062$\pm$0.008 nJ from embryo at 3 dpf, which increased to 0.158$\pm$0.020 and 0.200$\pm$0.023 nJ at 4 and 5 dpf, accounting for increases of 154% and 222%, respectively, from that at 3 dpf. It is noted that from 4 to 5 dpf, the increase in *SW* was 26%. The power generation of the developing embryonic heart was calculated to be 0.11$\pm$0.01 nano-Watts at 3 dpf, became 0.35$\pm$0.04 and 0.46$\pm$0.06 nano-Watts at 4 and 5 dpf, respectively, accounting for a 218% and 315% increase over that at 3 dpf.

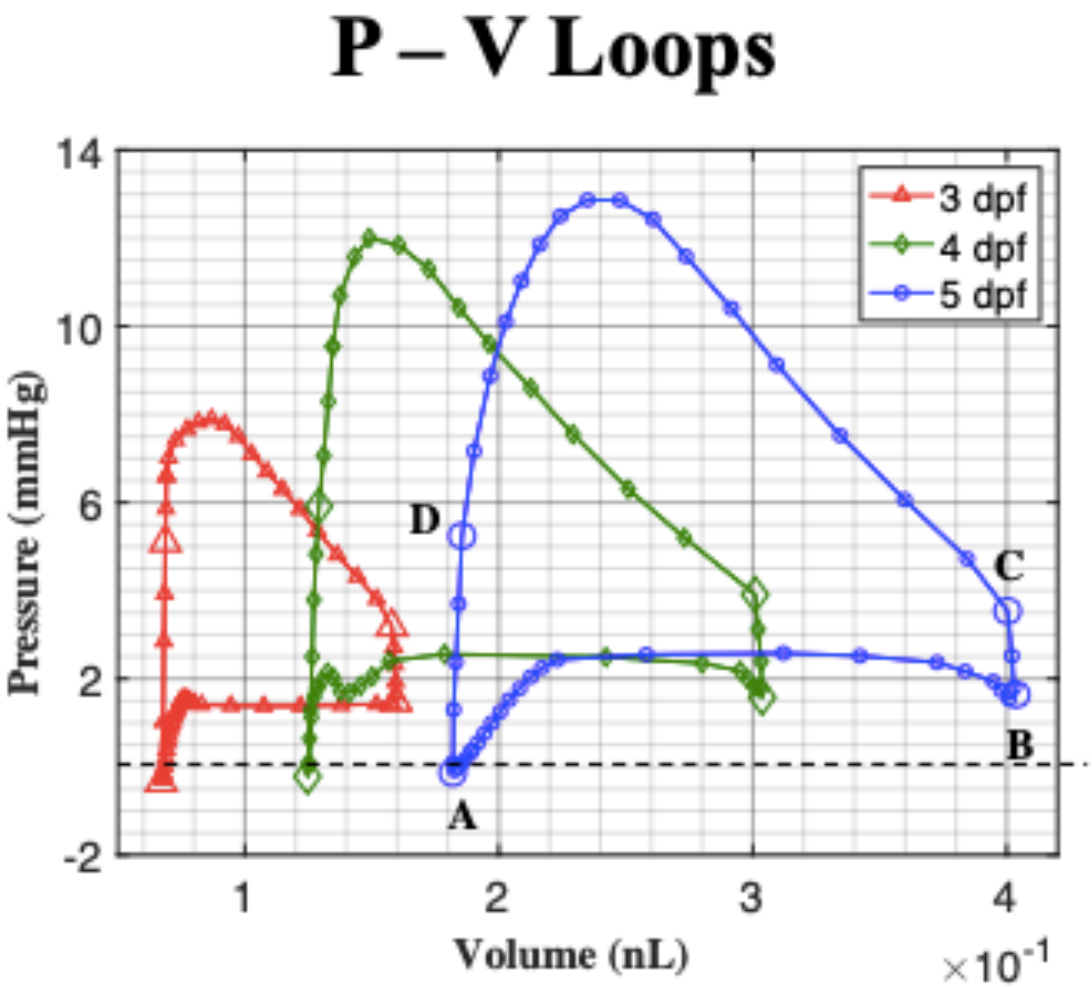

Figure 7: Representative pressure–volume (PV) loops of the developing zebrafish heart at 3, 4, and 5 dpf. Open markers A, B, C, D designate time steps with valve activities where A: AV valve open; B: AV valve close; C: VB valve open; D: VB valve close. Four phases of a cardiac cycle: Segment AB – ventricular filling; Segment BC - isovolumic contraction; Segment CD - ventricular ejection; and Segment DA - isovolumic relaxation;

BA pressure and TPR: To evaluate *TPR,* we calculated the mean of BA pressure $\overline{P_{BA}}$ from pressure-time recordings over a cardiac cycle in three fish per time point. $\overline{P_{BA}}$ was found to be 4.900±0.339 mmHg at 3 dpf, which increased to 9.865±0.646 and 9.944±0.045 mmHg for the 4 and 5 dpf groups, respectively. These changes correspond to 101% and 103% increases compared to 3 dpf. Statistically significant differences were noted from 3 to 4 dpf (p = 0.001)

and 3 to 5 dpf (p = 0.001), but not from 4 to 5 dpf (p = 0.9). Using the mean of $\overline{P_{BA}}$ values, a decreasing trend in *TPR* was established. At 3 dpf, *TPR* was found to be 0.504±0.035 (mmHg. min/nL). This value then dropped to 0.423±0.028 and 0.357±0.002 (mmHg. min/nL) in 4 and 5 dpf embryos, respectively, indicating a decrease of 16% and 29% respectively compared to 3 dpf. Statistically significant differences were noted from 3 to 4 dpf (p = 0.021), 3 to 5 (p = 0.001), and 4 to 5 dpf (p = 0.043). All data of BA pressure measurement are included in Supplementary Materials Fig. S3.

Discussion

a. Significance

During development, the heart transforms from a linear peristaltic tube into a multi-chambered pulsatile pump (*5*). Developmental changes in hemodynamic parameters have been reported in chick (*32-35*), in mouse (*57*) and in zebrafish (*36-38, 58*). Few studies have systematically assessed the changes in cardiac performance of the developing zebrafish, and to our knowledge, no studies have integrated multiple physiological signal detection techniques to build a pressure-volume (PV) loop model of the developing zebrafish heart. In this work, we quantified and compared the mechanical performance of the developing zebrafish heart at 3, 4 and 5 dpf through an array of hemodynamic parameters. We constructed the resultant PV loops of the embryonic zebrafish heart by combining the direct intra-ventricular pressure measurements with reconstructed ventricular volumes, which enabled measurement of the changing mechanical performance of the developing zebrafish heart.

Cardiac disease model organisms often retain phenotypes with altered cardiac morphology and compromised cardiovascular physiology. Genetic manipulation may result in gene variants with a phenotype that cannot be obviously morphologically defined. An adverse physiological phenotype in a model organism could be just as insidious as in humans, where a physical examination may be required to diagnose some cardiovascular pathology. Thus, there is a need for rigorous quantification methods of physiological function in intact small animal models to relate physiological data to other vertebrate models and human health.

b. Improving Hemodynamic Performance of the Developing Heart

It has been reported that cardiac physiology exhibits rapid changes during early development, with a rapidly increasing intra-ventricular pressure and *CO* to meet the demands of

the growing embryos (*3*). Our results show that in zebrafish, *HR* increased by approximately 15% from 3 to 4 dpf, and by 23% from 3 to 5 dpf. On the other hand, SV nearly doubled between 3 and 4 dpf, with further increase up to 120% at 5 dpf. We determined a resultant 142% increase in *CO* from 3 to 4 dpf, which became 178% at 5 from 3 dpf. Indeed, the increase in *CO* at 4 and 5 dpf was due mainly to the increase in SV. This is not surprising, since 3-4 dpf zebrafish largely rely on diffusion for oxygenation. Over the next days, inhibitory cholinergic tone develops, slowing the resting heart rate, and pumping efficiency increases as the valves and cardiac tissues mature. Our calculated *SV* and *CO* are systematically lower than values previously reported for zebrafish (*37*) which is unsurprising given that these studies relied on an empirical formula derived from brightfield microscopy image capture (*59*).

In both chick and mouse ventricles, *PSVP* increases faster than *EDVP* over early developmental stages (*32, 57*). Two studies (*36, 58*) have reported intra-ventricular pressure measurement for zebrafish embryos, but to our knowledge there is no published data which use a calculated *SW* to assess the mechanical pump performance of the zebrafish ventricle. Our calculations showed that the *SW* for the zebrafish heart on 4 dpf was 2.5 times that of the *SW* in 3 dpf hearts. At 5 dpf, the *SW* increased to 3.2x that of 3 dpf. It is therefore interesting to note the power generation of the developing zebrafish heart as compared to the human heart. Here, 3-5 dpf zebrafish hearts were found to generate between 0.1 ~ 0.46 nano-Watts of power, whereas that of a typical human adult generates closer to 1.4 watts (*60*).

Our analysis of the evolving mechanical function of the developing zebrafish heart indicates that significant improvement in cardiac performance occurs between 3 and 4 dpf. This is not surprising, since we see the valves becoming effective near 4 dpf. Comparatively smaller changes were detected between 4 and 5 dpf. The embryonic zebrafish heart generated higher

pressure throughout contributing to the increasing higher *CO* of the rapidly growing embryo. Collectively, our results suggest that the zebrafish heart is a well-developed functional organ near 5 dpf, in time for upcoming increased demand on the gills for respiration and osmoregulation (*61*).

TPR values were found to decrease in embryonic zebrafish from 3 to 4 to 5 dpf groups, corresponding to a 16% decrease from 3 to 4 dpf, and 29% decrease from 3 to 5 dpf. Our results suggest the combined effects of a higher *PSVP, SV, CO* and *SW* lead to a progressively more powerful and efficient working heart to achieve the noted improvement in functional capacity. Through the growth, there are more cardiomyocytes and ventricular mass engaged in the pumping effort of the heart to deliver oxygen and nutrients to the growing body mass of the zebrafish. The decrease in TPR from 3-5 dpf is indicative of the increasing complexity of the perfusion pattern in the developing zebrafish, a general pattern seen in chick and anuran embryos, and likely a vertebrate paradigm for hemodynamic development (*62*).

c. Examining the PV loop: negative intra-ventricular pressure

Our measurements showed intra-ventricular pressure dropped to negative values at the end of isovolumic relaxation (Fig. S2). We attributed this to the rapid isovolumic relaxation of the ventricular myocardium, along with a corresponding rapid ventricular pressure drop (high dp/dt). A slight negative intra-ventricular pressure can help to draw blood into the ventricle for 3 dpf embryos, when valve cushions are not yet fully functional valves. For embryos at 4, 5 dpf, the negative intra-ventricular pressure likely helps to open the AV valve. Blood influx immediately decelerates in the ventricle, converting its kinetic energy into potential energy, as intra-ventricular pressure increases. This transient event sets the stage for the filling phase.

d. A twostep filling phase, ECG signals and time of atrial contraction

Ventricular filling consists of two steps. In step 1, driven by the atrium-ventricular pressure gradients, the blood influx is relatively slow. The onset of step 2 is evidenced by both the rapid increase in flow rate, attributed to both atrial contraction (occurring just after the P wave in the ECG (Fig 3C)), and the rapid opening of the AV valve leaflets in embryonic zebrafish at 4, 5 dpf. We summarized the time duration for each of the two-step filling and the ejection phases in Table 3 with their respective contribution in volume and in percentage of the total volume increase through the filling phase. These data reveal that ventricular filling and ejection tasks take longer for embryonic zebrafish at 3 dpf compared to later stages, likely due to less developed cardiac tissue, valves and innervation.

Ventricular peak filling rate was almost 2 times the peak ejection rate. This relative increase was due in part to the relatively low ventricular pressure and hence low impedance throughout most of the filling phase but is primarily due to vigorous atrial contraction. Two-step filling has been previously reported for zebrafish embryos at 6.2 dpf (*63*) and adult zebrafish (*64*) with the majority of filling taking place during atrial systole.

Table 3

Two steps ventricular filling and their respective contribution, both in the unit of nL and % of the total volume increase, from embryonic zebrafish at 3, 4, and 5 dpf. Also listed are the corresponding time duration and ventricular volume decrease during the ejection phase.

	Filling						**Ejection**	
	Step 1			Step 2				
dpf	Δt (ms)	Volume increase		Δt (ms)	Volume increase		Δt (ms)	Volume decrease (nL)
		(nL)	%		(nL)	%		
3	210	0.015	16	70	0.077	84	180	0.091
4	130	0.032	18	70	0.147	82	150	0.175
5	140	0.041	18	90	0.181	82	160	0.22

e. Estimation of ventricular volume using 2D images with axisymmetric assumption

Other investigators have estimated ventricular volumes using 2D image sequences of the mid plane of the heart with an axisymmetric assumption(*37, 38, 59*). To assess the corresponding level of approximation in ventricular volume with the 2D approach, we manually segmented 2D image sequences of the mid-plane of embryonic zebrafish heart to delineate the endocardial boundary of the ventricle. From its enclosed area, we found the effective radius of the equivalent circle with the same surface area. At each time step, the ventricular volume was calculated from the corresponding equivalent circle based on axisymmetric spherical assumption (Fig. 8A). We found that the use of 2D images with axisymmetric assumption can lead to an underestimation

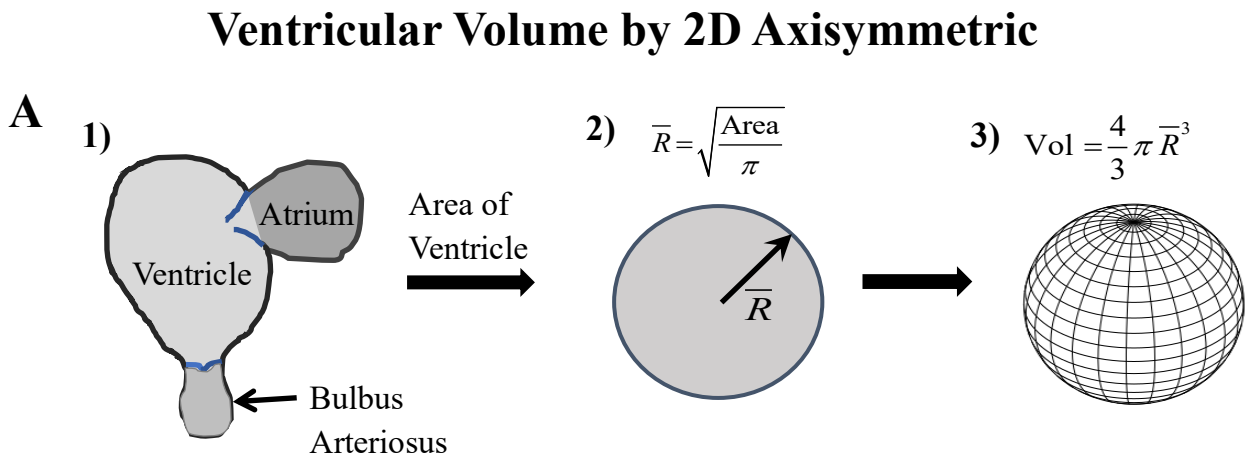

Fig. 8A

Figure 8: A) Method of ventricular volume measurement using 2D images of the heart. 1) By manual segmentation, endocardial perimeter of the ventricle was identified, 2) Equivalent radius was calculated from the ventricular area, 3) Ventricular volume was estimated using axisymmetric sphere assumption. **B)** Comparison between ventricular volume of developing zebrafish heart at 3, 4 and 5 dpf, estimated from 3D images and from 2D images using axisymmetric assumption.

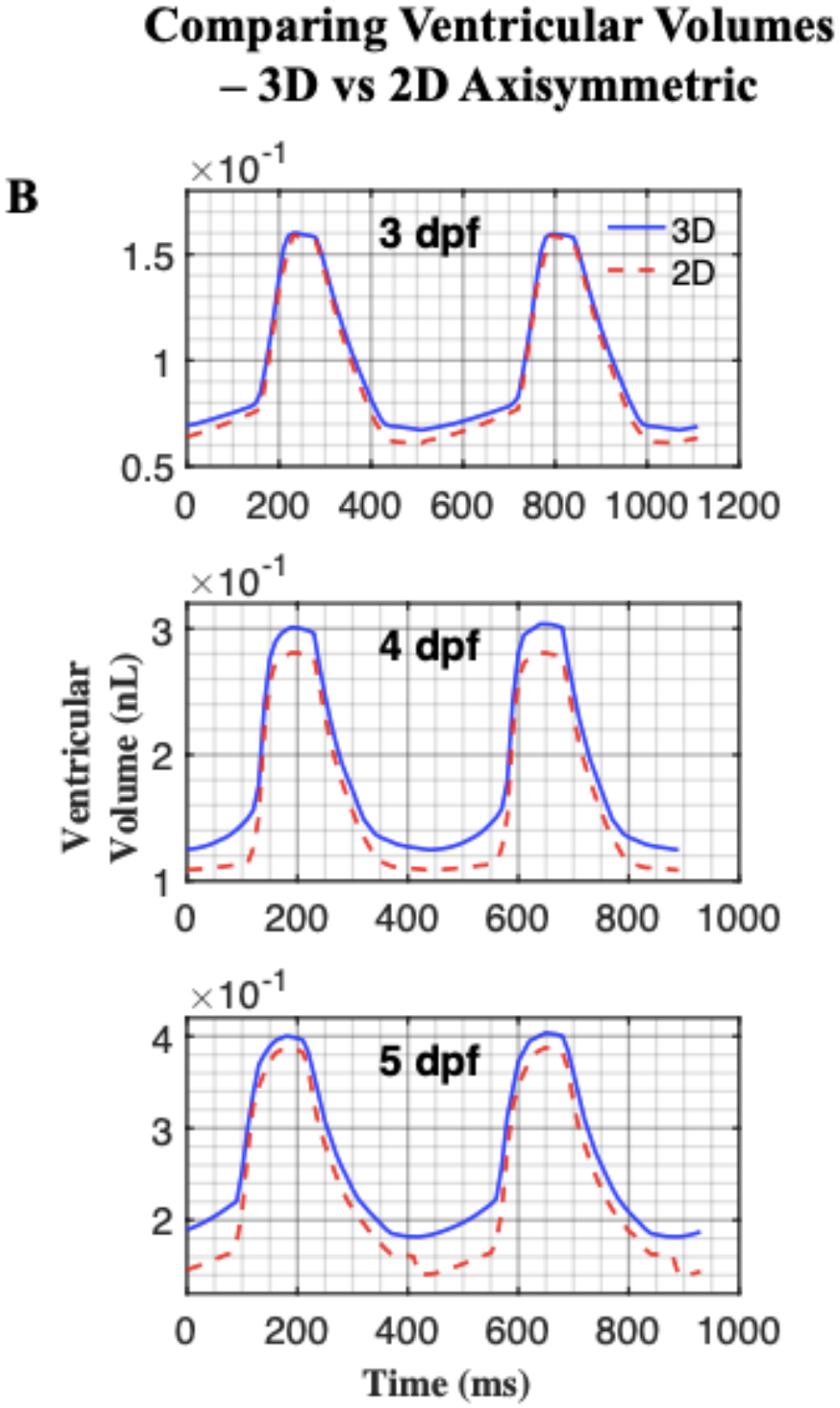
Comparing Ventricular Volumes
– 3D vs 2D Axisymmetric
B
×10^-1
3 dpf
3D
2D
1.5
1
0.5
0
200
400
600
800
1000
1200
×10^-1
4 dpf
Ventricular Volume (nL)
3
2
1
0
200
400
600
800
1000
×10^-1
5 dpf
4
3
2
0
200
400
600
800
1000
Time (ms)

Fig. 8B

artifact when calculating cardiac output. Indeed, for the 3 dpf, zebrafish, the 2D approach was associated with a 10% underestimation of the 3D calculated volume. Surprisingly, the 2D method underestimated up to 23% less volume for embryos at 4 and 5 dpf (Fig. 8B). Not surprisingly, this significant underestimation of ventricular volume occurred during the early part of ventricular filling, when the ventricle assumed a narrowed shape at the end of systole.

Limitations

Separate animals were used for pressure measurements and volume calculations. As such, PV loop data from cardiac cycles represent paired ventricular pressure and volume from separate embryos at each time point following the synchronization steps described in Methods. It was not possible to use the same animal for both pressure and volume measurement because direct measurement of ventricular pressure is destructive, rendering the organism unusable for additional experiments. Otherwise, early attempts to complete imaging prior to pressure recordings proved unfeasible due to the time required for acquiring micro-pressure measurements and the prolonged effects of anesthesia to capture both measurements from one fish (>2 h). Further, though the addition of PTU to suppress pigmentation is generally accepted as being unharmful, we do note that PTU blocks the conversion of thyroid hormone, the master regulator of vertebrate metamorphosis. Though PTU addition is fairly common in such studies and the developmental progression here appears to proceed normally, it is not possible that PTU causes a hidden, yet deleterious effect on the developmental program (*65, 66*). An additional limitation to this study is the use of transgenic organisms. Here, we assumed that the gene variants in our experimental organisms had no effect on the physiological phenotype. Ironically, this study was initiated to develop new techniques to detect fine scale physiological changes

using direct pressure measures combined with advanced imaging modality (SPIM). As such, these limitations point out knowledge gaps in the acquisition of real time physiological data from small model organisms and the need to develop experimental tools to detect unseen, yet potentially insidious physiological effects. With the emergence of the zebrafish as a premier biomedical model, it is prudent to consider the need for higher throughput, non-destructive and high-resolution measures of animal physiology.

Conclusions

We reported the development of hemodynamic parameters of the embryonic zebrafish ventricle at 3, 4 and 5 dpf. At each time point, dynamic measurements of ventricular pressure and volume allowed a 4D re-construction of changing pressure and volume during the cardiac cycle. This enabled, for the first time, the creation of a pressure-volume loop of the ventricle of the developing zebrafish. Improving mechanical performance of the heart as a pump was described in terms of increasing degree of stroke work performed by the ventricular myocardium. Our results revealed significant increases in peak systolic pressure, stroke volume, cardiac output, stroke work. Further, a concomitant decrease in *TPR* from 3 to 5 dpf tracked the increasing mechanical performance, indicating the development of an increasingly complex vascular pattern. These changes reflect both the very early stages of heart development at 3 dpf prior to heart valve formation, then later stages of the developing embryo heart at 4 and 5 dpf. Together these data illustrate increasing pumping efficiency in the developing zebrafish heart, to meet environmental challenges and further highlight the utility of capturing reliable physiological data at early developmental time points. Such physiological measures are increasingly important for the future of phenomics efforts, which seek to match complex phenotypes with underlying variations in genotype.

Supplementary Figures

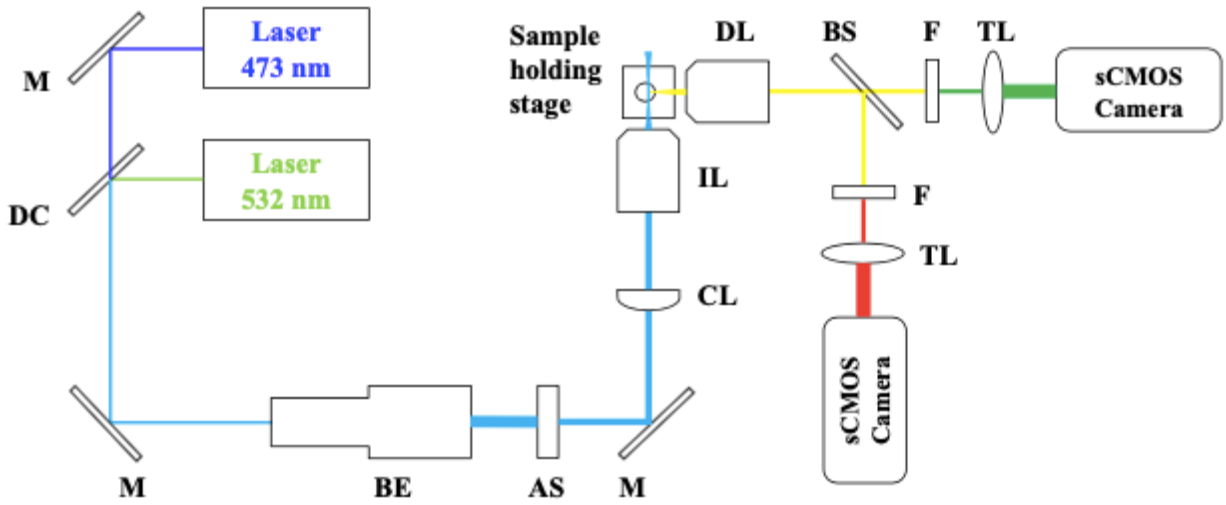

Fig. S1: Schematic of SPIM setup where a cylindrical lens converts the laser beam to a thin light sheet that illuminates a thin slice of the sample and this slice is captured by a high-speed camera. M: Mirror, DC: Dichroic Mirror, BE: Beam Expander, AS: Adjustable Slit, CL: Cylindrical Lens, IL: Illumination Lens, DL: Detection Lens, BS: Beam Splitter, F: Filter, TL: Tube Lens.

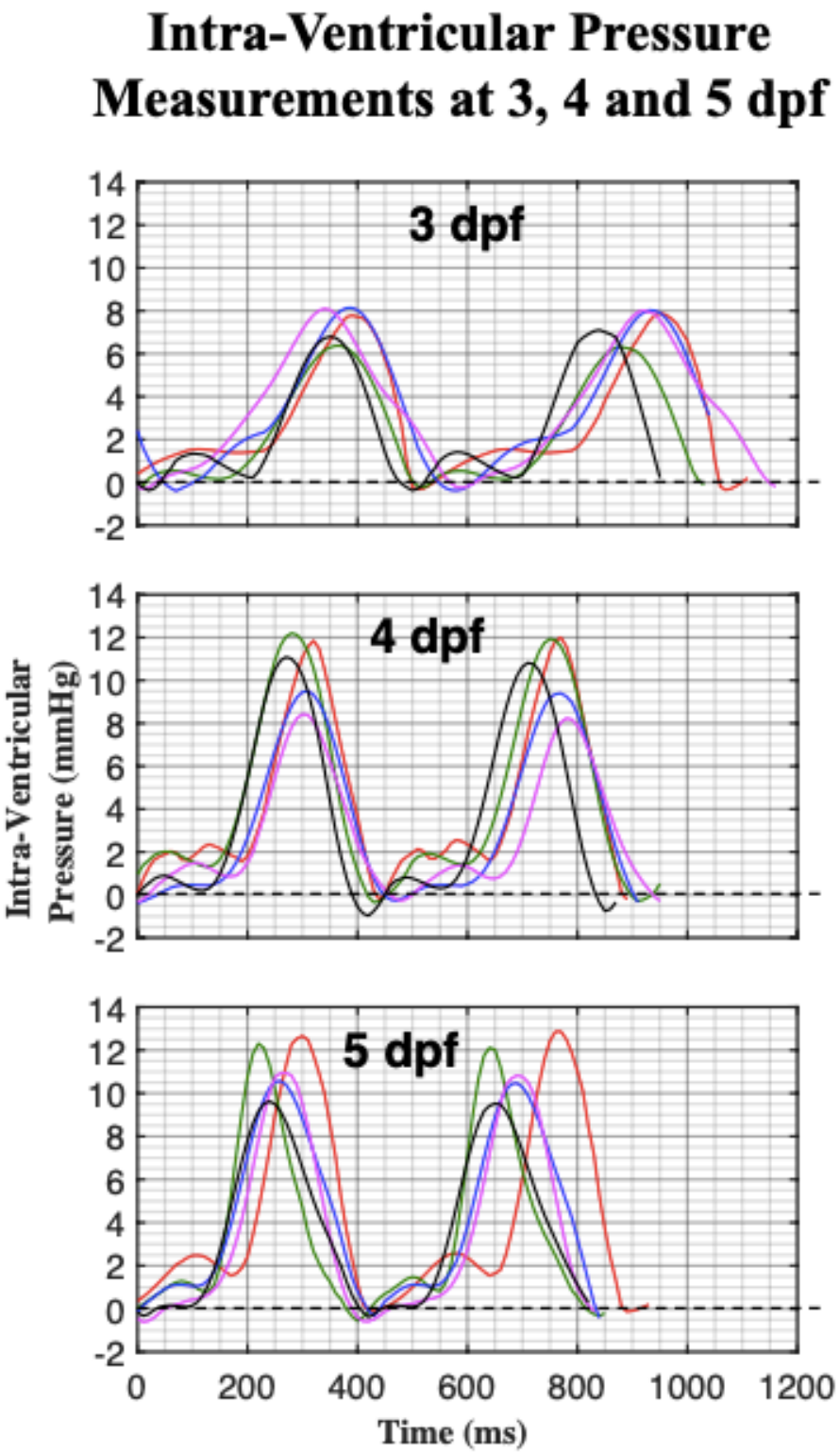

Fig. S2: Intra-ventricular pressure measurements from embryonic zebrafish of 3, 4, and 5 dpf group, with n = 5 for each group. Intra-ventricular pressure consistently dropped to negative values before bouncing back at the end of isovolumic relaxation for all cases.

Bulbus Arteriosus Pressure Measurements at 3, 4 and 5 dpf

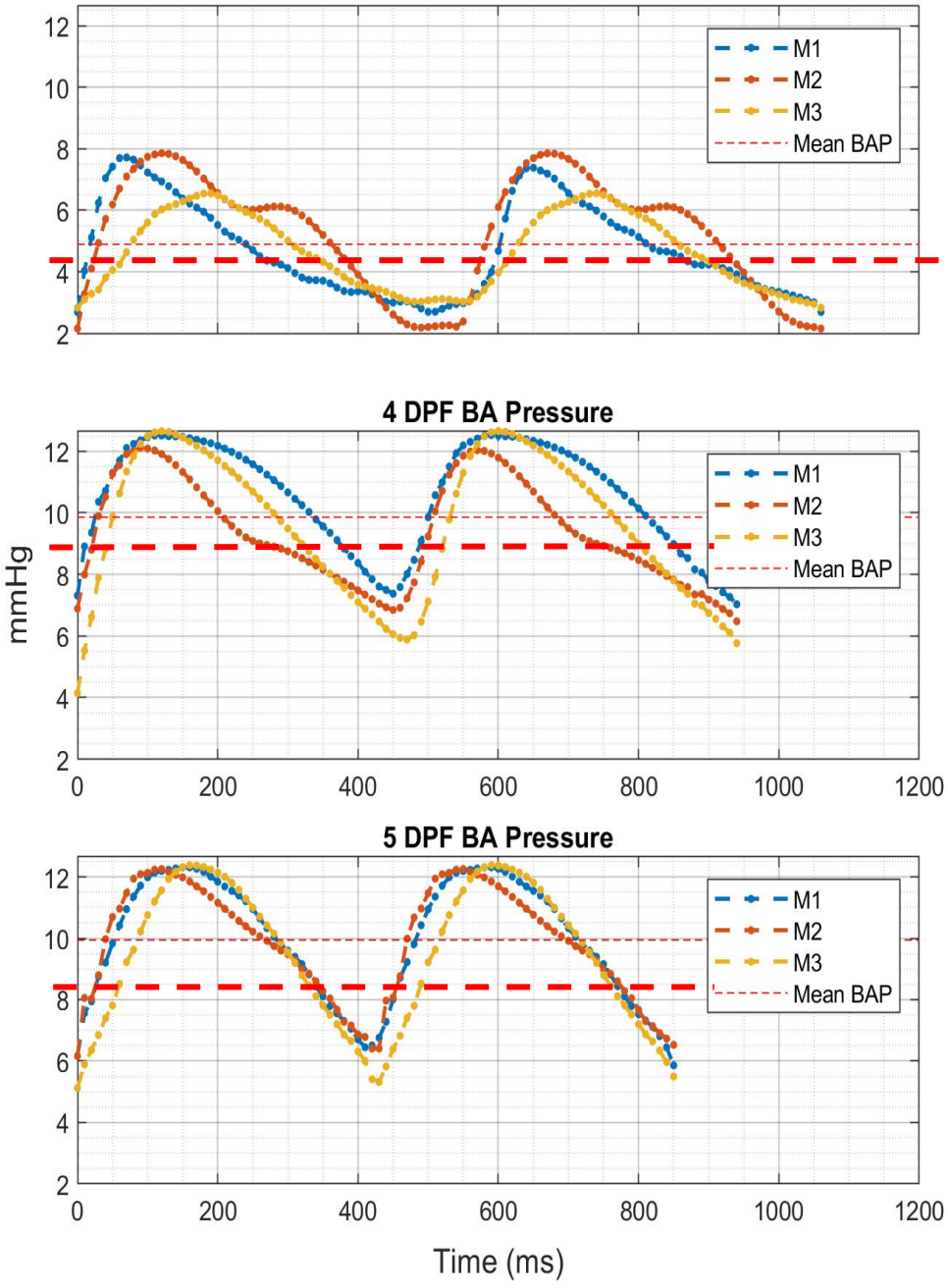

Fig. S3: Pressure measurements from Bulbus Arteriosus (BA) of embryonic zebrafish of 3, 4 and 5 dpf group, with n = 3 for each group. Red horizontal dash line is the mean of $\overline{P_{BA}}$ for each group, where $\overline{P_{BA}} = \frac{\int_{t_1}^{t_2} P_{BA}(t)\,dt}{(t_2 - t_1)}$ with $P_{BA}(t)$ from BA pressure recordings and t_1, t_2 denote the start and end time point of a cardiac cycle.

CHAPTER 3

VENTRICULAR WALL DEFORMATION & CONTRACTILE FUNCTION OF THE DEVELOPING HEART OF ZEBRAFISH *IN-VIVO*

Introduction

The heart is an electrically controlled mechanical pump delivering oxygenated blood for the organism to function with flexibility and adaptability to the changing demand and the working conditions. In vertebrate embryos, the heart is the first organ that starts to function (*4*). Originating as a valveless linear tube, through the processes of growth, remodeling and morphogenesis, it transforms into a multi-chambered pulsatile pump with flow regulating valves (*5*).

The zebrafish is widely used as model for *in vivo* studies of the genetic, morphological, and functional aspects of cardiovascular development. Its advantages include high fecundity, external fertilization, rapid organ development, ease of genetic manipulation and optically transparent body (*8, 9, 29, 49, 67*). Especially with the attribute of optical transparency, the morphology can be noninvasively imaged throughout cardiac development, facilitating inference of *in-vivo* functions of the embryonic heart. With sequenced genome and application of modern genetics techniques, disorders of human heart development such as congenital heart defects and cardiomyopathy have been studied using zebrafish as model (*67*).

Unlike the human heart, which has four-chamber and four-valve configuration, zebrafish heart has one atrium, one ventricle, with atrio-ventricular (AV) valve and ventriculo-bulbar (VB) valve serving to regulate the blood flow to meet entire body's metabolic needs. Because of the conservation of the genetic networks regulating vertebrate heart development, zebrafish adopt similar cellular and molecular strategies to assemble its heart (*28, 67*). In zebrafish, peristaltic contraction of the valveless linear heart tube starts around 24 hours post fertilization (hpf). Initiation of chamber formation through cardiac looping occurs at 33 hpf, followed by transformation of the pumping mechanism to sequential chamber contractions at 36 hpf (*28*). Primitive valve leaflets appear around 40 hpf from endocardial cushions which are regional wall thickening in the AV canal and outflow tract. Maturation of the valve leaflets to functioning valves is completed by 96 to 120 hpf (*8, 49*). The embryonic heart starts functioning well before its structural organogenesis is complete and undergoes substantial changes in morphology while continuing to pump blood to satisfy the metabolic needs of the embryo (*4, 5*). In addition to genetic factors, environmental factors such as biomechanical cues modulate the early stages of heart development, from looping and trabeculation to chamber and valve formation (*8, 9, 14, 29, 49, 68*). Thus, cardiac development is affected by early cardiac function with altered function leading to compensatory remodeling of the heart (*34, 35, 69*).

Function of the heart is commonly described in terms of volume-based parameters such as stroke volume, ejection fraction, pressure-volume loops which measure the overall functional performance of the ventricle. We have recently showed improving mechanical performance of the developing heart, commensurate with the observed changes in valve development, chamber morphology and vascular network, for the zebrafish model (*70*). The developing zebrafish ventricle generated higher pressure resulting in increased stroke volume and cardiac output to

meet the demand of the rapidly growing embryo. Since the generation of higher ventricular pressure, stroke volume and cardiac output of a beating heart is the effect of synchronized contractile deformation of cardiomyocytes in the ventricular wall collectively, there is a need to understand how the cyclic myocardium wall deformation contribute to the improving mechanical performance of the heart at different stage of development.

In this work, we studied regional ventricular myocardial wall deformation of developing heart through cardiac cycles. Using images from selective plane illumination microscopy (SPIM), we reconstructed ventricular wall deformation of embryonic zebrafish hearts *in-vivo*. We tracked the movement of triads of fluorescing nuclei of myocytes in the ventricular myocardium to characterize the regional deformation. We also measured the intra-ventricular pressure (*IVP*). At 3, 4, 5 days post fertilization (dpf), we examined regional deformation in the equatorial (EQ), apex (AP) and outflow (OT) regions. At each region, we found area changes, principal stretches and assessed the degrees of anisotropic deformation. From the results we inferred ventricular compliance (*VC*) during filling, and systolic performance Index (*SPI*) during ejection phase. Through diastolic filling, the heart prepares its ventricular myocardium for the ensuing active contractile deformation to pump blood during systolic ejection. Our results provide insights into the cyclic deformation of the ventricular wall myocardium and their contributions to the contractile function.

Materials and Methods

Zebrafish handling and preparation for imaging

Transgenic zebrafish embryos Tg(*cmlc2:* nuc – egfp) at 3, 4 and 5 dpf were used in this study. The *cmlc2* promoter is expressed with enhanced green fluorescent protein (egfp) in the nuclei of ventricular cardiomyocytes. In order to maintain transparency of zebrafish embryos incubated at 28^0C, phenylthiourea (PTU) at 0.003% was added to the E3 medium at 20 hpf to suppress pigmentation (*53*). To image the heart, embryos were anesthetized in 0.05% tricaine, immersed in 0.5% low melting point agarose, having a refractive index close to that of water and biological tissue. Before solidification of agarose, the embryos were transferred to fluorinated ethylene propylene (FEP) tube for vertical mounting on a stage providing translation and rotation (*1*) of the preparation for the study. All embryos used were obtained from fertilized eggs, bred in the animal care facility and all experiments were performed in compliance with our Institutional Animal Care & Use Committee (IACUC) guidelines.

Acquisition and Reconstruction of 4-D images of the beating heart of embryonic zebrafish

Images of the beating zebrafish hearts were acquired using a modified version of SPIM (*9, 71*) as described previously (*70*). Excitation for gfp signals was provided by 473 nm laser light. A 20X water dipping objective lens of high numerical aperture (NA = 0.5) was used for detection, which helped to eliminate spherical aberrations by minimizing refractive index mismatch. For acquisition of dynamic 3D volumes, the sample was moved along the detection axis at a fixed step size of 0.65 μm while slice sequences of zebrafish heart were captured from the rostral to the caudal end. Using a digital camera (Hamamatsu, ORCA Flash 4.0 sCMOS), 150 – 280 overlapping z-slices were recorded with each slice sequence consisting of 300 frames (512 x 512 pixels) imaged with 10 milliseconds exposure. The process of image acquisition was

controlled by a code written in LABVIEW (National Instruments). As the slice sequences were acquired in a non-gated manner, with acquisition starting at a random moment in the cardiac cycle, the acquired sequences were processed with our previously developed MATLAB (MathWorks) code (*9, 29*) that minimized the error of cardiac phase of each layer. 4D images reconstructed by post acquisition synchronization (*54*) are with voxel sizes of 0.325 x 0.325 x 0.65 μm^3.

Image processing and segmentation of cardiomyocytes

The reconstructed 4D images of the embryonic zebrafish heart were processed to reduce noise and enhance contrast. Background subtraction was performed, followed by contrast optimization through the application of a sigmoid shaped intensity transfer function. 3D segmentation of the cardiomyocyte nuclei at each time point was achieved by applying a threshold and watershed transform to the processed images. A code written in MATLAB (MathWorks) performed the processing and segmentation.

Cardiomyocyte tracking

Using the centroids of segmented cardiomyocyte nuclei as their instantaneous locations in 3D space, we considered all possible identifications of the old positions with the new positions and chose that identification which resulted in the minimal total squared displacement. Using this approach, we tracked segmented cardiomyocytes through the cardiac cycle with an adapted code in MATLAB (MathWorks) developed by John C. Crocker, University of Chicago. Timed positions and trajectories of cardiomyocytes providing their 3D motion referenced in ground coordinates were stored for deformation analysis.

Quantifying regional myocardial deformation

Representative images of reconstructed ventricular myocardium showing fluorescing cardiomyocyte nuclei at the end of isovolumic relaxation, and the end of diastolic filling are presented in Fig. 1A, B. Three neighboring nuclei markers (~ 15 to 25 μm) forming a triangular region was chosen from each of the equatorial (EQ), apex (AP) and outflow (OT) region. By following marker movements, we calculated their respective regional deformation through a cardiac cycle. A slice-cut through the midsection of the ventricle revealed the one-cell thickness of the myocardium at early stage of development (Fig. 1C, D) supporting the use of thin-wall membrane model.

Illustrated in Fig. 2A for EQ region, a triad of three neighboring nuclei markers A, B, C forming a triangular region was chosen. Using ground coordinate system **XYZ** as the reference, the position vector for each of the nuclei markers at its centroid can be denoted as $\boldsymbol{X}$. For referencing the deformation of the region through a cardiac cycle, adopting Lagrangian approach, we chose the region's configuration at the end of isovolumic relaxation (or the start of ventricular filling) as the initial reference (State 1) since it is the state when the myocardium is least deformed. All regional deformation through a cardiac cycle was referenced with respect to State 1.

At time *t* into a cardiac cycle, the nuclei makers labeled as a, b, c now occupy new position in the deformed configuration denoted as position vector $\boldsymbol{x}$. The movement and deformation can be described as (*72*)

$$\boldsymbol{x} = \zeta(\boldsymbol{X}, t) \tag{1}$$

from which the deformation gradient $\boldsymbol{F}$ can be obtained as $\boldsymbol{F} = \frac{\partial \boldsymbol{x}}{\partial \boldsymbol{X}}$ (where $F_{iJ} = \frac{\partial x_i}{\partial X_J}$) (2)

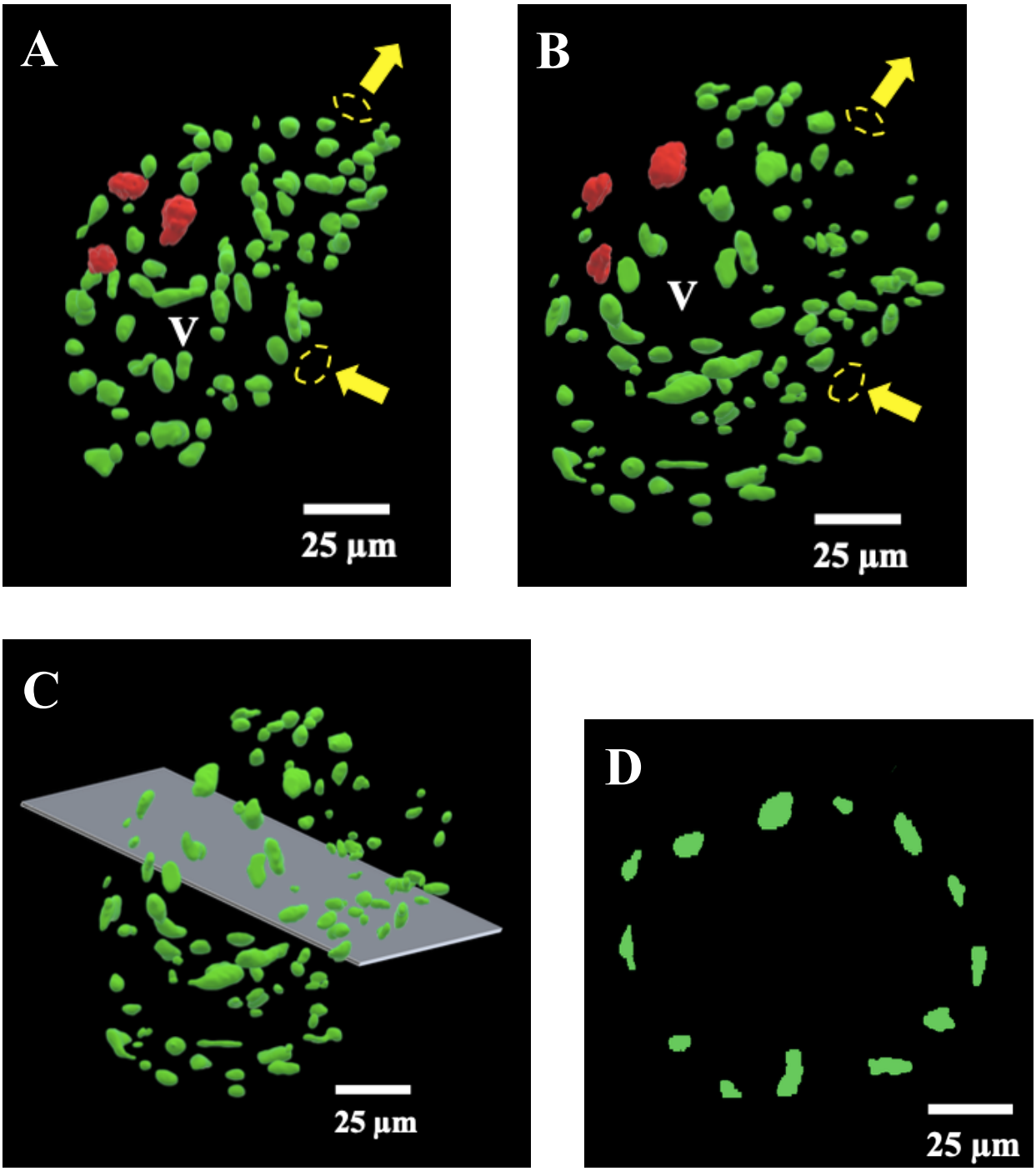

Figure 1: Representative SPIM images of developing Tg*(cmlc2:* egfp - nuc*)* zebrafish heart at 4 days post fertilization (dpf). Ventricular cardiomyocyte nuclei **A)** at State 1 (End of Isovolumic Relaxation), **B)** at State 2 (End Diastole). In **(A)** and **(B)**, red nuclei served as markers in the equatorial region of the ventricle and yellow arrows represent inflow through AV valve and outflow through VB valve. V: Ventricle. **C)** A cutting plane passing through the ventricle (at State 2) isolates the myocytes. **D)** Myocyte nuclei in the transverse cross section representing a thin myocardial wall.

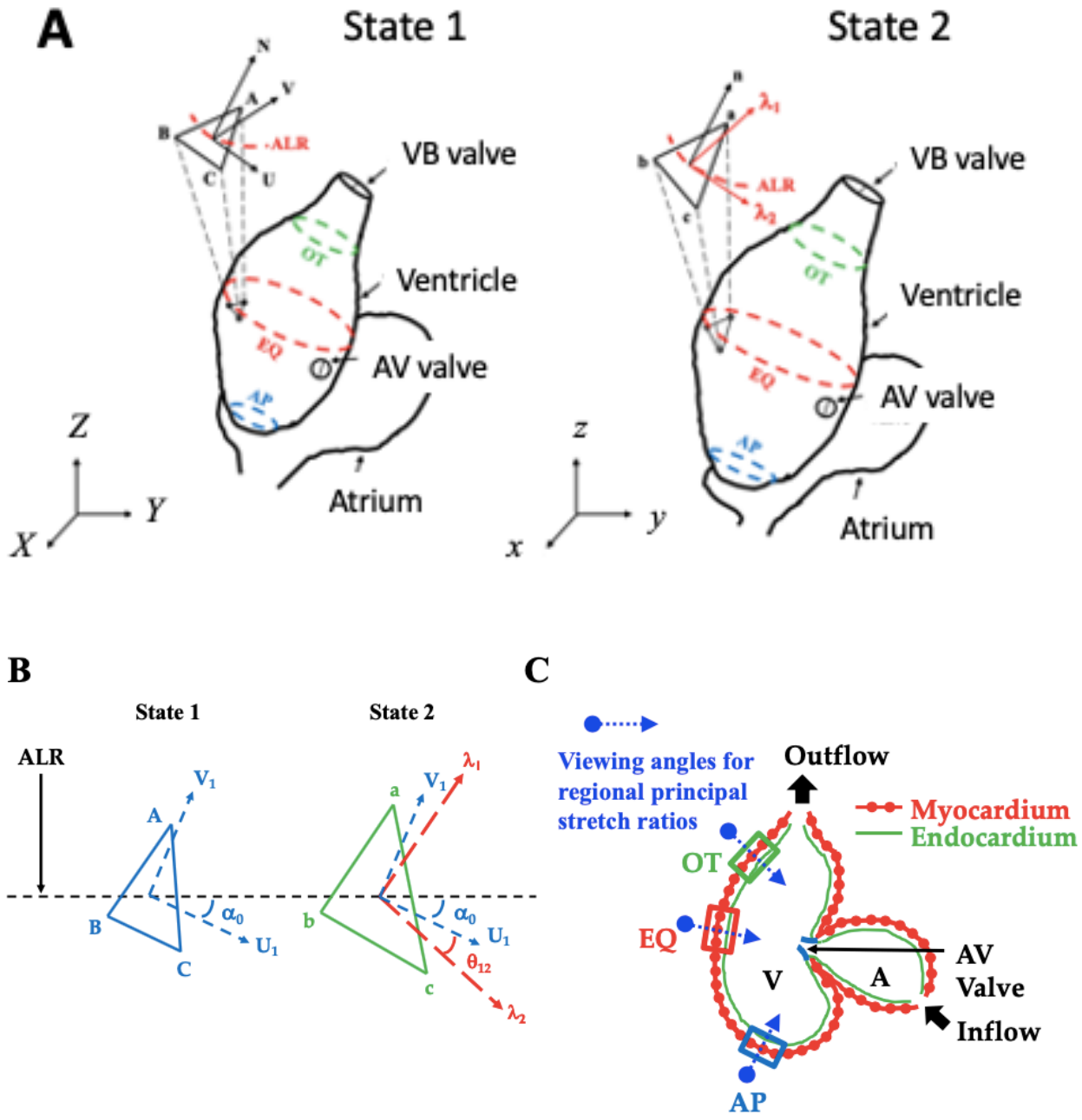

Figure 2: Regional deformation is estimated from the relative movements of three cardiomyocytes on the ventricular wall which served as markers. **(A)** Triangle ABC represents the reference configuration at the end of isovolumic relaxation (State 1) and **UVN** denotes the local coordinate system, triangle abc represents the corresponding deformed configuration at end diastole (State 2); **ALR:** Anatomical Latitude Reference Line; λ_1, λ_2**:** Principal Stretch components. 3 regions were analyzed: Outflow **(OT)**, Equatorial **(EQ)** and Apex **(AP)**. **(B)** Principal directions resolved in terms of **ALR** where α_{02} **(=** $\alpha_0 + \theta_{12}$**):** angle of λ_2 from **ALR** at (State 2), α_0**:** angle between $\mathbf{U}_1$ and **ALR** at (State 1) and θ_{12}**:** angle of λ_2 from $\mathbf{U}_1$ at (State 2). **(C)** 2D projection view of the zebrafish heart showing the 3 regions (OT, EQ, AP) analyzed.

F may differ from point to point in the region ABC but becomes a constant when the triangle is small enough to warrant the assumption of local homogeneous deformation. That is,

$$\boldsymbol{x} = \boldsymbol{F} \bullet \boldsymbol{X} \tag{3}$$

With marker coordinates of the region known at the deformed and the initial reference configuration, ***F*** can be determined from (3). To evaluate the in-plane deformation gradient ***F***, local coordinate system can be used that facilitate the removal of rigid body motion and the isolation of regional deformation (*73*). At each time point, local in-plane coordinate system ***UVN*** was established at the centroid of the triangle ABC. ***U*** was a unit vector chosen to parallel to side BC, ***N*** a unit vector perpendicular from plane ABC, and ***V*** obtained as the cross product of ***N*** x ***U***. At each time point *t*, the marker coordinates were transformed from ground coordinate system ***XYZ*** to local coordinate system ***UVN*** and the in-plane deformation gradient ***F*** of the region was computed from Eq. (3), written in matrix form as

$$\begin{bmatrix} u_a & u_b & u_c \\ v_a & v_b & v_c \end{bmatrix} = \begin{bmatrix} F_{11} & F_{12} \\ F_{21} & F_{22} \end{bmatrix} \begin{bmatrix} U_A & U_B & U_C \\ V_A & V_B & V_C \end{bmatrix} \tag{4}$$

Eq. (4) is an over determined system of equations with four unknowns ($F_{11}, F_{12}, F_{21}, F_{22}$) and six equations. With ***F*** known, components of the symmetric finite (Green) strain tensor ***E*** were calculated, where, $\boldsymbol{E} = \frac{1}{2}\ (\boldsymbol{F^T} \bullet \boldsymbol{F} - \boldsymbol{I})$ (5)

In-plane principal strains were then determined by solving the eigenvalue problem. The corresponding principal stretches were found from $\lambda_i = \sqrt{2\,E_i + 1} \qquad i = 1, 2$ (6)

where E_i represent principal strain components and λ_i represent principal stretch components.

Both principal stretch components λ_1 and λ_2 were expressed as ratios with respect to their reference values at State 1 (end of isovolumic relaxation). Principal directions at States 2 (end diastole, ED), 3 (end of isovolumic contraction) and 4 (end systole, ES) were resolved in terms of anatomical latitude reference line (*ALR* in Fig. 2B). Area ratio *AR*, representing the changes in the area of the triangular region ABC with respect to the reference area at the end of isovolumic relaxation were also calculated at each time point. All calculations were done in a code written in MATLAB (MathWorks).

Measurement of Intra-Ventricular Pressure

Separate embryos were used for Intra-ventricular pressure (*IVP*) recording and image acquisition, because of the invasive nature of the pressure measurement. For each of 3, 4 and 5 dpf group, we measured the *IVP* of five embryonic zebrafish using a servo null micro-pressure system (World Precision Instruments, 900A). A glass micro-pipette having a tip diameter 2 ~ 5 μm, filled with electrolyte at 1 M NaCl served as the probe. With the tip of the probe inserted in the ventricular cavity, the fluid level in the micro-pipette changed in response to the instantaneous ventricular pressure. It was restored by a system-generated compensatory pressure to offset the changes due to ventricular pressure (*74*). The dynamic response of the system was assessed by applying known pressure pulses of 5 ~ 20 mmHg and the system was calibrated prior to each measurement. Pressure signals sampled at 100 Hz, were passed through an IIR Butterworth filter to remove the high frequency noise. A code was written for identifying the cut-off frequencies and filtering the signals running in MATLAB (MathWorks). The *IVP* reported herein are relative pressure with the fluid pressure just outside the heart used as reference.

Ventricular Myocardial Wall Compliance during Filling

During filling from State 1 to 2, ventricular wall myocardium undergoes passive deformation in response to the increasing blood volume driven by the atrium-ventricle pressure gradients and atrial contraction. To compare the differences in the passive deformation properties of the developing ventricle at operation, we calculated ventricular compliance *VC* for each from

$$VC = \frac{\Delta(AR)}{\Delta p} = \frac{AR_{state\,2} - AR_{state\,1}}{P_{State\,2} - P_{State\,1}} = \frac{AR_{End\,Diastole} - 1}{EDVP - ERVP} \quad (7)$$

where *EDVP* denotes end diastolic ventricular pressure, *ERVP* denotes end relaxation ventricular pressure with both determined from *IVP* measurements.

Systolic Performance Index

To compare the potential of ventricular wall myocardium in generating IVP to eject blood during systole through contractile deformation among dpf groups, we calculated Systolic Performance Index (SPI) from

$$SPI = \frac{\Delta p}{\Delta(AR)} = \frac{PSVP - EDVP}{AR_{State\,2} - AR_{State\,4}} \quad (8)$$

where *PSVP* denotes peak systolic ventricular pressure, *EDVP* denotes end diastolic ventricular pressure obtained from *IVP* measurements.

Statistical Analysis

Results of area ratio (*AR*), principal stretch components (λ_1 and λ_2) at States 1, 2, 3 and 4, were expressed as mean ± SD (n = 3) for each of the three regions EQ, AP, OT in 3, 4 and 5 dpf groups. From *IVP* measurements *PSVP*, *EDVP* and *ERVP* were expressed as mean ± SD (n = 5)

for each of 3, 4 and 5 dpf groups. Differences in λ_1 and λ_2 at a specific region at State 2 (ED) and State 4 (ES), were analyzed by two sample *t*-test. Regional differences in *AR*, λ_1 and λ_2 at ED and ES were tested by one-way ANOVA test. Differences in *VC*, *SPI* and regional *AR*, among 3, 4 and 5 dpf group were analyzed by one-way ANOVA test. Tukey's multiple comparison test was performed when significant difference was detected. Statistical testing was performed in ***R*** (https://www.r-project.org/) with $p < 0.05$ considered as statistically significant.

Results

Introduction to Results

Representative time courses of area ratio *AR* and the corresponding principal stretch components λ_1, λ_2 from one cardiac cycle are presented in Fig. 3 for the three analyzed regions of the embryos at 3, 4, and 5 dpf. Red vertical dash lines delineate the four phases of the cardiac cycle: filling, isovolumic contraction, ejection, and isovolumic relaxation. Principal directions were resolved with respect to the anatomical latitude reference line (*ALR*) at the analyzed region of the ventricle (Fig 2B), with principal stretch component λ_2 developing near the latitudinal direction and its paired λ_1 near the longitudinal direction. Key results for *AR* and paired λ_1, λ_2 are summarized with statistics in Fig. 4 for *AR,* in Fig. 7 for λ_1, λ_2. Results of passive mechanical properties of ventricular wall myocardium inferred from *IVP* recordings and the corresponding wall deformation during filling are presented in Fig 5 A, B. Results of ventricular myocardium's capacity to generate *IVP* during active contractile ejection phase are presented in Figs. 6A, B, C. Finally, we presented the results on the regional anisotropic deformation of the myocardium and their differences in 3, 4 and 5 dpf groups in Fig. 8.

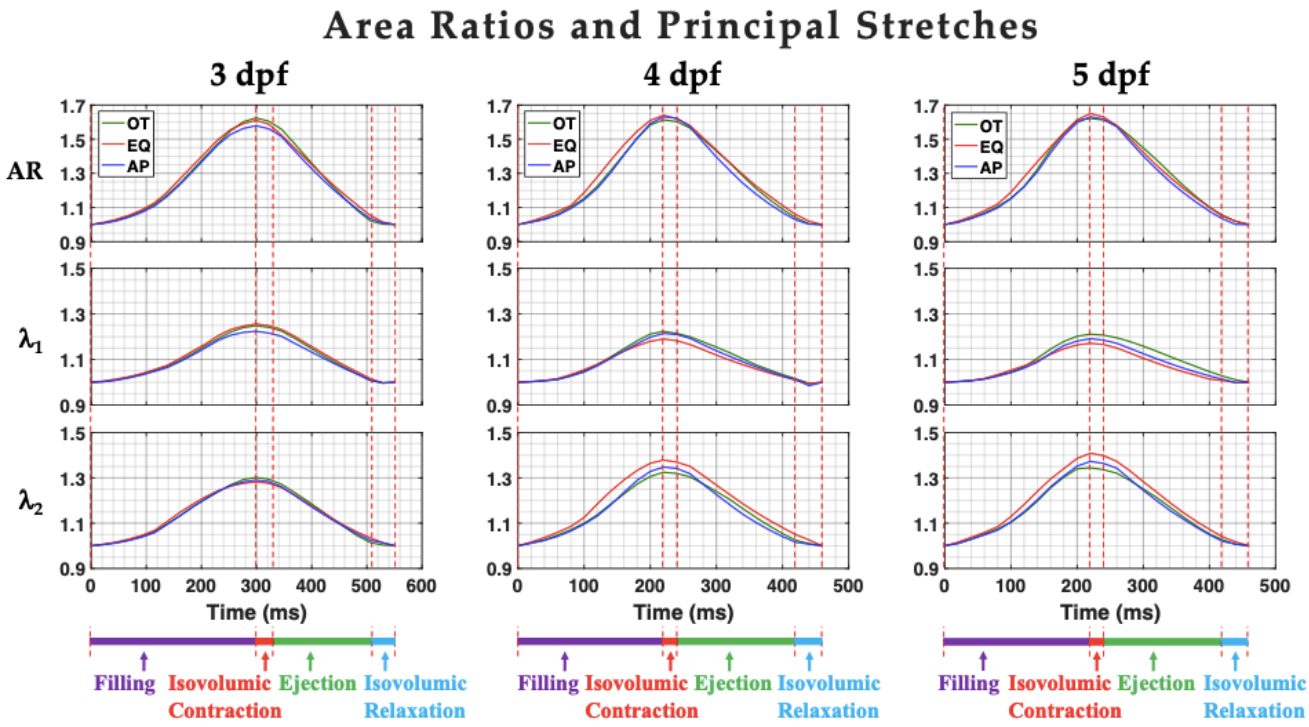

Figure 3: Representative time courses of Area Ratio **(AR)** and Principal Stretches: λ_1, λ_2 for one cardiac cycle at Outflow (**OT**), Equatorial (**EQ**) and Apex (**AP**) regions of developing Tg*(cmlc2:* egfp - nuc*)* zebrafish heart at 3, 4 and 5 days post fertilization (dpf). Four phases in the cardiac cycle can be identified as shown.

Area Ratios (Fig. 4)

For embryos at 3 dpf, *AR* at ED were found to be 1.63 ± 0.07, 1.59 ± 0.05 and 1.6 ± 0.06 at EQ, AP and OT regions respectively. At 4 and 5 dpf, the corresponding values of end diastolic *AR* were 1.67 ± 0.06, 1.62 ± 0.01, 1.63 ± 0.05 and 1.64 ± 0.04, 1.6 ± 0.06, 1.6 ± 0.04. No significant regional difference in end diastolic *AR* was detected at 3, 4 or 5 dpf.

From EQ, AP and OT region of 3 dpf embryos, *AR* at ES were found to be 1.01 ± 0.04, 1.003 ± 0.02 and 1.017 ± 0.03 respectively. The corresponding end systolic *AR* at 4, 5 dpf were 1.007 ± 0.02, 0.987 ± 0.01, 1.013 ± 0.02 and 1.037 ± 0.01, 1.003 ± 0.01, 1.03 ± 0.01. At 5 dpf,

end systolic *AR* was significantly lower at AP region. However, such regional difference in end systolic *AR* was not found at 3 or 4 dpf.

Comparison of *AR* from EQ region at ED and ES among 3, 4 and 5 dpf groups did not reveal any significant difference. For the AP and OT regions, similarly, the values of respective *AR* at ED and at ES did not differ significantly among 3, 4 and 5 dpf groups.

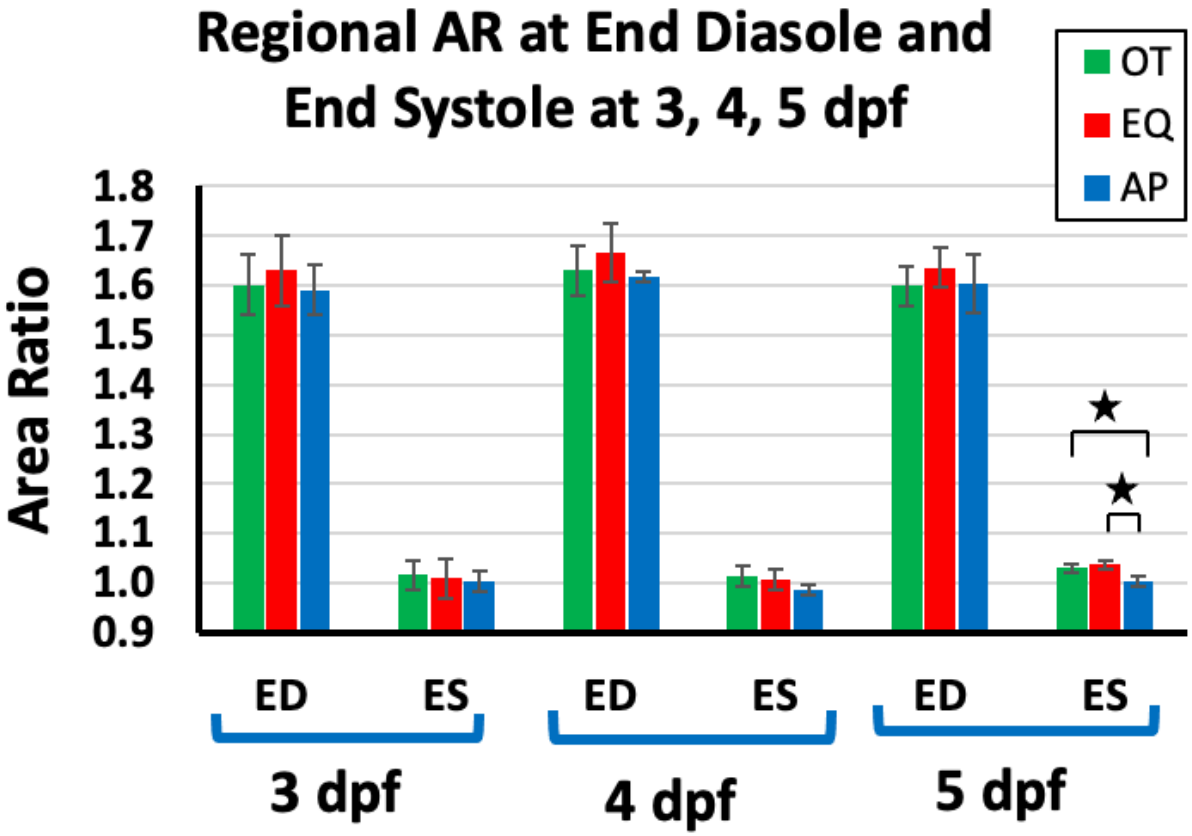

Figure 4: Comparison of regional area ratios at end diastole and end systole during a cardiac cycle at Outflow (**OT**), Equatorial (**EQ**) and Apex (**AP**) regions of developing zebrafish heart at 3-, 4- and 5-days post fertilization (dpf). **AR:** Area Ratio, **ED:** End Diastole, **ES:** End Systole. Statistically significant differences are denoted by *.

Passive Deformation Response (Fig. 5 A, B)

Recorded *IVP* tracings showed small amplitudes (peak 2 - 2.4 mmHg) with oscillations seen in some of them indicating the effects of kinetic energy of the incoming flow. All recorded *IVP* tracing during filling were plotted against averaged *AR* (Fig. 5A). We chose to use the averaged *AR* from 3 regions for each dpf group, since we did not see their significant differences. To quantitatively compare the differences in the passive deformation properties of the developing myocardium, we calculated their ventricular compliance (*VC*). From 3 dpf, the *VC* was found to be 0.41 ± 0.03 $mmHg^{-1}$, being significantly higher than 0.33 ± 0.03 $mmHg^{-1}$ and 0.31 ± 0.02 $mmHg^{-1}$ for 4 and 5 dpf, with $p < 0.05$ respectively (Fig. 5B). Results showed decreasing compliance and increasing stiffness of the ventricular wall myocardium from 3 to 4, to 5 dpf groups as the cardiac development proceeds.

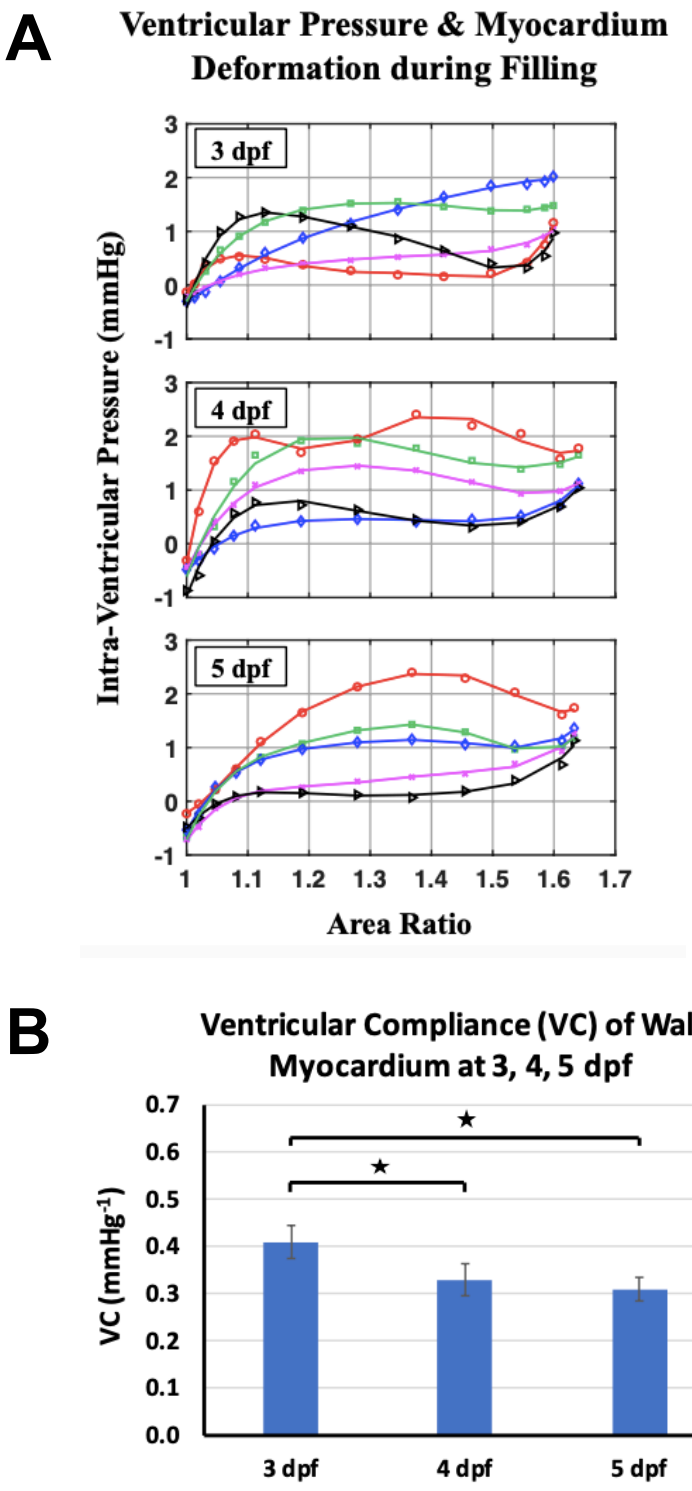

Figure 5: Passive response of ventricular myocardium of developing zebrafish heart at 3-, 4- and 5-days post fertilization (dpf). **A)** Changes in intra-ventricular pressure (n = 5) with area ratio (regional average at each dpf) during filling phase of a cardiac cycle. **B)** Comparison of ventricular compliance of myocardial wall. **VC:** Ventricular Compliance. Statistically significant differences are denoted by *.

Contractile Deformation During Ejection (Fig. 6 A, B, C)

Recorded *IVP* from ED (State 2) to ES (State 4) was plotted against decreasing averaged *AR*. Follow the results from Fig. 4, we chose to use the averaged *AR* from 3 regions for each dpf group in Fig. 6A with the data fitted to a 5^{th} order polynomial. The average of the responses as represented by the fitted curve showed that 3 dpf embryos reached the peak of 7.5 mmHg at $AR = 1.24$, whereas the peak *IVP* of 10.45 mmHg for 4 dpf embryos occurred at $AR = 1.27$, and 11 mmHg for 5 dpf embryos occurred at $AR = 1.28$.

Derivatives of the fitted *IVP* with respect to the decreasing *AR*, at different levels of *AR* during systole show higher levels of pressure-generating potential at the onset of systole: being 56 and 47 mmHg from 5, 4 dpf groups, respectively, and 28 mmHg from 3 dpf group (Fig. 6B). Calculated values of systolic performance index (*SPI*), indicating the pressure generating capacity of ventricular wall myocardium, were found to be 10.27 ± 0.83 mmHg for 3 dpf embryos. At 4 and 5 dpf, we saw significant increases in *SPI*, being 14.71 ± 1.97 and 16.86 ± 1.85 mmHg, with $p < 0.05$ respectively (Fig. 6C).

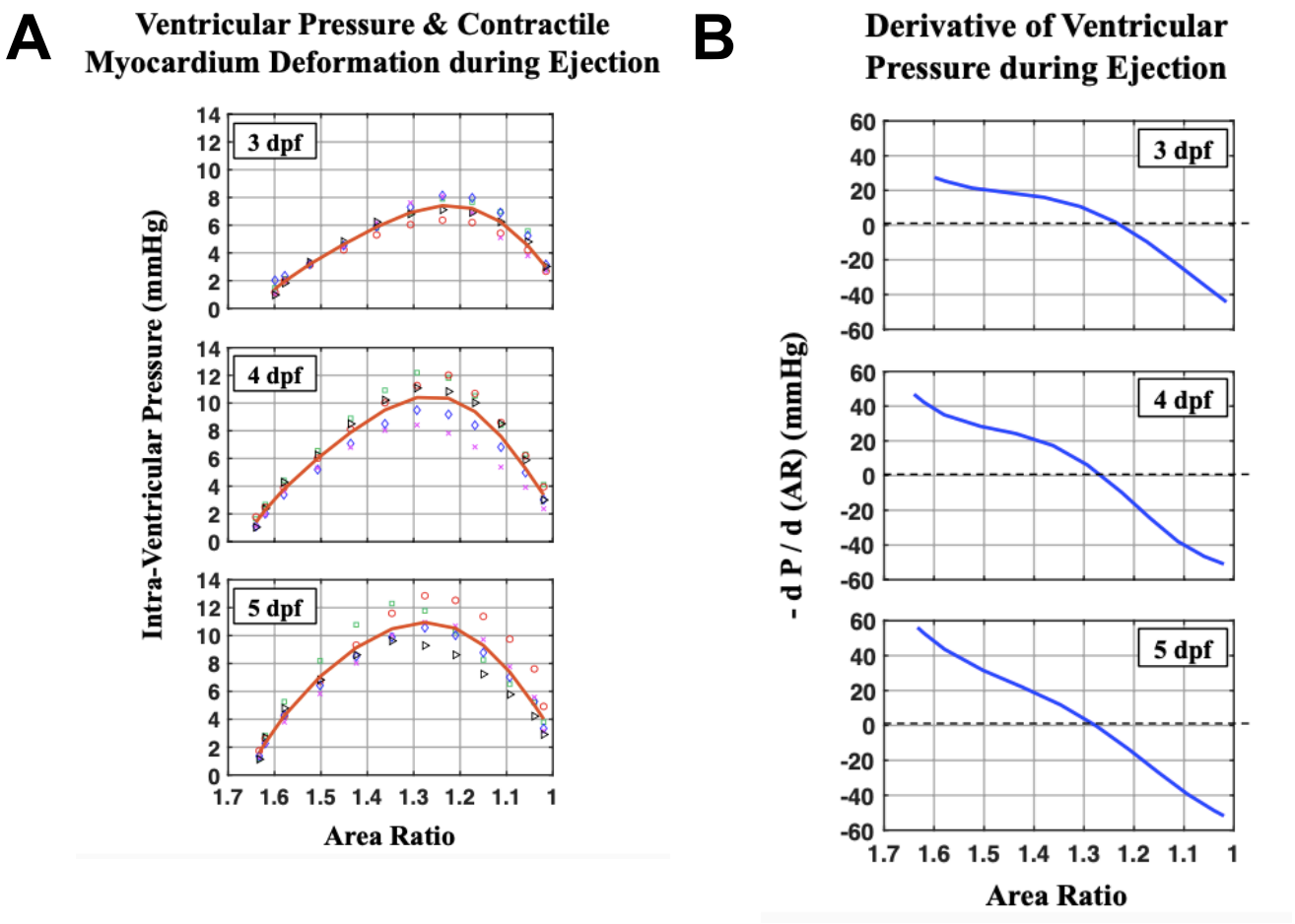

Figure 6: Active contractile response of ventricular myocardium of developing zebrafish heart at 3-, 4- and 5-days post fertilization (dpf). **A)** Generation of intra-ventricular pressure (n = 5) with area ratio (regional average at each dpf) during ejection phase of a cardiac cycle. Fitted curves represent

characteristic response. **B)** The intensity of pressure generation during ejection calculated as the negative derivative of characteristic pressure with respect to area ratio. **C)** Comparison of systolic performance index of contracting myocardium. **SPI:** Systolic Performance Index. Statistically significant differences are denoted by *.

Principal Stretches (Fig. 7):

From 3 dpf embryos at ED state, the paired (λ_2, λ_1) were found to be (1.303 ± 0.04, 1.253 ± 0.02), (1.293 ± 0.025, 1.23 ± 0.02) and (1.293 ± 0.04, 1.237 ± 0.015) at EQ, AP and OT region, respectively. Only at the *AP* region, λ_2 and λ_1 was found significantly different from each other ($p < 0.05$). The corresponding (λ_2, λ_1) pairs at ES state were found to be (1.007 ± 0.04, 1.003 ± 0.012), (1.013 ± 0.006, 0.993 ± 0.015), and (1.02 ± 0.017, 0.997 ± 0.012) at EQ, AP and OT region, respectively. None of the three regions exhibited significant difference in the end systolic λ_2 and λ_1.

From 4 dpf embryos at ED state, the paired (λ_2, λ_1) were found to be (1.39 ± 0.036, 1.2 ± 0.017), (1.327 ± 0.025, 1.22 ± 0.017) and (1.337 ± 0.038, 1.22 ± 0.01) at EQ, AP and OT region, respectively. For all three regions, end diastolic λ_2 was significantly higher than λ_1 ($p < 0.05$). Their corresponding (λ_2, λ_1) pairs at ES were found to be (1.02 ± 0.01, 0.987 ± 0.006), (1.0 ± 0.01, 0.987 ± 0.006) and (1.02 ± 0.01, 0.993 ± 0.006) at EQ, AP and OT region, respectively. At EQ and OT regions, end systolic λ_2 and λ_1 differed significantly ($p < 0.05$).

From the 5 dpf embryos at ED state, the (λ_2, λ_1) pairs were found to be (1.403 ± 0.021, 1.167 ± 0.015), (1.357 ± 0.023, 1.183 ± 0.021) and (1.327 ± 0.032, 1.207 ± 0.006) at EQ, AP and OT region, respectively. Similar to the 4 dpf group, end diastolic λ_2 was significantly higher than λ_1 in all three regions ($p < 0.05$). Their corresponding paired (λ_2, λ_1) at ES state were found

significantly different in all three regions as well ($p < 0.05$), being (1.027 ± 0.006, 1.01 ± 0), (1.017 ± 0.006, 0.987 ± 0.006) and (1.027 ± 0.006, 1.003 ± 0.0012) at EQ, AP and OT region, respectively. From 5 dpf embryos, significant regional difference was detected between EQ and OT regions for both λ_2 and λ_1 at ED state and between EQ and AP regions for λ_1 at ES state. However, such regional difference in principal stretches was not found at 4 and 3 dpf.

Anisotropic deformation responses (Figs. 8 A, B, C)

To assess the degree of anisotropic deformation, we calculated the ratio of λ_2 to λ_1 in the three analyzed regions at each of State 1, 2, 3 and 4 for each of 3, 4 and 5 dpf groups. From 3 dpf embryos, (λ_2/λ_1) ratio at ED were found to be 1.04 ± 0.024, 1.051 ± 0.009 and 1.046 ± 0.025 at EQ, AP and OT region, respectively. From 4 dpf group, the corresponding (λ_2/λ_1) ratio at ED were found to be 1.158 ± 0.015, 1.088 ± 0.035, 1.096 ± 0.023. From 5 dpf group, the corresponding (λ_2/λ_1) ratio were found to be 1.203 ± 0.003, 1.146 ± 0.005, 1.099 ± 0.022. The results show that, at 4, 5 dpf, the ventricles underwent anisotropic deformation through a cardiac cycle that favors the latitudinal direction. At 3 dpf, the deformation is near isotropic.

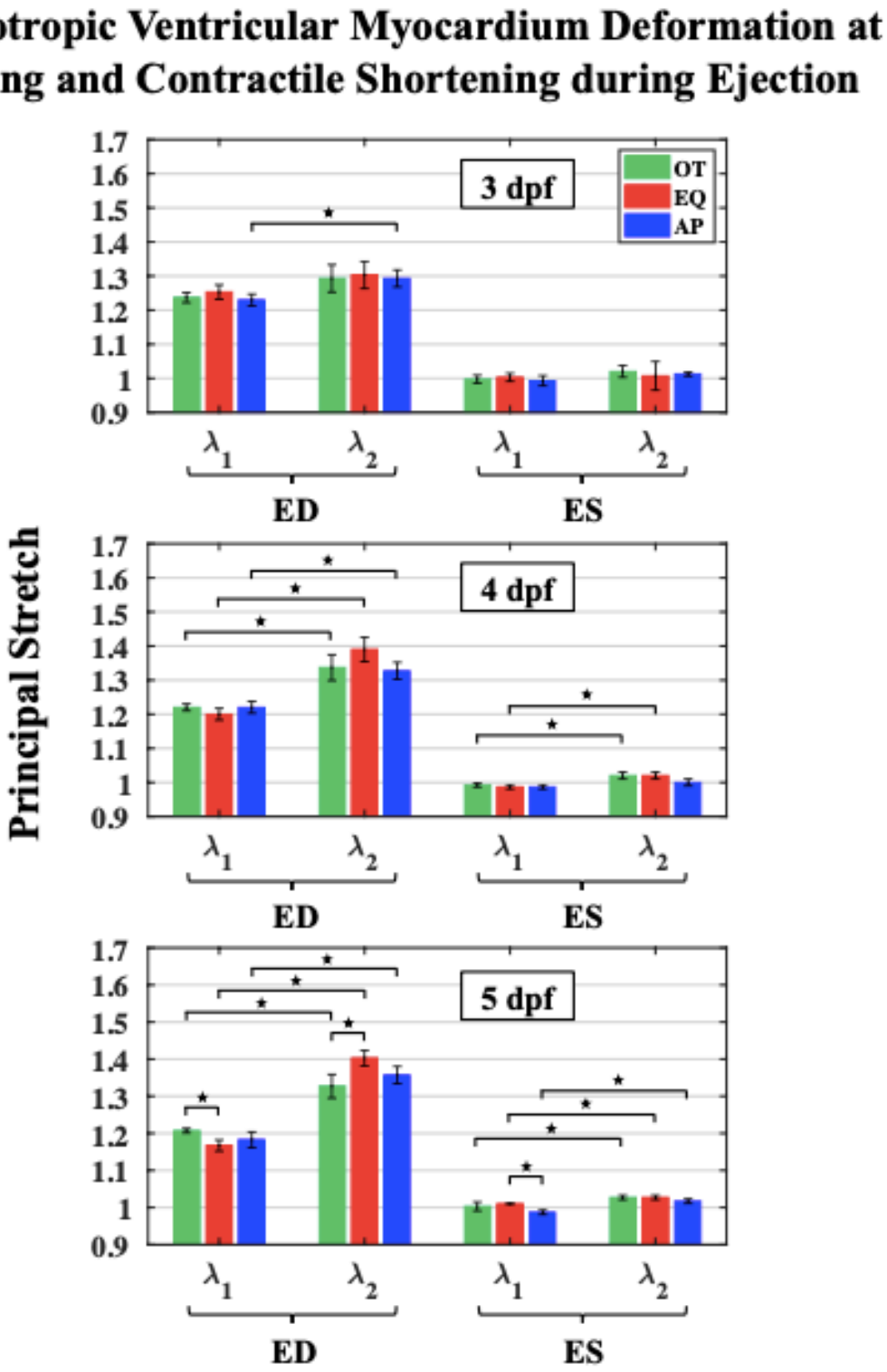

Figure 7: Comparison of regional principal stretches (λ_1, λ_2) at end diastole and end systole during a cardiac cycle at Outflow (**OT**), Equatorial (**EQ**) and Apex (**AP**) regions of developing zebrafish heart at 3-, 4- and 5-days post fertilization (dpf). **λ_1:** Principal Stretch along

longitudinal direction, λ_2**:** Principal Stretch along latitudinal direction **ED:** End Diastole, **ES:** End Systole. Statistically significant differences are denoted by *.

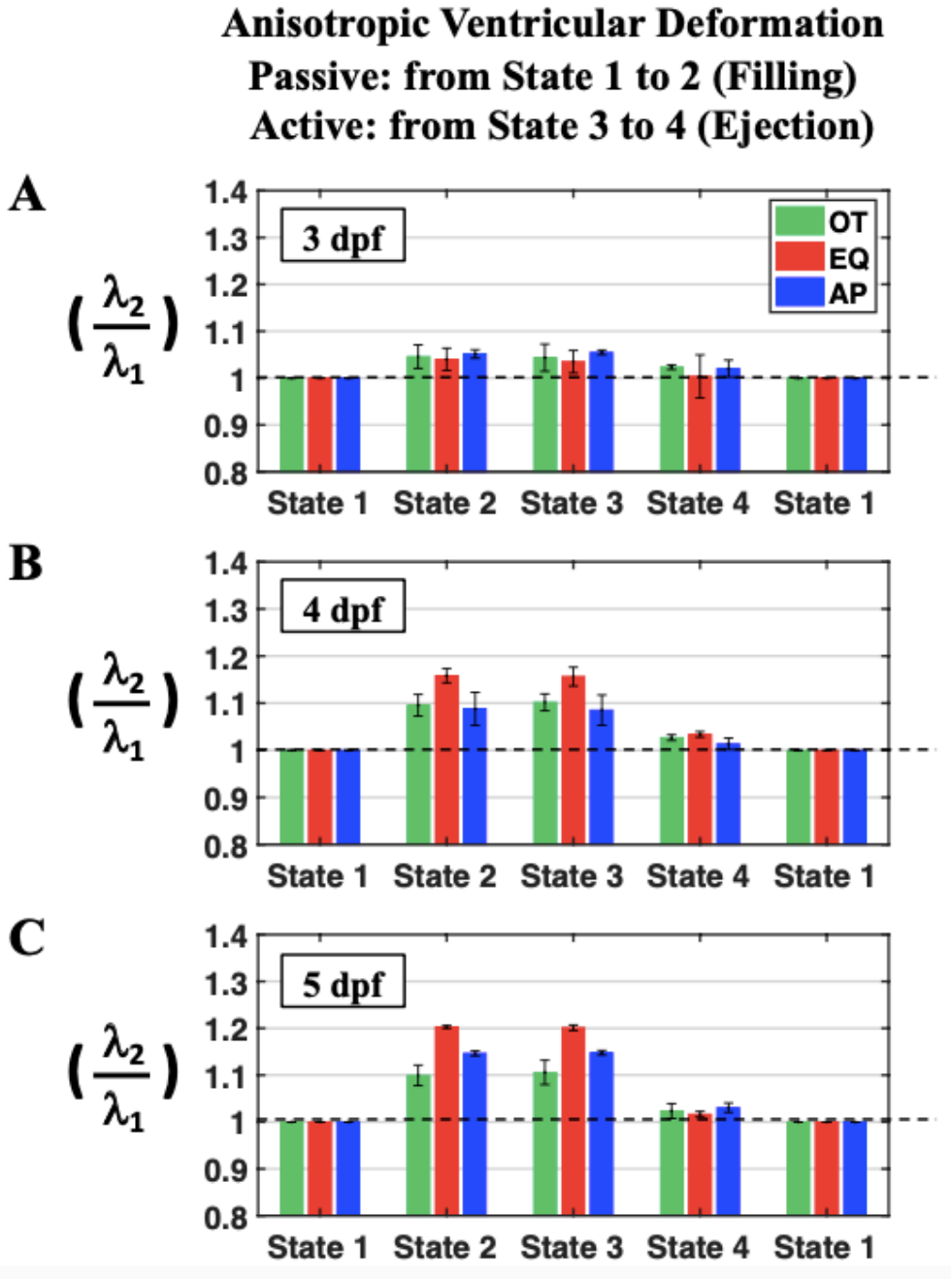

Figure 8: Ratios of principal stretch components λ_2 to λ_1 at states 1 - 4 of a cardiac cycle at Outflow (**OT**), Equatorial (**EQ**) and Apex (**AP**) regions of developing Tg*(cmlc2:* egfp - nuc*)* zebrafish heart at **(A)** 3, **(B)** 4 and **(C)** 5 days post fertilization (dpf). **State 1:** End of isovolumic relaxation, **State 2:** End diastole, **State 3:** End of isovolumic contraction, **State 4:** End systole

Discussion:

Significance

Mechanical performance of the embryonic ventricle has been described in terms of intra-ventricular pressure (*34, 35, 57*), cardiac output (*34, 35, 37*) and dimension (*57*). But these indicators are not sensitive to regional differences in ventricular function, considering the dramatic morphological changes that the ventricles undergo during development. Myocardial deformation in 3D has been analyzed in mature canine left ventricle by tracking columns of implanted lead beads using biplane cineradiography (*75*). In another study, regional deformation differences in the systolic contraction of canine right ventricular free wall were characterized in terms of in-plane principal stretches (*73*). Developmental changes in epicardial wall strain have been studied in left and right ventricle of embryonic chick (*12*) by tracking positions of attached microspheres in single projection of 2D images from one camera (*12, 76*).

For embryonic zebrafish, the assessment of regional ventricular wall deformation and how they contribute to the evolving cardiac functions are questions yet to be answered. In this study, we reconstructed 4D images of the beating heart of zebrafish embryos with fluorescing myocyte nuclei. Moving coordinates of the myocyte markers were tracked through the cardiac cycle for analyzing regional deformation. In our study, animals were free from the effects of surgical intervention and subsequent scars. Combining regional wall strains with *IVP* recordings enabled us to infer the passive and active mechanical properties of the developing ventricular wall myocardium at operation. The increasing degrees of anisotropic ventricular deformation favoring latitudinal direction through a cardiac cycle from 3 to 4, to 5 dpf suggests the evolving changes in the passive deformation during filling that prepare the ventricular wall myocardium for a more effective active contractile deformation to eject blood during the ensuing systole.

Passive Mechanical Properties

Our results showed that *AR* at ED was ~ 1.6 across 3, 4 and 5 dpf groups. End diastolic *AR* did not exhibit significant regional difference for any of the 3, 4 and 5 dpf groups. For end systolic *AR*, regional difference was found only in 5 dpf embryos. Comparison of region-specific *AR* at ED and ES among 3, 4 and 5 dpf groups also did not indicate any significant differences.

Combination of the calculated *AR* with the *IVP* measurements during filling phase enabled us to infer the passive mechanical property of the developing zebrafish ventricle in terms of *VC*. Values of *VC* for 4 and 5 dpf groups were found to be significantly lower than that of 3 dpf group, indicating that ventricular myocardium became stiffer through development. A study on chick heart has shown that myocardial stiffness increases with embryonic age up to Hamburger-Hamilton stage 26 (*77*).

Active Mechanical Properties

The capacity of the developing ventricle to generate pressure for ejecting blood during systole was assessed by comparing *SPI* that relate the *IVP* generated during systolic ejection to the decreasing *AR*. Characteristic responses, described by the fitted curves at 3, 4 and 5 dpf, revealed that for approximately the same levels of *AR* decrease in contractile deformation during systole, 5 and 4 dpf embryos developed significantly higher peak systolic *IVP* than 3 dpf. The intensity and strength of the pressure generation potential during systole was examined by taking the derivative of the characteristic *IVP* with respect to the decreasing *AR*. Compared to the value of 28 mmHg from 3 dpf group at the beginning of systole, embryos at 4 and 5 dpf had much higher starting potential, being 47 and 56 mmHg. Through systole, as more ventricular blood was ejected with accompanying ventricular volume drop, there was a corresponding decrease in the rate of ventricular pressure increase, which eventually reached zero. Beyond which, the

ventricular pressure started to drop with further decrease in ventricular volume and decreasing myocardium contractile deformation in *AR* until reaching the end of systole when the VB-valve closed. In terms of *SPI,* we assessed the capacity of the developing ventricles to generate *IVP* to eject blood during systole. Our results showed increasing trends in *SPI* with statistically significant increase from 3 to 4 dpf group, and from 3 to 5 dpf group. With the growth of the ventricle through the developmental period, more cardiomyocytes compacted in myocardium participate in the pumping function enabling generation of higher ventricular pressure at faster rates during systole.

Anisotropic Deformation of Ventricular Myocardium in Developing Hearts

From a study on epicardial strain of chick embryos at Hamburger-Hamilton (*78*) stages 21, 24, 27 and 31, it was reported that the pattern of ventricular wall deformation during systole changes from isotropic to chamber specific anisotropic during development (*12*). In another study the authors studied the mechanical properties of the atrium of zebrafish embryos at 2dpf to infer their isotropic or transversely isotropic deformation at pressurization (*79*). From our results of 3 dpf embryos, principal stretches λ_1 and λ_2 did not differ significantly at ES, except at AP region during ED where significant differences were noted. The index for anisotropic deformation (λ_2/λ_1) ratio was ~ 1.05 at ED for 3 dpf embryos. On the other hand, from 4 dpf embryos, λ_1 and λ_2 was significantly different in all three regions at ED, and in two of the three regions at ES. For the 5 dpf group, λ_1 and λ_2 significantly differed in all three regions at both ED and ES. The index for anisotropic deformation (λ_2/λ_1) ratio at ED reached ~ 1.16 and ~ 1.2 for 4 and 5 dpf embryos respectively. Our findings suggest that, at 3 dpf, myocardial deformation is isotropic, or slightly anisotropic at best favoring the latitudinal (or circumferential) direction over the longitudinal. At 4 and 5 dpf, the developing zebrafish ventricle becomes more anisotropic,

clearly favoring the latitudinal direction. At ED state, we noted significant regional difference in λ_1 between EQ and OT region for 5 dpf group, and in λ_2 for 5 dpf as well. For 4 dpf embryos, regional differences in λ_1 and λ_2 at ED was present, although it was not statistically significant.

Directional Differences in Ventricular Chamber Deformation

We measured the lengths of major axis and two minor axes of the ventricular chamber at States 1, 2, 3, 4 from embryos at 3, 4, 5 dpf groups (Fig. S1). Using their respective dimensions at State 1 as the references, we calculated the dimensional changes of the major axis and the averaged minor axes at State 2 (ED) and State 4 (ES). From these dimensional changes, we obtained the ratios between the averaged minor and the major axis directions. Following these steps, we assessed the differences in dimensional changes of the ventricular chamber among 3, 4, 5 dpf groups. Summarized in Fig S2, results from 3 dpf group at State 2 show a near uniform expansion (or slightly anisotropic expansion favoring latitudinal direction) through ventricular filling with a ratio of 1.03 ± 0.04 (n=3). From 4 and 5 dpf embryos the ratios were found to be 1.13 ± 0.03 and 1.15 ± 0.03 (n=3 for each dpf group), suggesting expansion favors the latitudinal directions through ventricular filling. These results support the anisotropic behaviors of ventricular wall myocardium in terms of (λ_2/λ_1) ratios (Fig. 8) derived from the regional stretch at OT, EQ and AP regions.

Conclusions:

We characterized the regional deformation of the ventricle of developing zebrafish embryos at 3, 4, 5 dpf. In terms of *AR* and principal stretches λ_1, λ_2, we compared regional differences in EQ, AP and OT and examined their evolving changes through the development from 3, 4, to 5 dpf. Although we did not see statistically significant differences in regional *AR*, the deformation was anisotropic favors the direction along the anatomical latitudinal reference line of the region. The ventricular wall myocardium was found to have higher *VC* at 3 dpf than 4 and 5 dpf groups. On the other hand, the ventricular myocardium was found to have higher *SPI* at 4,5 dpf than that 3 dpf.

Our results indicated approximately the same level of increase in area ratios during the filling phase across 3, 4 and 5 dpf groups accompanied by the absence of any significant regional differences. The developing myocardium also becomes stiffer from 3 to 5 dpf and generates higher ventricular pressure at faster rates during ejection.

As the deformation was resolved into principal stretches λ_1 and λ_2, acting along longitudinal and latitudinal directions respectively, differences were noticed. For 3 dpf embryos, λ_2 was significantly larger than λ_1 only at the AP region at ED. From 4 and 5 dpf groups, end diastolic λ_2 was larger than λ_1 in all three regions and differences between λ_2 and λ_1 also existed at end systolic state. At 5 dpf, significant regional difference was detected in both λ_2 and λ_1.

Overall, our results suggest that along with the developmental changes in morphology, vasculature and maturation of valves, the embryos at 4, 5 dpf underwent anisotropic deformation favoring latitudinal direction.

Supplementary Figures

FISH ID	STATE 1	STATE 2	STATE 3	STATE 4
3 dpf Mar 3, 2020	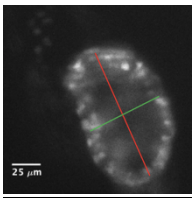	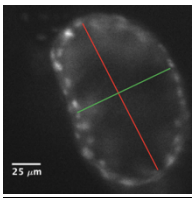	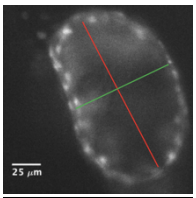	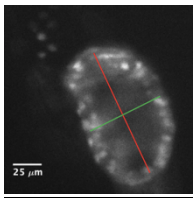
3 dpf Nov 2, 2019	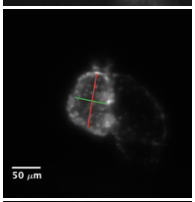	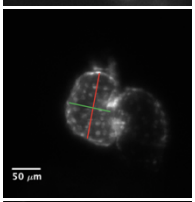	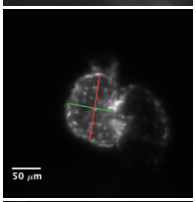	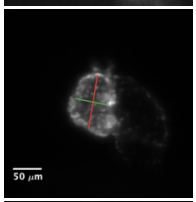
3 dpf Mar 3, 2020 (#2)	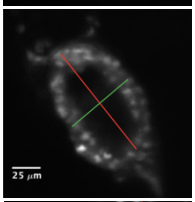	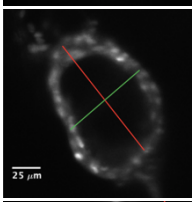	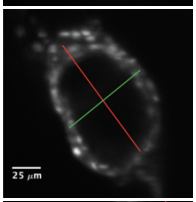	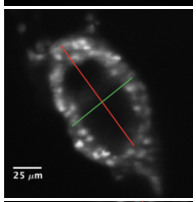
4 dpf Mar 4, 2020	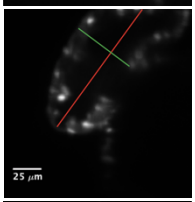	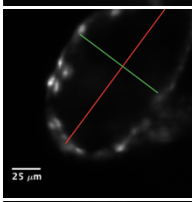	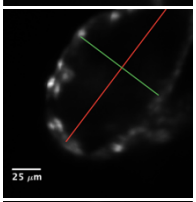	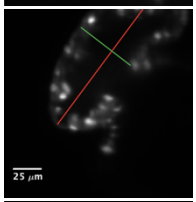
4 dpf Jun 1, 2020	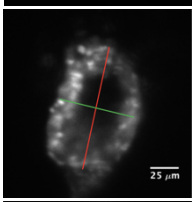	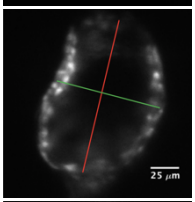	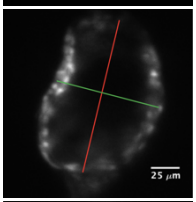	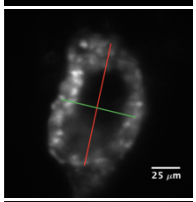
4 dpf Nov 3, 2019	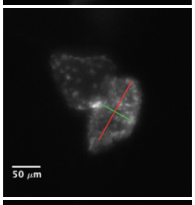	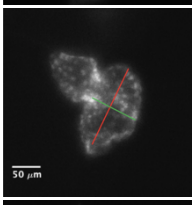	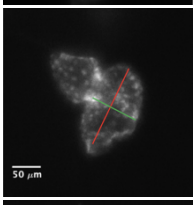	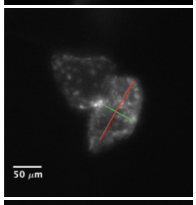
5 dpf Nov 4, 2019	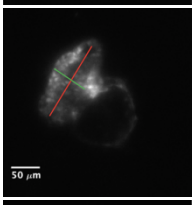	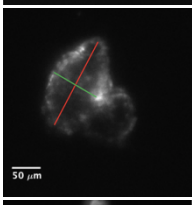	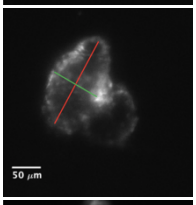	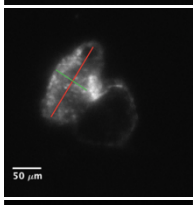
5 dpf Feb 26, 2020	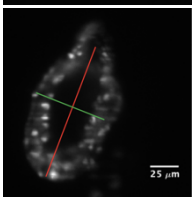	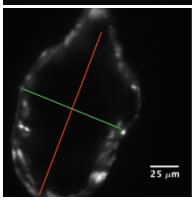	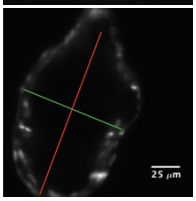	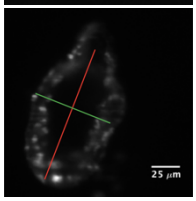

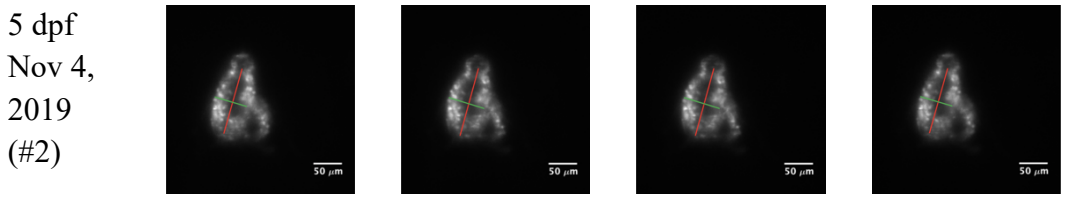

Fig S1: Lengths of major axis and two minor axes of the ventricle were measured at states 1, 2, 3, 4 from zebrafish embryos at 3, 4, 5 days post fertilization (dpf) groups. Red line: Length of major axis, Green line: Length of minor axis. **State 1:** End of isovolumic relaxation, **State 2:** End diastole, **State 3:** End of isovolumic contraction, **State 4:** End systole

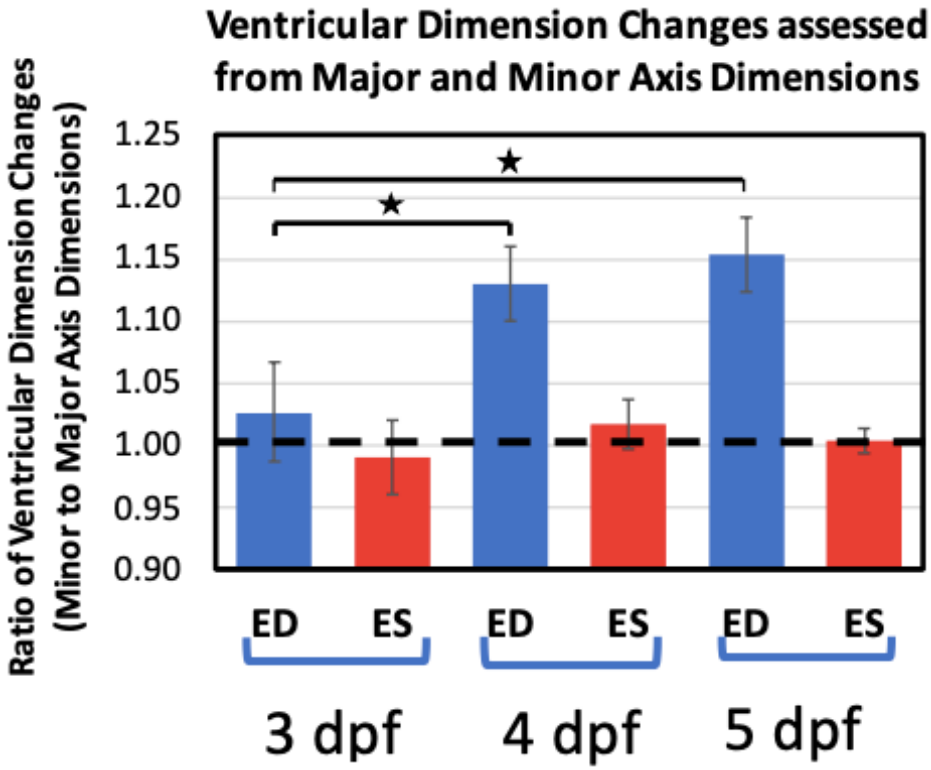

Fig S2: Comparison of changes in ventricular dimension at end diastole and end systole during a cardiac cycle of developing zebrafish heart at 3-, 4- and 5-days post fertilization (dpf). Using the dimensions at end of isovolumic relaxation as reference, changes in dimensions of major axis and averaged minor axes were calculated at ED and ES and ratios of these changes were computed. **ED:** End Diastole, **ES:** End Systole. Statistically significant differences are denoted by *.

CHAPTER 4

MAPPING OF VENTRICULAR WALL DEFORMATION OF THE DEVELOPING HEART OF ZEBRAFISH

Introduction

Unique features of zebrafish including high fertility, rapid development of organs, external fertilization, ease of genetic manipulation, optical transparency and relatively low cost of maintenance has led to its emergence as a popular model organism for biomedical research (*28, 67*). Researchers have used embryonic zebrafish to study cardiovascular development and diseases including congenital heart defects, cardiomyopathy and arrythmia (*8, 9, 29, 49, 67, 70*). Zebrafish hearts develop following the same steps as the human heart in spite of only having systemic circulation. After formation as a hollow linear tube, the developing heart undergoes a remarkable transformation in terms of morphogenesis and mechanical properties (*5*). The developing heart starts to pump blood well before the completion of its structure, implying that early function of the heart affects its own development (*4*). Relatively few studies have explored the functional aspects of cardiac development in zebrafish (*36, 37*).

Volume-based parameters such as stroke volume, cardiac output and ejection fraction are generally used to evaluate the overall function of the heart. The ejection of blood occurs as a result of deformation of the ventricle. As the ventricle lacks homogeneity with respect to local shape, tissue composition, activation and perfusion, regional evaluation of deformation is required to quantify regional function. Through the cardiac cycle, the heart undergoes complex three-dimensional deformation, which can be quantified in terms of ventricular wall strain. Multi-dimensional deformations can be described by principal strain analysis which identifies the effective directions along which strains develop as well as the magnitude of the strains (*41*). Many of the studies from mammals, chicken, etc. are based on thick-walled model of the ventricle where transmural changes in myofibers play important role in the resulting anisotropic deformation.

In our previous study, we developed a method to quantify the regional deformation of the ventricular myocardial wall of embryonic zebrafish in terms of regional area ratios and in plane principal stretches. Fluorescing cardiomyocyte nuclei of a transgenic variety of zebrafish served as markers and the changes in their three-dimensional position during the cardiac cycle enabled estimation of regional deformation in the equatorial and outflow regions on the free outer wall of developing ventricle at 3-, 4- and 5-days post fertilization (dpf). Our results did not indicate significant differences in regional area ratios but with development from 3 to 5 dpf, the deformation became anisotropic favoring the latitudinal direction. Here, we extend our previous study and create a map of regional deformation by moving along the circumference from the outer wall to the inner wall at two different axial positions: the equatorial plane and the outflow plane. Hearts of zebrafish embryos were imaged at 3, 4 and 5 dpf using selective plane illumination microscopy (SPIM) and the ventricular wall deformation was reconstructed.

Trajectories of trio of fluorescing myocyte nuclei were constructed at each region which allowed estimation of area changes, principal stretches, and the degrees of anisotropic deformation. This mapping of regional deformation will allow assessment of the coordination of regions in the mechanical function of the ventricle as a pressure-generating pump and facilitate the examination of the changing deformation characteristics through development from 3 to 5 dpf.

Materials and Methods

Using the method that we developed to characterize the regional deformation of the developing ventricular myocardium of zebrafish by tracking the moving three-dimensional coordinates of the fluorescing cardiomyocyte nuclei through cardiac cycles, mapping of ventricular wall deformation of zebrafish hearts at 3, 4 and 5 dpf was accomplished. The main steps of the procedures were preparation of zebrafish embryos for imaging, reconstruction of 4-D images of the beating heart of zebrafish embryo, segmentation and tracking of myocyte nuclei from the images and computation of regional deformation by strain analysis (described in detail in chapter 3).

Preparation of zebrafish embryos for imaging

Embryos were obtained from fertilized eggs collected from adult zebrafish that were bred and maintained at the UTA animal care facility and experiments were performed in compliance with our Institutional Animal Care and Use Committee (IACUC) protocols. Transgenic zebrafish embryos Tg(*cmlc2:* nuc – egfp) at 3, 4 and 5 dpf expressing enhanced green fluorescent protein (eGFP) in cardiomyocyte nuclei were used in this study. Transparency of zebrafish embryos incubated at 28^0C, was maintained by addition of 0.003% phenylthiourea (PTU) to the E3 medium at 20 hours post fertilization (hpf) that suppressed pigmentation (*53*). Before capturing images, embryos were anesthetized in 0.05% tricaine and immersed in 0.5% low melting point agarose, that have refractive indices similar to that of water and biological tissue. The embryos immersed in melted agarose were then transferred to fluorinated ethylene propylene (FEP) tube to provide a physiological environment in which optical clarity for fluorescence imaging was established.

4-D images of the beating heart of zebrafish embryo

Using SPIM, a light sheet fluorescence microscopy technique, images of the transgenic zebrafish hearts were acquired with high spatial and temporal resolution. In SPIM, a thin volume of the sample around the focal plane of the detection objective lens, is illuminated from the side by a focused thin sheet of laser light (*71*). The sample is placed at the intersection of the illumination and the detection axes which are orthogonal to each other. The emitted light from the fluorophores in the focal plane of the detection objective lens is collected by the detection optics and forms the image. Excitation for gfp signal was provided by 473 nm laser light and a 20X water dipping objective lens (NA = 0.5) was used for detection. For acquisition of dynamic 3D volumes, the sample was moved along the detection axis at a fixed step size of 0.65 μm and slice sequences of transgenic zebrafish Tg*(cmlc2:* nuc - egfp) heart were captured from the rostral to the caudal end, at 3, 4 and 5 dpf. Each slice sequence consisted of 300 frames (512 x 512 pixels), imaged at 10 milliseconds exposure time per frame and 150 – 280 overlapping z-slices were recorded using a digital camera (Hamamatsu, ORCA Flash 4.0 sCMOS). 4D images were reconstructed from the slice sequences afterwards with voxel size of 0.325 x 0.325 x 0.65 μm^3. The image acquisition process was controlled by a code written in LABVIEW (National Instruments). As the zebrafish embryo is embedded in aqueous media during imaging, there are higher possibilities for spherical aberrations if air objectives are used for detection. Water dipping objectives help to eliminate spherical aberrations by minimizing refractive index mismatch. The higher numerical aperture of the water-dipping objective improved the resolution of the images that aided in tracking individual cardiomyocytes. Because of the difficulty of gating the acquisition for a very small organism like zebrfish embryo, slice sequences were acquired in a non-gated manner. The acquired slice sequences were then processed with our

previously developed software (*9, 29*). A MATLAB (MathWorks) code was used to rearrange the slice sequences by post acquisition synchronization (*54*).

Segmentation and tracking of myocyte nuclei

Using a MATLAB (MathWorks) code, the myocyte nuclei were segmented at each time point from the reconstructed 4D images by noise reduction, contrast enhancement and application of a threshold and watershed transform. For tracking segmented cardiomyocytes through the cardiac cycle, a MATLAB (MathWorks) code (John C. Crocker, University of Chicago) was adapted. Using the centroids of the segmented nuclei as their locations in 3D space, the code considered all possible identifications of the old positions with the new positions and chose that identification which provided the minimal total squared displacement. Trajectories of cardiomyocytes, providing their three-dimensional motion in ground coordinates, were stored for analyzing myocardial deformation.

Analyzing regional deformation

For mapping of ventricular wall deformation, we divided the ventricular surface into 8 sub-regions to systematically examine the differences in deformation characteristics along circumferences at different axial positions and the differences in three dpf groups. Illustrated in Fig. 1 are the eight ventricular regions analyzed in this study. Four regions along the equatorial plane were studied: 9 o'clock (on the outer wall), 12 o'clock, 6 o'clock and 3 o'clock (on the inner wall or wall shared with the atrium). Similarly, four regions along the outflow tract plane were studied: 9 o'clock (on the outer wall), 12 o'clock, 6 o'clock and 3 o'clock (on the inner wall or wall shared with the atrium).

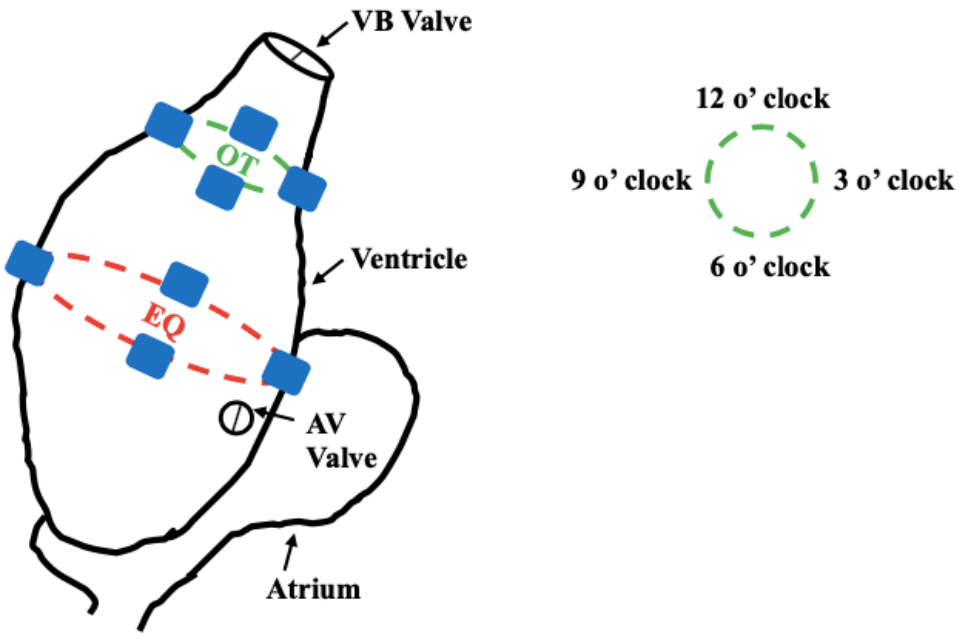

Figure 1: Schematic of embryonic zebrafish heart with blue boxes indicating the regions on the equatorial plane and the outflow tract plane where regional deformation was analyzed. 9 o'clock region is on the outer wall and 3 o'clock region is on the inner wall or wall shared with the atrium. **EQ:** Equatorial, **OT:** Outflow tract.

At early stages of development, ventricular myocardium of zebrafish is one-cell thick and therefore, it was considered as a thin-walled membrane. Three neighboring cardiomyocyte nuclei, which served as markers, were used to characterize the regional deformation of the myocardium through a cardiac cycle. The three markers, forming small triangular region, were used to estimate the magnitudes and directions of in-plane principal stretch under the assumption of homogeneous deformation. The end of isovolumic relaxation was chosen as the reference state (State 1) as it represents the least deformed state of the myocardium. The two principal stretch components λ_1 and λ_2 were presented as ratios relative to their reference values at the end of isovolumic relaxation. At each time point, the area ratio, AR, which is the ratio of the area of the marker triangle to the reference area at the end of isovolumic relaxation was also computed. A MATLAB (MathWorks) code was used for analyzing deformation.

Statistical Analysis

Results of area ratio (*AR*), ratio of principal stretch components (λ_2/λ_1) at end diastole were expressed as mean ± SD (n = 3) for each of the eight analyzed regions in 3, 4 and 5 dpf groups. Regional differences in *AR* and (λ_2/λ_1) ratio at ED were tested by one-way ANOVA test. Tukey's multiple comparison test was performed when significant difference was detected. Differences in *AR* and (λ_2/λ_1) ratio at State 2 (ED) between corresponding regions of the upper ring and the center ring were analyzed by two sample *t*-test. Statistical tests were carried out in ***R*** (https://www.r-project.org/) and $p < 0.05$ was considered as statistically significant.

Results

At each of the studied regions of the ventricle, principal directions were expressed relative to the anatomical latitude reference line (*ALR*) with λ_2 being the principal stretch component acting near the latitudinal direction and λ_1 being the principal stretch component acting near the longitudinal direction. Results for *AR* of the analyzed regions along the upper ring and along the center ring are summarized with statistics in Figs. 2, 3, 4 for embryonic zebrafish at 3, 4, and 5 dpf, respectively. In Fig. 5, *AR* of the corresponding regions along the upper ring and along the center ring are compared. Results for regional anisotropic deformation of the myocardium in 3, 4 and 5 dpf groups are presented in Figs. 6 and 7 for the upper ring and the center ring respectively. The degree of anisotropic deformation between analogous regions of the upper ring and the center ring are compared in Fig. 8.

Area Ratios at 3 dpf (Fig. 2)

For the upper ring of 3 dpf embryos, *AR* at ED were found to be 1.6 ± 0.07, 1.55 ± 0.02, 1.54 ± 0.05 and 1.35 ± 0.02 at 9 o'clock, 12 o'clock, 6 o'clock and 3 o'clock regions respectively. The corresponding values of end diastolic *AR* were 1.63 ± 0.07, 1.57 ± 0.08, 1.57 ± 0.07 and 1.34 ± 0.04, for the center ring. In both the upper and the center ring, 3 o'clock region had a significantly lower *AR* compared to the other three regions.

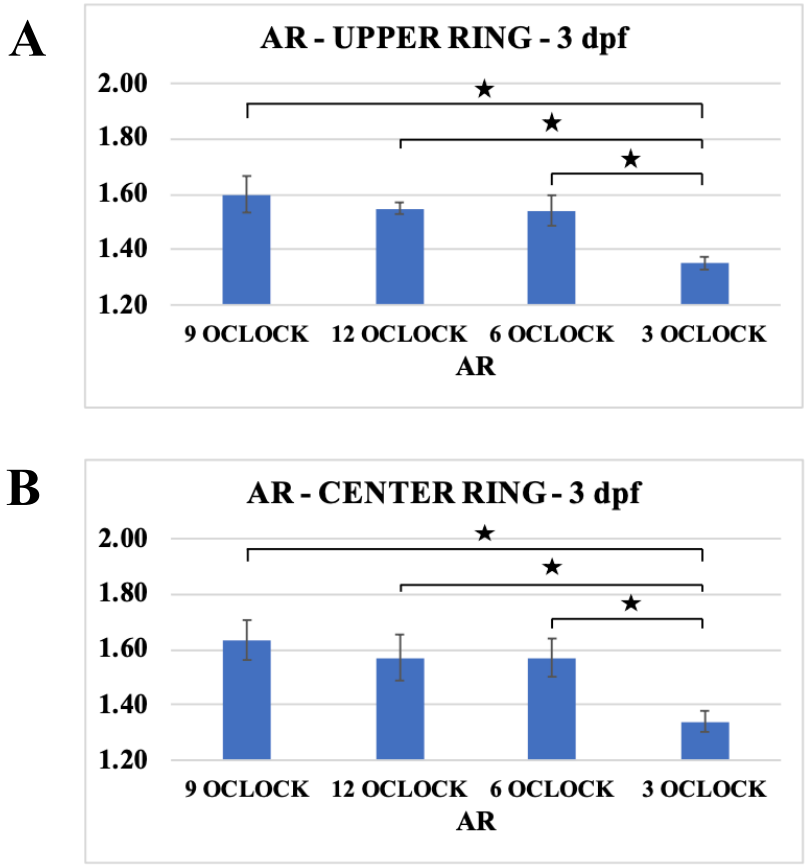

Figure 2: Comparison of regional area ratios at end diastole during a cardiac cycle at 9 o'clock, 12 o'clock, 6 o'clock and 3 o'clock regions along **A)** Upper ring, **B)** Center ring of developing zebrafish heart at 3 days post fertilization (dpf). **AR:** Area Ratio. Statistically significant differences are denoted by *.

Area Ratios at 4 dpf (Fig. 3)

From 4 dpf embryos, end diastolic *AR* were found to be 1.63 ± 0.06, 1.55 ± 0.05, 1.55 ± 0.04 and 1.36 ± 0.02 at 9 o'clock, 12 o'clock, 6 o'clock and 3 o'clock regions of the upper ring respectively. For the center ring, the corresponding values of *AR* at ED were 1.67 ± 0.07, 1.59 ± 0.04, 1.59 ± 0.04 and 1.36 ± 0.02. Similar to the 3 dpf group, *AR* at 3 o'clock region was significantly lower for both the upper and the center ring.

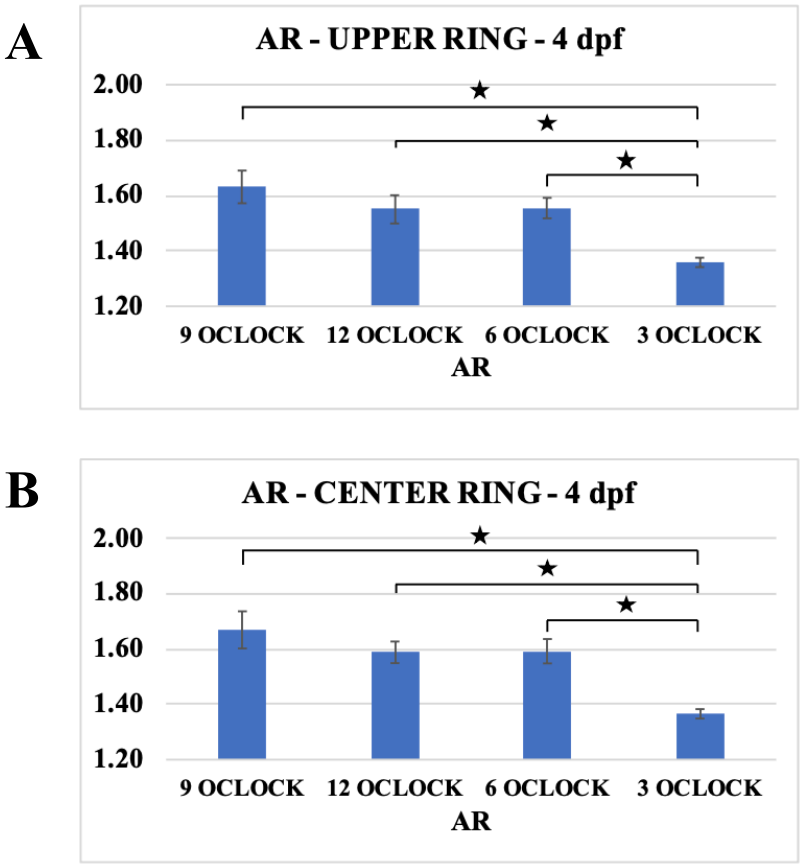

Figure 3: Comparison of regional area ratios at end diastole during a cardiac cycle at 9 o'clock, 12 o'clock, 6 o'clock and 3 o'clock regions along **A)** Upper ring, **B)** Center ring of developing zebrafish heart at 4 days post fertilization (dpf). **AR:** Area Ratio. Statistically significant differences are denoted by *.

Area Ratios at 5 dpf (Fig. 4)

For the 5 dpf group, end diastolic *AR* at 9 o'clock, 12 o'clock, 6 o'clock and 3 o'clock regions of the upper ring were found to be 1.6 ± 0.05, 1.54 ± 0.03, 1.54 ± 0.05 and 1.36 ± 0.03 respectively. The corresponding values of *AR* at the center ring were 1.64 ± 0.05, 1.56 ± 0.06, 1.57 ± 0.03 and 1.37 ± 0.03. Like the 3 dpf and 4 dpf groups, 3 o'clock regions of both the upper and the center ring exhibited significantly lower *AR* than the other regions.

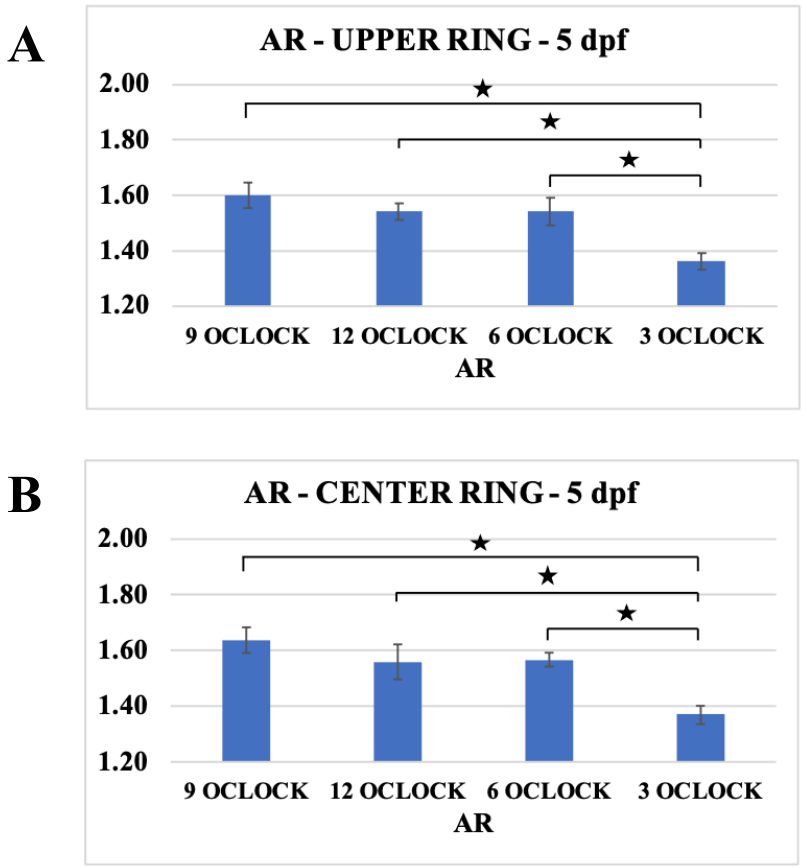

Figure 4: Comparison of regional area ratios at end diastole during a cardiac cycle at 9 o'clock, 12 o'clock, 6 o'clock and 3 o'clock regions along **A)** Upper ring, **B)** Center ring of developing zebrafish heart at 5 days post fertilization (dpf). **AR:** Area Ratio. Statistically significant differences are denoted by *.

Area Ratios: Upper Ring vs Center Ring (Fig. 5)

Comparison of regional *AR* between analogous regions of the upper ring and the center ring did not reveal statistically significant difference for the 3 dpf group. Similar trends were observed at 4 and 5 dpf with absence of significant difference between corresponding regions of the upper ring and the center ring.

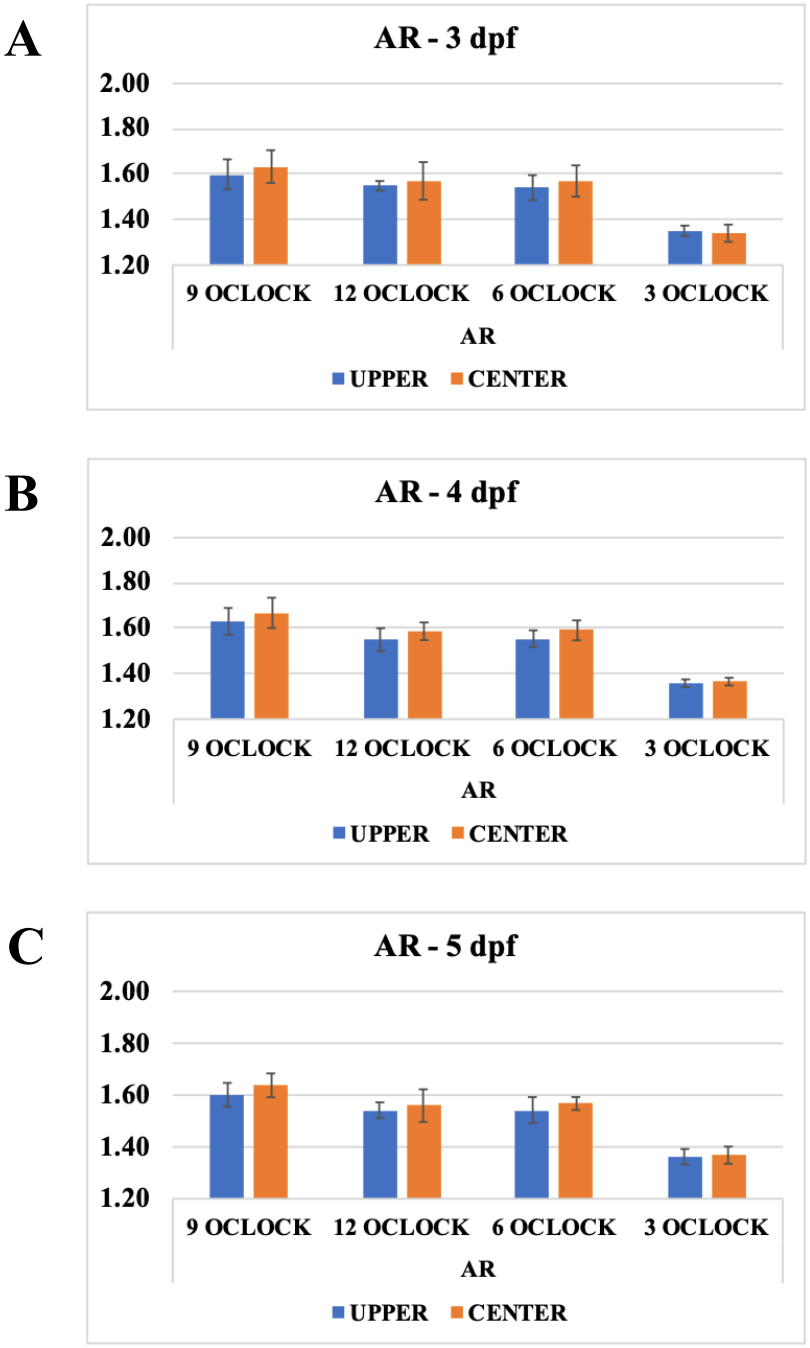

Figure 5: Regional end diastolic area ratios at corresponding 9 o'clock, 12 o'clock, 6 o'clock and 3 o'clock regions of the upper ring and center ring of developing zebrafish heart at **A)** 3, **B)** 4 and **C)** 5 days post fertilization (dpf). **AR:** Area Ratio.

Anisotropic deformation responses (Figs. 6, 7)

Anisotropy of deformation was quantified in terms of the ratio of λ_2 to λ_1 for each analyzed region at end diastole (State 2) for each of 3, 4 and 5 dpf groups. For the upper ring of 3 dpf embryos, (λ_2/λ_1) ratio at ED were found to be 1.046 ± 0.025, 1.041 ± 0.022, 1.047 ± 0.024 and 1.09 ± 0.024 at 9 o'clock, 12 o'clock, 6 o'clock and 3 o'clock regions, respectively. The corresponding values of end diastolic (λ_2/λ_1) ratio were 1.096 ± 0.023, 1.113 ± 0.019, 1.104 ± 0.019 and 1.15 ± 0.005 at 4 dpf and 1.099 ± 0.022, 1.107 ± 0.022, 1.107 ± 0.019 and 1.153 ± 0.013 at 5 dpf.

At 9 o'clock, 12 o'clock, 6 o'clock and 3 o'clock regions along the center ring, (λ_2/λ_1) ratio at ED were 1.04 ± 0.024, 1.043 ± 0.02, 1.043 ± 0.028 and 1.135 ± 0.028, respectively, for the 3 dpf group. At 4 and 5 dpf, the analogous values were 1.158 ± 0.015, 1.16 ± 0.018, 1.162 ± 0.014, 1.2 ± 0.005 and 1.203 ± 0.003, 1.192 ± 0.005, 1.192 ± 0.008, 1.21 ± 0.019. For the center ring of 3 and 4 dpf groups, end diastolic (λ_2/λ_1) ratio at region is significantly higher than the other three regions. But such regional difference is not observed for the center ring at 5 dpf.

Anisotropic deformation: Upper Ring vs Center Ring (Fig. 8)

Equivalent regions of the upper ring and the center ring did not differ significantly in terms of regional end diastolic (λ_2/λ_1) ratio for the 3 dpf group. However, from the 4 dpf embryos, regions along the center ring were found to have significantly higher (λ_2/λ_1) ratio at ED. This trend in anisotropic deformation also existed at 5 dpf with the center ring displaying higher degree of anisotropy.

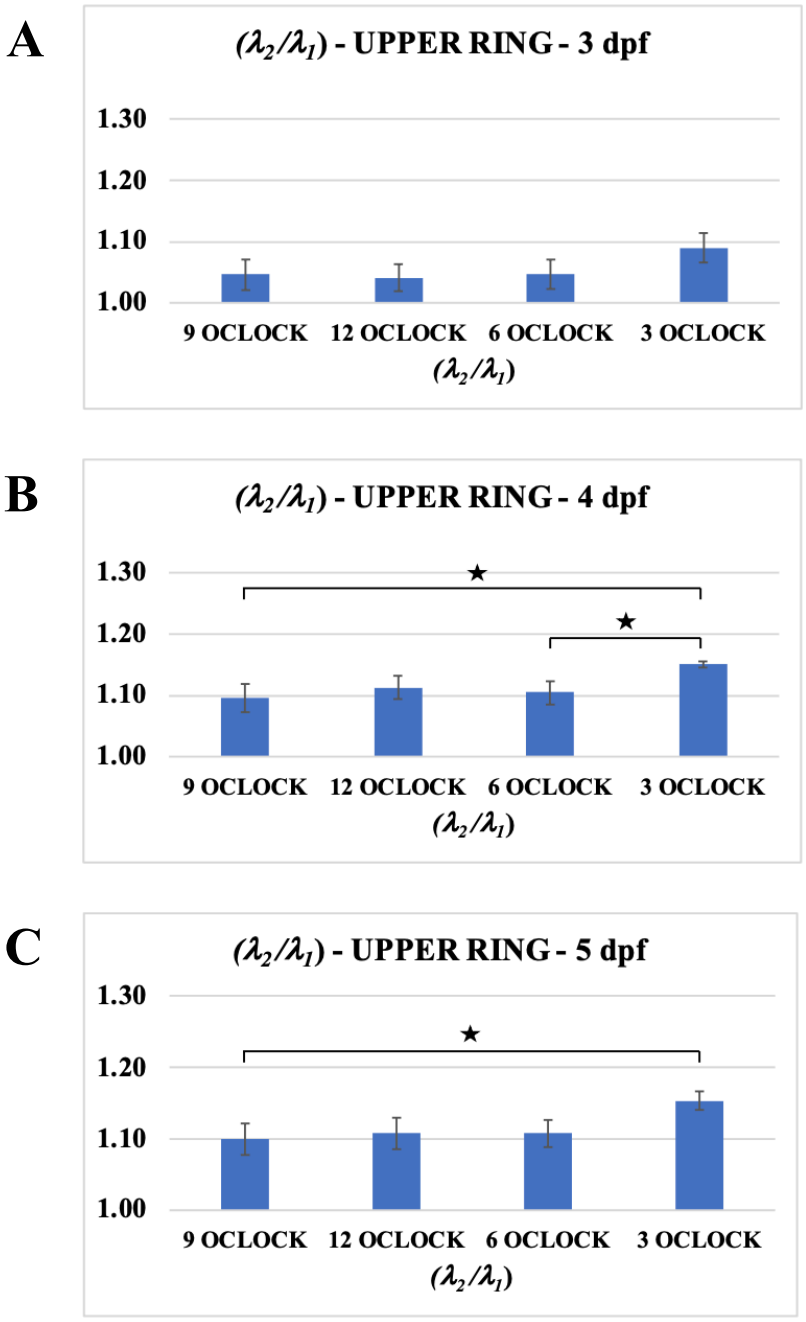

Figure 6: Comparison of ratios of principal stretch components λ_2 to λ_1 at end diastole during a cardiac cycle at 9 o'clock, 12 o'clock, 6 o'clock and 3 o'clock regions along the upper ring of developing zebrafish heart at **A)** 3, **B)** 4 and **C)** 5 days post fertilization (dpf). Statistically significant differences are denoted by *.

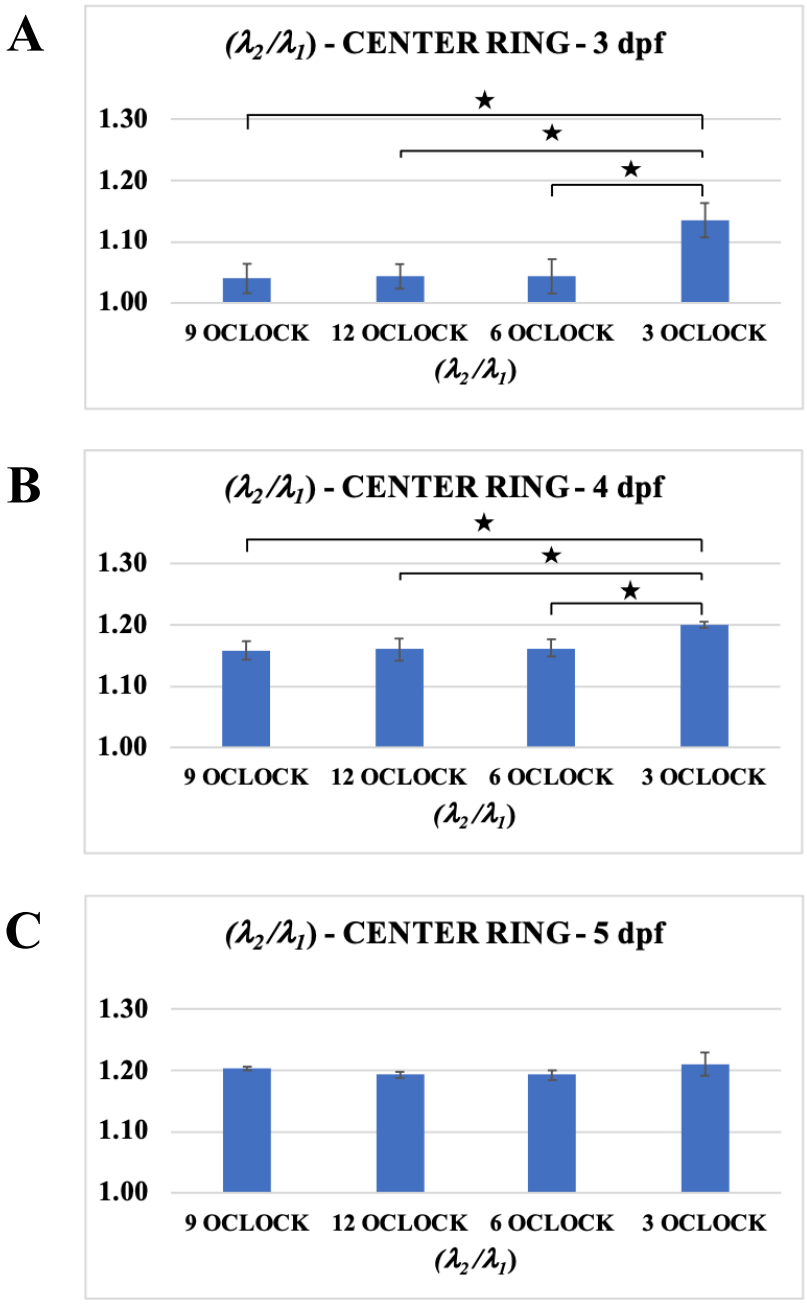

Figure 7: Comparison of ratios of principal stretch components λ_2 to λ_1 at end diastole during a cardiac cycle at 9 o'clock, 12 o'clock, 6 o'clock and 3 o'clock regions along the center ring of developing zebrafish heart at **A)** 3, **B)** 4 and **C)** 5 days post fertilization (dpf). Statistically significant differences are denoted by *.

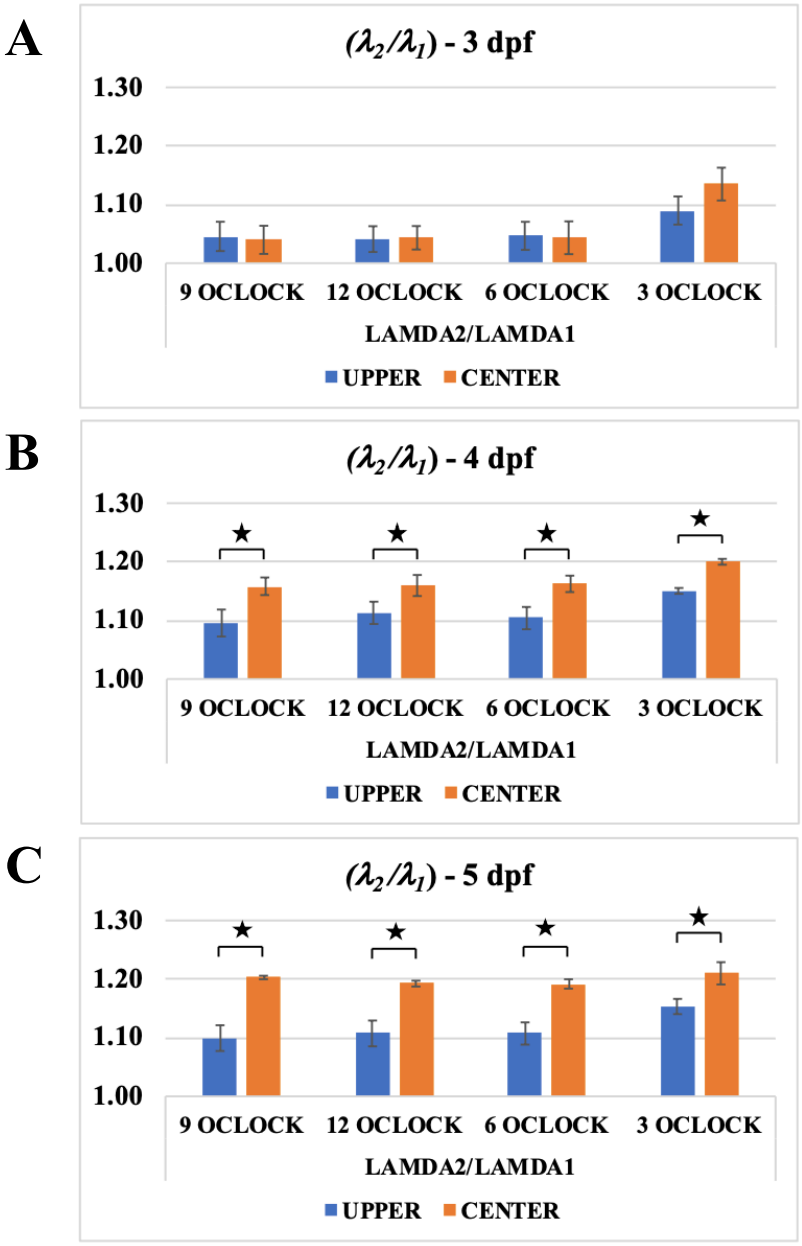

Figure 8: Ratios of principal stretch components λ_2 to λ_1 at corresponding 9 o'clock, 12 o'clock, 6 o'clock and 3 o'clock regions of the upper ring and center ring of developing zebrafish heart at **A)** 3, **B)** 4 and **C)** 5 days post fertilization (dpf). Statistically significant differences are denoted by *.

Discussion

To quantify the function of the developing heart, various parameters including intra-ventricular pressure (*32, 34, 35, 57*), cardiac output (*34, 35, 37*) and ventricular dimensions (*57*) have been used. As these indicators provide a measure of the overall function, assessment of regional function is desired to unravel potential regional differences in deformation. Regional ventricular function has been studied in mature animals by implanting radiopaque metallic beads and analyzing regional myocardial deformation by tracking the position of the beads through cardiac cycles (*73, 75, 80, 81*). Two-dimensional finite deformation of the developing ventricle of chicken embryo has been investigated at different Hamburger-Hamilton (*78*) stages by placing microspheres on the epicardial surface (*12, 76, 82*).

In this study, we used our previously developed method for quantifying regional ventricular wall deformation of zebrafish embryo and mapped the deformation of regions along the circumference at different axial positions. By tracking the three-dimensional positions of fluorescing myocyte nuclei in reconstructed 4D images of the beating heart of zebrafish embryo, we estimated the regional deformation through the cardiac cycles.

Changes in ventricular wall deformation pattern from isotropic to chamber specific anisotropic over the course of cardiac development has been reported for chick embryos (*12*). In another study on embryonic chick heart, the authors examined regional epicardial strain during the early phase of cardiac looping (*82*). Regional differences, in terms of longitudinal strain, were detected near the inner curvature which elongated by 5-10 % during systole (*82*). Assessment of regional finite strains in mature canine left ventricle revealed that the magnitude of end diastolic and end systolic strains is of the same level for anterior and posterior walls but the principal directions are different (*83*).

Our results indicated that *AR* continues to decrease along the latitude from 9 o'clock through 12 and 6 o'clock to 3 o'clock region. *AR* at 12 and 6 o'clock regions are of the same level. Although the *AR* at 9 o'clock region is slightly higher than that at 12 and 6 o'clock regions, the difference is not significant statistically. However, *AR* at 3 o'clock region is significantly lower than those at 9, 12 and 6 o'clock regions. These trends are observed in all 3 groups (3, 4 and 5 dpf) for both the upper and center ring. It appears that *AR* at 9, 12 and 6 o'clock regions which are on the free (outer) wall of the ventricle are of the same level. On the other hand, *AR* at 3 o'clock region which is on the wall shared by the ventricle and the atrium is much lower.

Inspection of regional *AR* of equivalent regions of 3 dpf embryos from the upper ring and the center ring did not indicate the presence of significant difference. For 4 and 5 dpf groups also, analogous regions of the upper ring and the center ring did not exhibit significant difference in terms of regional *AR*. However, as the anisotropic deformation responses of corresponding regions of the upper ring and the center ring were compared in terms of the index, end diastolic (λ_2/λ_1) ratios, differences were detected. For 4 dpf embryos, regions on the center ring consistently had higher values of (λ_2/λ_1) ratio than those on the upper ring. This trend continued at 5dpf with the difference between the center ring and the upper ring becoming greater. But such difference in anisotropic deformation was not observed for 3 dpf group. With development of the ventricular myocardial wall, regions on the center ring undergo a higher degree of anisotropic deformation.

From the center ring of 3 dpf group, the index for anisotropic deformation, end diastolic (λ_2/λ_1) ratios at 9, 12 and 6 o'clock regions are of the same level at ~ 1.04. The (λ_2/λ_1) ratio at ED at 3 o'clock region is much higher and significantly different than those at 9, 12 and 6 o'clock regions. At 4 dpf, the end diastolic (λ_2/λ_1) ratios at 9, 12 and 6 o'clock regions along the

center ring are again of the same level but have increased to a much higher value of ~ 1.16. The ratio at 3 o'clock region has also increased and is still significantly higher than those at 9, 12 and 6 o'clock regions. At 5 dpf, the end diastolic (λ_2/λ_1) ratios at 9, 12 and 6 o'clock regions along the center ring have further increased to the level of ~ 1.2. However, the ratio at 3 o'clock region increased by a small amount and is no longer significantly different than those at 9, 12 and 6 o'clock regions. This suggests that through development from 3 to 4, 5 dpf, the anisotropic response becomes more prominent in the regions on the outer wall compared to regions on the inner wall.

Conclusions

We created a map of the regional ventricular wall deformation of developing zebrafish hearts at 3, 4, 5 dpf. Differences among 9 o'clock, 12 o'clock, 6 o'clock and 3 o'clock regions along the circumference and between corresponding regions of the upper ring and the center ring were examined in terms of *AR* and the index for anisotropic deformation, end diastolic (λ_2/λ_1) ratio. We also assessed their evolving changes through the development from 3 to 4 and 5 dpf. *AR* at 3 o'clock region is much lower than the other three regions on the free ventricular wall. Between analogous regions of the upper ring and the center ring, *AR* did not differ for any of the dpf groups. For 4 and 5 dpf embryos, regions on the center ring exhibited higher values of (λ_2/λ_1) ratio than those on the upper ring. At 5 dpf, the regional difference in (λ_2/λ_1) ratio at the center ring disappeared. Overall, our results suggest an increasingly anisotropic deformation of regions on the outer wall with ventricular development from 3 to 4, 5 dpf.

CHAPTER 5

Discussion

Functional aspects of heart development in zebrafish have been analyzed in a small number of studies. Intra-ventricular pressure of embryonic zebrafish heart has been reported by Hu *et al* and Kopp *et al*. Bagatto *et al* analyzed the changes in heart rate, stroke volume and cardiac output with the development of the heart. In our study, we analyzed the changes in overall & regional function of the ventricle through developmental stages. We constructed the first pressure-volume loop model for the embryonic zebrafish heart which enabled estimation of the stroke work of the developing ventricle for the first time. Our analysis of the changing hemodynamic parameters indicated that peak systolic ventricular pressure, stroke volume, cardiac output, stroke work, cardiac power significantly increases while total peripheral resistance significantly decreases over the development from 3 to 5 days post fertilization (dpf). Mechanical performance of the developing heart of zebrafish improves from 3 to 4 and 5 dpf with maturation of valves, changes in morphology and increasing complexity of the vascular network.

Generation of ventricular pressure and resulting cardiac output of a developing heart is the effect of synchronized motion of cardiomyocytes in the ventricular wall collectively. To understand how the cyclic deformation of ventricular wall myocardium contribute to the improving mechanical performance of the heart at different stages of development, we characterized the regional deformation of ventricular wall of zebrafish embryos through cardiac cycles in terms of regional area ratios and principal stretches. We also estimated the passive

deformation properties of the ventricle during the filling phase, and the active contractile function during ejection. Using selective plane illumination microscopy (SPIM), we reconstructed the deformation of the ventricular wall of embryonic zebrafish *in vivo* at 3-, 4- and 5-days post fertilization (dpf). By tracking the motion of three neighboring fluorescing myocyte nuclei of the ventricular myocardium, we quantified the deformation in the equatorial, apex and outflow regions of zebrafish ventricle. Our results reveal that at 4 and 5 dpf, principal stretch along the latitudinal direction is significantly larger than the principal stretch along the longitudinal direction suggesting anisotropic deformation. The compliance of ventricular myocardium is significantly lower at 4, 5 dpf that that at 3 dpf, indicating an increase in myocardial stiffness through development. Higher systolic performance index at 4 and 5 dpf suggested their higher capacity to generate higher ventricular pressure at faster rates during contractile ejection.

Using our developed method for estimation of regional deformation, we created a map of deformation at regions along the circumference at different axial positions. This mapping of regional ventricular wall deformation revealed not only the regional differences in area ratio and degree of anisotropy but also the tethering effects due to the presence of AV valve and its opening closure through a cardiac cycle when regulating blood flow.

Results from these studies help us to understand the increasing efficiency of the early-stage zebrafish heart occurring in time with changes in valve development, chamber morphology and increasing complexity of the vascular network. Physiological measurements from these studies will be beneficial to phenomics efforts and facilitate translational relevance of the zebrafish model.

Limitations

In our study, different zebrafish embryos of the same age group were used for capturing images of the heart for ventricular volume computation and measurement of intra-ventricular pressure. Data of intra-ventricular pressure and ventricular volume were synchronized later for generation of pressure-volume loops. Similarly, separate embryonic zebrafish of a different transgenic variety and of the same dpf group were utilized for acquisition of images for regional deformation estimation. Data of regional area ratios and intra-ventricular pressure were synchronized afterwards for estimating performance of the developing ventricle. It was not possible to measure intra-ventricular pressure and acquire SPIM images of the heart simultaneously due to different sample mounting requirements of servo null micro pressure measurement system and SPIM imaging. Development of techniques to simultaneously image the motion of the beating heart and to record intra-ventricular pressure will facilitate quantification of mechanical properties with greater ease.

Future Studies

The maximum shortening of the sarcomere, the contractile unit of the myocardium, is about 10 – 15 % (*31*). However, the complex three-dimensional organization of myofibers in the myocardium results in blood ejection fraction of ~ 50 – 60%. In zebrafish, sarcomeres have formed by 2 dpf and synchronized beats of the heart tube have replaced peristaltic waves (*84*). The developmental increase in the stiffness of cardiac muscle of chick embryo has been related to higher expressions of certain proteins: actomyosin contractile proteins, sarcoplasmic calcium channel SERCA and collagen I (*77*). Cardiac titin, the largest known cytoskeletal protein, affects

diastolic function of the heart by contributing to passive tension resulting from stretch (*85, 86*). Our results of *VC* and *SPI* suggest an increase in expressions of contractile proteins and collagen with the development of zebrafish heart. To establish the molecular basis, future studies on mechanical properties of embryonic zebrafish heart can explore the expression trends of myofibrillar proteins.

Previous studies on mature hearts have related ventricular wall deformation with transmural myofiber orientation (*75, 80*). Smaller variation in principal direction compared to transmural variation in fiber direction has been reported (*75*). The architecture of the embryonic ventricle is different from the adult heart as the ventricular wall is predominantly trabecular with a thin compact layer. Tobita et al (*87*) analyzed the myofiber architecture of developing left ventricle of chick embryos and found that in the compact myocardium, the orientation of transmural myofiber angles was circumferential at early stages and shifted to more longitudinal direction in the outer compact myocardium at later stages of development. In zebrafish, formation of trabeculae starts around 60 hpf (*19*) and trabeculation progresses through 3 to 5 dpf. Based on our results of increasingly anisotropic deformation pattern through development, with latitudinal direction being preferred, it is likely that a circumferential fiber orientation also develops in the compact myocardium layer. Future studies can determine the transmural distribution of myofiber direction in developing zebrafish to identify relationship with ventricular deformation.

REFERENCES

1. M. Weber, J. Huisken, In vivo imaging of cardiac development and function in zebrafish using light sheet microscopy. *Swiss medical weekly* **145**, w14227 (2015).
2. B. Bijnens, M. Cikes, C. Butakoff, M. Sitges, F. Crispi, Myocardial motion and deformation: What does it tell us and how does it relate to function? *Fetal diagnosis and therapy* **32**, 5-16 (2012).
3. S. Goenezen, M. Y. Rennie, S. Rugonyi, Biomechanics of early cardiac development. *Biomechanics and modeling in mechanobiology* **11**, 1187-1204 (2012).
4. T. Bartman, J. Hove, Mechanics and function in heart morphogenesis. *Developmental Dynamics* **233**, 373-381 (2005).
5. L. A. Taber, R. Perucchio, Modeling Heart Development. *Journal of Elasticity* **61**, 165-197 (2000).
6. D. Srivastava, Genetic regulation of cardiogenesis and congenital heart disease. *Annual review of pathology* **1**, 199-213 (2006).
7. T. Banjo *et al.*, Haemodynamically dependent valvulogenesis of zebrafish heart is mediated by flow-dependent expression of miR-21. *Nature communications* **4**, 1978 (2013).
8. J. Vermot *et al.*, Reversing Blood Flows Act through klf2a to Ensure Normal Valvulogenesis in the Developing Heart. *PLoS biology* **7**, e1000246 (2009).
9. J. Lee *et al.*, 4-Dimensional light-sheet microscopy to elucidate shear stress modulation of cardiac trabeculation. *J Clin Invest* **126**, 3158 (2016).
10. E. Steed, F. Boselli, J. Vermot, Hemodynamics driven cardiac valve morphogenesis. *Biochim Biophys Acta* **1863**, 1760-1766 (2016).

11. J. R. Hove *et al.*, Intracardiac fluid forces are an essential epigenetic factor for embryonic cardiogenesis. *Nature (London)* **421**, 172-177 (2003).

12. K. Tobita, B. B. Keller, Right and left ventricular wall deformation patterns in normal and left heart hypoplasia chick embryos. *American journal of physiology. Heart and circulatory physiology* **279**, H959-H969 (2000).

13. L. A. Taber, Mechanical aspects of cardiac development. *Progress in Biophysics and Molecular Biology* **69**, 237-255 (1998).

14. D. A. Voronov, P. W. Alford, G. Xu, L. A. Taber, The role of mechanical forces in dextral rotation during cardiac looping in the chick embryo. *Developmental biology* **272**, 339-350 (2004).

15. J. B. Caulfield, T. K. Borg, The collagen network of the heart. *Laboratory investigation* **40**, 364 (1979).

16. K. Kamino, A. Hirota, S. Fujii, Localization of pacemaking activity in early embryonic heart monitored using voltage-sensitive dye. *Nature* **290**, 595-597 (1981).

17. J. Männer, L. Thrane, K. Norozi, T. M. Yelbuz, In vivo imaging of the cyclic changes in cross-sectional shape of the ventricular segment of pulsating embryonic chick hearts at stages 14 to 17: A contribution to the understanding of the ontogenesis of cardiac pumping function. *Developmental Dynamics* **238**, 3273-3284 (2009).

18. G. del Monte-Nieto *et al.*, Control of cardiac jelly dynamics by NOTCH1 and NRG1 defines the building plan for trabeculation. *Nature (London)* **557**, 439-445 (2018).

19. S. J. Rasouli, D. Y. R. Stainier, Regulation of cardiomyocyte behavior in zebrafish trabeculation by Neuregulin 2a signaling. *Nature communications* **8**, 15281 (2017).

20. M. Wagner, M. A. Q. Siddiqui, Signal transduction in early heart development (II): ventricular chamber specification, trabeculation, and heart valve formation. *Experimental biology and medicine (Maywood, N.J.)* **232**, 866 (2007).

21. M. Yang, L. A. Taber, E. B. Clark, A nonliner poroelastic model for the trabecular embryonic heart. *Journal of biomechanical engineering* **116**, 213 (1994).

22. W. W. Burggren, B. B. Keller, Eds., *Development of cardiovascular systems: Molecules to organisms*, (Cambridge University Press, Cambridge, UK, 1997).

23. G. van den Berg, A. F. M. Moorman, Concepts of cardiac development in retrospect. *Pediatric cardiology* **30**, 580-587 (2009).

24. B. Hogers, M. C. DeRuiter, A. C. Gittenberger-de Groot, R. E. Poelmann, Extraembryonic venous obstructions lead to cardiovascular malformations and can be embryolethal. *Cardiovasc Res* **41**, 87-99 (1999).

25. L. Ma, M.-F. Lu, R. J. Schwartz, J. F. Martin, Bmp2 is essential for cardiac cushion epithelial-mesenchymal transition and myocardial patterning. *Development* **132**, 5601-5611 (2005).

26. J. Li *et al.*, The expression profile analysis of NKX2-5 knock-out embryonic mice to explore the pathogenesis of congenital heart disease. *J Cardiol* **66**, 527-531 (2015).

27. B. J. Martinsen, Reference guide to the stages of chick heart embryology. *Dev Dyn* **233**, 1217-1237 (2005).

28. H. C. Yalcin, A. Amindari, J. T. Butcher, A. Althani, M. Yacoub, Heart function and hemodynamic analysis for zebrafish embryos. *Developmental Dynamics* **246**, 868-880 (2017).

29. J. Lee *et al.*, Spatial and temporal variations in hemodynamic forces initiate cardiac trabeculation. *JCI Insight* **3**, (2018).

30. B. Pelster, W. W. Burggren, Disruption of Hemoglobin Oxygen Transport Does Not Impact Oxygen-Dependent Physiological Processes in Developing Embryos of Zebra Fish (Danio rerio). *Circulation research* **79**, 358-362 (1996).

31. E. H. Sonnenblick, J. Ross, J. W. Covell, H. M. Spotnitz, D. Spiro, The Ultrastructure of the Heart in Systole and Diastole: >Changes In Sarcomere Length. *Circulation research* **21**, 423-431 (1967).

32. N. Hu, E. B. Clark, Hemodynamics of the stage 12 to stage 29 chick embryo. *Circulation research* **65**, 1665-1670 (1989).

33. B. B. Keller, J. P. Tinney, N. Hu, Embryonic ventricular diastolic and systolic pressure-volume relations. *Cardiology in the young* **4**, 19-27 (1994).

34. S. Stekelenburg-de Vos *et al.*, Systolic and diastolic ventricular function assessed by pressure-volume loops in the stage 21 venous clipped chick embryo. *Pediatric research* **57**, 16-21 (2005).

35. S. Stekelenburg-de Vos, P. Steendijk, N. T. Ursem, J. W. Wladimiroff, R. E. Poelmann, Systolic and diastolic ventricular function in the normal and extra-embryonic venous clipped chicken embryo of stage 24: a pressure-volume loop assessment. *Ultrasound Obstet Gynecol* **30**, 325-331 (2007).

36. N. Hu, D. Sedmera, H. J. Yost, E. B. Clark, Structure and function of the developing zebrafish heart. *Anat Rec* **260**, 148-157 (2000).

37. B. Bagatto, W. Burggren, A Three-Dimensional Functional Assessment of Heart and Vessel Development in the Larva of the Zebrafish (Danio rerio). *Physiological and biochemical zoology* **79**, 194-201 (2005).

38. J. T. Shin, E. V. Pomerantsev, J. D. Mably, C. A. MacRae, High-resolution cardiovascular function confirms functional orthology of myocardial contractility pathways in zebrafish. *Physiol. Genomics* **42**, 300-309 (2010).

39. G. P. Pedrizzetti *et al.*, Three-Dimensional Principal Strain Analysis for Characterizing Subclinical Changes in Left Ventricular Function. *Journal of the American Society of Echocardiography* **27**, 1041-1050.e1041 (2014).

40. H. Geyer *et al.*, Assessment of Myocardial Mechanics Using Speckle Tracking Echocardiography: Fundamentals and Clinical Applications. *Journal of the American Society of Echocardiography* **23**, 351-369 (2010).

41. S. Timoshenko, J. N. Goodier, *Theory of elasticity*. (McGraw-Hill, New York, ed. 3d, 1969).

42. G. P. Aurigemma, K. H. Silver, M. A. Priest, W. H. Gaasch, Geometric changes allow normal ejection fraction despite depressed myocardial shortening in hypertensive left ventricular hypertrophy. *Journal of the American College of Cardiology* **26**, 195-202 (1995).

43. C. Parsai *et al.*, Toward understanding response to cardiac resynchronization therapy: left ventricular dyssynchrony is only one of multiple mechanisms. *European Heart Journal* **30**, 940-949 (2009).

44. W. W. Burggren, J. F. Santin, M. R. Antich, Cardio-respiratory development in bird embryos: new insights from a venerable animal model. *Revista brasileira de zootecnia* **45**, 709-728 (2016).

45. H. E. Salman, B. Ramazanli, M. M. Yavuz, H. C. Yalcin, Biomechanical Investigation of Disturbed Hemodynamics-Induced Tissue Degeneration in Abdominal Aortic Aneurysms Using Computational and Experimental Techniques. *Frontiers in Bioengineering and Biotechnology* **7**, (2019).

46. Z. Z. Zakaria *et al.*, Using Zebrafish for Investigating the Molecular Mechanisms of Drug-Induced Cardiotoxicity. *Biomed Research International*, (2018).

47. W. W. Burggren, B. Dubansky, N. M. Bautista, in *Fish Physiology,* A. K. Gamperl, T. E. Gillis, A. P. Farrell, C. J. Brauner, Eds. (Academic Press, 2017), vol. 36, pp. 107-184.

48. Y. Moriyama *et al.*, Evolution of the fish heart by sub/neofunctionalization of an elastin gene. *Nat Commun* **7**, 10397 (2016).

49. P. J. Scherz, J. Huisken, P. Sahai-Hernandez, D. Y. Stainier, High-speed imaging of developing heart valves reveals interplay of morphogenesis and function. *Development* **135**, 1179-1187 (2008).

50. S. Gurung, B. Dubansky, C. A. Virgen, G. F. Verbeck, D. W. Murphy, Effects of crude oil vapors on the cardiovascular flow of embryonic Gulf killifish. *Science of The Total Environment* **751**, 141627 (2021).

51. E. Kirkman, Mechanical events and the pressure–volume relationships. *Anaesthesia & Intensive Care Medicine* **19**, 314-317 (2018).

52. K. R. Walley, Left ventricular function: time-varying elastance and left ventricular aortic coupling. *Critical Care* **20**, (2016).

53. M. Westerfield, *The zebrafish book : a guide for the laboratory use of zebrafish (Brachydanio rerio)*. (M. Westerfield, Eugene, OR, 1993).

54. M. Liebling, A. S. Forouhar, M. Gharib, S. E. Fraser, M. E. Dickinson, Four-dimensional cardiac imaging in living embryos via postacquisition synchronization of nongated slice sequences. *Journal of biomedical optics* **10**, 054001-0540010 (2005).

55. V. Messerschmidt *et al.*, Light-sheet Fluorescence Microscopy to Capture 4-Dimensional Images of the Effects of Modulating Shear Stress on the Developing Zebrafish Heart. *Journal of visualized experiments : JoVE*, (2018).

56. S. S. Dhillon *et al.*, Optimisation of Embryonic and Larval ECG Measurement in Zebrafish for Quantifying the Effect of QT Prolonging Drugs. *PLoS ONE* **8**, e60552 (2013).

57. T. Ishiwata, M. Nakazawa, W. T. Pu, S. G. Tevosian, S. Izumo, Developmental Changes in Ventricular Diastolic Function Correlate With Changes in Ventricular Myoarchitecture in Normal Mouse Embryos. *Circulation Research: Journal of the American Heart Association* **93**, 857-865 (2003).

58. R. Kopp, T. Schwerte, B. Pelster, Cardiac performance in the zebrafish breakdance mutant. *J. Exp. Biol.* **208**, 2123-2134 (2005).

59. P. Perrichon, M. Grosell, W. W. Burggren, Heart Performance Determination by Visualization in Larval Fishes: Influence of Alternative Models for Heart Shape and Volume. *Frontiers in Physiology* **8**, (2017).

60. D. Houghton *et al.*, The effect of age on the relationship between cardiac and vascular function. *Mech Ageing Dev* **153**, 1-6 (2016).

61. P. Rombough, The functional ontogeny of the teleost gill: Which comes first, gas or ion exchange? *Comp. Biochem. Physiol. A-Mol. Integr. Physiol.* **148**, 732-742 (2007).

62. P. C. Hou, W. W. Burggren, Cardiac output and peripheral resistance during larval development in the anuran amphibian Xenopus laevis. *Am J Physiol* **269**, R1126-1132 (1995).

63. M. Liebling *et al.*, Rapid three-dimensional imaging and analysis of the beating embryonic heart reveals functional changes during development. *Dev Dyn* **235**, 2940-2948 (2006).

64. L. W. Wang *et al.*, Standardized echocardiographic assessment of cardiac function in normal adult zebrafish and heart disease models. *Disease models & mechanisms* **10**, 63-76 (2017).

65. Z. R. Li *et al.*, Phenylthiourea Specifically Reduces Zebrafish Eye Size. *PLoS ONE* **7**, 14 (2012).

66. W. D. Wang, Y. Wang, H. J. Wen, D. R. Buhler, C. H. Hu, Phenylthiourea as a weak activator of aryl hydrocarbon receptor inhibiting 2,3,7,8-tetrachlorodibenzo-p-dioxin-induced CYP1A1 transcription in zebrafish embryo. *Biochem. Pharmacol.* **68**, 63-71 (2004).

67. D. R. Brown, L. A. Samsa, L. Qian, J. Liu, Advances in the Study of Heart Development and Disease Using Zebrafish. *J Cardiovasc Dev Dis* **3**, (2016).

68. L. A. Samsa *et al.*, Cardiac contraction activates endocardial Notch signaling to modulate chamber maturation in zebrafish. *Development* **142**, 4080-4091 (2015).

69. K. Tobita, E. A. Schroder, J. P. Tinney, J. B. Garrison, B. B. Keller, Regional passive ventricular stress-strain relations during development of altered loads in chick embryo. *Am J Physiol Heart Circ Physiol* **282**, H2386-2396 (2002).

70. N. Salehin *et al.*, Assessing Pressure–Volume Relationship in Developing Heart of Zebrafish In-Vivo. *Annals of Biomedical Engineering*, (2021).

71. J. Huisken, D. Y. R. Stainier, Selective plane illumination microscopy techniques in developmental biology. *Development (Cambridge)* **136**, 1963-1975 (2009).

72. Y. C. Fung, *Foundations of solid mechanics*. (Prentice-Hall, Englewood, 1965).

73. C. J. Chuong, M. S. Sacks, G. Templeton, F. Schwiep, R. L. Johnson, Jr., Regional deformation and contractile function in canine right ventricular free wall. *AJP - Heart and Circulatory Physiology* **260**, H1224-H1235 (1991).

74. R. J. Petrie, H. Koo, Direct measurement of intracellular pressure. *Current protocols in cell biology* **63**, 12.19.11 (2014).

75. L. K. Waldman, Y. C. Fung, J. W. Covell, Transmural myocardial deformation in the canine left ventricle. Normal in vivo three-dimensional finite strains. *Circulation research* **57**, 152-163 (1985).

76. P. Ling, L. A. Taber, J. D. Humphrey, Approach to Quantify the Mechanical Behavior of the Intact Embryonic Chick Heart. *Annals of Biomedical Engineering* **30**, 636-645 (2002).

77. S. Majkut *et al.*, Heart-Specific Stiffening in Early Embryos Parallels Matrix and Myosin Expression to Optimize Beating. *Current biology* **23**, 2434-2439 (2013).

78. V. Hamburger, H. L. Hamilton, A series of normal stages in the development of the chick embryo. 1951. *Dev Dyn* **195**, 231-272 (1992).

79. A. Gendernalik, B. Zebhi, N. Ahuja, D. Garrity, D. Bark, In Vivo Pressurization of the Zebrafish Embryonic Heart as a Tool to Characterize Tissue Properties During Development. *Ann Biomed Eng* **49**, 834-845 (2021).

80. L. K. Waldman, D. Nosan, F. Villarreal, J. W. Covell, Relation between transmural deformation and local myofiber direction in canine left ventricle. *Circ Res* **63**, 550-562 (1988).

81. J. I. Fann *et al.*, Regional epicardial and endocardial two-dimensional finite deformations in canine left ventricle. *American journal of physiology. Heart and circulatory physiology* **261**, H1402-H1410 (1991).

82. P. W. Alford, L. A. Taber, Regional epicardial strain in the embryonic chick heart during the early looping stages. *J Biomech* **36**, 1135-1141 (2003).

83. F. J. Villarreal, W. Y. Lew, Finite strains in anterior and posterior wall of canine left ventricle. *Am J Physiol* **259**, H1409-1418 (1990).

84. A. M. Ebert *et al.*, Calcium extrusion is critical for cardiac morphogenesis and rhythm in embryonic zebrafish hearts. *Proc Natl Acad Sci U S A* **102**, 17705-17710 (2005).

85. M. H. Radke *et al.*, Targeted deletion of titin N2B region leads to diastolic dysfunction and cardiac atrophy. *Proc Natl Acad Sci U S A* **104**, 3444-3449 (2007).

86. W. A. Linke *et al.*, I-band titin in cardiac muscle is a three-element molecular spring and is critical for maintaining thin filament structure. *J Cell Biol* **146**, 631-644 (1999).

87. K. Tobita, J. B. Garrison, L. J. Liu, J. P. Tinney, B. B. Keller, Three-dimensional myofiber architecture of the embryonic left ventricle during normal development and altered mechanical loads. *Anat Rec A Discov Mol Cell Evol Biol* **283**, 193-201 (2005).